

FAR-INFRARED STUDIES OF
BIS-TETRAMETHYLTETRASELENAFULVALENE SALTS
[(TMTSF)₂X, X=(ClO₄, SbF₆ & AsF₆)]

by

HON KIE NG, B.Sc.(Hons.)

A Thesis

*Submitted to the School of Graduate Studies
in Partial Fulfilment of the Requirements
for the Degree
Doctor of Philosophy*

McMaster University

September 1984

FAR-INFRARED STUDIES
OF
ORGANIC SUPERCONDUCTORS

DOCTOR OF PHILOSOPHY (1984)
(Physics)

McMASTER UNIVERSITY
Hamilton, Ontario

TITLE: Far-infrared Studies of
bis-tetramethyltetraselenafulvalene Salts
[(TMTSF)₂X, X=(ClO₄, SbF₆ & AsF₆)]

AUTHOR: Hon Kie Ng, B.Sc.(Hons.)
University of Canterbury, Christchurch,
New Zealand

SUPERVISOR: Dr. T. Timusk

NUMBER OF PAGES: *xiv*, 99

ABSTRACT

Detailed far-infrared reflectivity measurements were done for three organic compounds, *bis*-tetramethyltetraselenafulvalene (TMTSF) perchlorate (ClO_4), hexafluoroantimonate (SbF_6) and hexafluoroarsenate (AsF_6). One of these compounds ($\text{TMTSF})_2\text{ClO}_4$, was also studied by measuring the transmission through a grid of crystals. The grid technique was used to enhance the absorption of a material brought on by the application of a magnetic field. The ($\text{TMTSF})_2\text{ClO}_4$ compound shows an increased absorption below ≈ 3.8 meV with a field of 0.2 Tesla.

The reflectance data were Kramers-Kronig transformed to get the real part of the frequency dependent conductivity $\sigma_1(\omega)$, and the real part of the dielectric constant $\epsilon_1(\omega)$. In the metallic state, $\sigma_1(\omega)$ can be described by two relaxation times. The first is an extremely long lifetime τ_c ($> 10^{-11}$ s) needed to account for the high dc conductivity (10^4 - 10^5 $(\Omega\cdot\text{cm})^{-1}$). We shall call this the 'zero frequency mode'. The high frequency 'tail' of the zero frequency mode can be seen in ($\text{TMTSF})_2\text{SbF}_6$ and AsF_6 . An effective mass M^* of 250-650 m^* was obtained for the zero frequency mode. The second is the frequency dependent scattering time τ_p due to phonons (Holstein process). In the Holstein process, the conductivity profile shows an initial increase in $\sigma_1(\omega)$ as a

function of frequency before levelling off at the limiting value of τ_p .

None of the three compounds in the semiconducting (spin density waves (SDW)) state show the well developed SDW gap that is predicted theoretically. For $(\text{TMTSF})_2\text{ClO}_4$, a gap of 20 cm^{-1} was observed in the 'quenched state' while for $(\text{TMTSF})_2\text{SbF}_6$ it is $\approx 180 \text{ cm}^{-1}$. In the latter compound, 'phase phonons' accompanied the SDW transition. This is the first observation of phase phonons in the SDW state. The third compound studied, $(\text{TMTSF})_2\text{AsF}_6$, did not show any identifiable SDW gap.

獻給

我的祖母和母親

ACKNOWLEDGEMENTS

It gives me great pleasure to thank my supervisor, Dr. T. Timusk, for his help, guidance, humor and unfailing support throughout the project. Special thanks should also be given to Dr. J.P. Carbotte and Dr. E. Fenton for valuable discussion.

I would like to thank Dr. K. Bechgaard for providing the good quality samples, and to Mme. C. Weyl for mounting the samples. I am indebted to Dr. D. Jérôme for communicating first hand information.

I am grateful to Mrs. H. Kennelly and Cheryl McCallion for their accurate typing, and to Doug Bonn and Neil McKay for proofreading the manuscript.

I thank Mr. W. Scott for the endless supply of liquid helium, and others in and around the lab for useful interactions.

TABLE OF CONTENTS

	PAGE
<i>Abstract</i>	<i>iii</i>
<i>Dedication</i>	<i>v</i>
<i>Acknowledgements</i>	<i>vi</i>
<i>List of Tables</i>	<i>ix</i>
<i>List of Figures</i>	<i>x</i>
<i>Glossary</i>	<i>xiii</i>
CHAPTER 1 INTRODUCTION	1
1.1 Mechanisms for High dc Conductivity	3
1.2 Interpretations of Other Experimental Results in Terms of Single Particle Transport and/or Fluctuation Superconductivity	6
1.3 Other Optical Experiments	9
CHAPTER 2 EXPERIMENTAL TECHNIQUES	12
2.1 Introduction	12
2.2 Sample Preparation	12
2.3 a. Sample Mounting - Grids as Infrared Absorbers	13
b. Sample Mounting - Reflectivity	14
2.4 a. Apparatus - Michelson Interferometers	14
b. Apparatus - Probes	16
2.5 Magneto-Absorption: Results and Discussion	20
2.6 Reflectivity - Raw Data	28

CHAPTER 3	REFLECTIVITY MEASUREMENTS AND ANALYSIS	32
3.1	Introduction	32
3.2	Kramers-Kronig Transformation	33
3.3	Absolute Far-Infrared Reflectance of (TMTSF) ₂ ClO ₄ , SbF ₆ and AsF ₆ .	36
3.4	Discussion	45
	a. Common Features	47
	b. Unique Features	65
	c. Effects of Thermal Cycling	84
CHAPTER 4	SUMMARY AND CONCLUSIONS	88
4.1	Suggestions for Future Experiments	91
APPENDIX		93
BIBLIOGRAPHY		94

LIST OF TABLES

<u>TABLE</u>		<u>PAGE</u>
1	A list of values of λ_{tr} for the three compounds and some superconducting elements.	55
2	Half-width and effective mass of the zero frequency mode for the three compounds.	61
3	Parameters used in fitting the spin density wave conductivity of $(TMTSF)_2SbF_6$.	73

LIST OF FIGURES

<u>FIGURE</u>		<u>PAGE</u>
1.1	A detailed view of the TMTSF molecules and one of the compounds studied, $(\text{TMTSF})_2\text{ClO}_4$.	2
2.1	Schematic diagram of the common insert and probe used in the magneto-absorption experiments.	17
2.2	Secondary insert and reflectivity probe. The whole system was designed as an anti-cryostat and can be fitted into the common insert (Fig. 2.1). Inset illustrates the sample mounting.	19
2.3	Magneto-absorption of niobium and lead grids. The natural logarithm of the ratio of the transmission in the superconducting to the normal state is plotted as a function of frequency.	23
2.4	Magneto-absorption of a grid of $(\text{TMTSF})_2\text{ClO}_4$. There is a pronounced onset of magneto-absorption below 3.8 meV.	25
2.5	An example of the uncorrected reflectance from a mosaic of crystals before and after evaporating gold on the sample.	29
3.1	Absolute reflectance of $(\text{TMTSF})_2\text{ClO}_4$ for both $E a$ and $E\perp a$ to 400 cm^{-1} .	38
3.2	Polarized reflectance of $(\text{TMTSF})_2\text{SbF}_6$. Three lines appear as the sample was cooled to 2K for $E a$. In the $E\perp a$ direction, there is little observable change up to 30K.	39
3.3	Reflectance measurements of $(\text{TMTSF})_2\text{AsF}_6$ up to $\approx 500\text{ cm}^{-1}$.	40
3.4	Detailed reflectance of $(\text{TMTSF})_2\text{ClO}_4$ in the R-state from $5\text{-}60\text{ cm}^{-1}$. The measurements were for $E a$.	43

<u>FIGURE</u>		<u>PAGE</u>
3.5	A corresponding measurement as a function of temperature in the $E \perp a$ direction.	44
3.6	Reflectance of $(\text{TMTSF})_2\text{AsF}_6$ for $E \parallel a$ in the low frequency end as a function of temperature.	46
3.7	Frequency dependent conductivity of $(\text{TMTSF})_2\text{ClO}_4$ at 2K.	48
3.8	Frequency dependent conductivity of $(\text{TMTSF})_2\text{SbF}_6$ in the $E \parallel a$ direction at 2K and 19K.	49
3.9	Frequency dependent conductivity of $(\text{TMTSF})_2\text{AsF}_6$ in the $E \parallel a$ direction. The Holstein fit to 2K is also shown.	50
3.10	Assumed form $\alpha^2 \text{tr}(\omega)F(\omega)$ used to fit $\sigma_1(\omega)$ of $(\text{TMTSF})_2\text{AsF}_6$. This $\alpha^2 F$ can also be used to fit $\sigma_1(\omega)$ of the other two compounds.	53
3.11	Real part of the dielectric constant for $(\text{TMTSF})_2\text{ClO}_4$ at 2K.	59
3.12	Frequency dependent conductivity of $(\text{TMTSF})_2\text{SbF}_6$ in the $E \perp a$ direction at 2K.	62
3.13	Frequency dependent conductivity of $(\text{TMTSF})_2\text{AsF}_6$ in the $E \perp a$ direction, at 2K and 25K. Note the significant difference in $\sigma_1(\omega)$ below $\approx 67 \text{ cm}^{-1}$.	63
3.14	Temperature dependence of $\sigma_1(\omega)$ of $(\text{TMTSF})_2\text{SbF}_6$ in the $100\text{-}300 \text{ cm}^{-1}$.	66
3.15	Plot of integrated intensity of peak A' versus temperature, and shift in frequency versus temperature.	68
3.16	The SDW part of $\sigma_1(\omega)$ of $(\text{TMTSF})_2\text{SbF}_6$ at 2K and theoretical fit.	70
3.17	Detailed temperature dependence of the 7 cm^{-1} and 25 cm^{-1} peaks for $(\text{TMTSF})_2\text{ClO}_4$ in the $E \parallel a$ direction.	75
3.18	Corresponding temperature dependence of $\sigma_1(\omega)$ of $(\text{TMTSF})_2\text{ClO}_4$ in the $E \perp a$ direction in the low frequency end.	76

<u>FIGURE</u>		<u>PAGE</u>
3.19	Magnetic field dependence of the 25 cm^{-1} peak of $(\text{TMTSF})_2\text{ClO}_4$ at 2K.	78
3.20	Reflectance and corresponding conductivity of $(\text{TMTSF})_2\text{ClO}_4$ when cooled at a rate of $\approx 40\text{-}50 \text{ K/min}$ from $\approx 70\text{K}$.	80
3.21	Reflectance of $(\text{TMTSF})_2\text{ClO}_4$ in the R-state and Q-state at 2K. The Q-state was obtained by cooling at a rate of $\approx 70 \text{ K/min}$ from 30K.	81
3.22	Detailed temperature dependence of $(\text{TMTSF})_2\text{AsF}_6$ at the low frequency end.	83
3.23	An example of the effect of thermal cycling on the 7 cm^{-1} and 25 cm^{-1} peaks of a sample of $(\text{TMTSF})_2\text{ClO}_4$.	86

GLOSSARY

A	absorbance
AsF ₆	hexafluoroarsenate
BCS	Bardeen-Cooper-Schrieffer
CDW	charge density waves
ClO ₄	perchlorate
e	electron charge
e-p	electron-phonon
FSC	fluctuation superconductivity
FWHM	full width at half maximum
g	grid spacing
H _{c2}	superconducting critical field (type 2)
ħ	Planck's constant
k	imaginary part of refractive index
m	free electron mass
m*	single particle effective mass
M*	effective mass of zero frequency mode
MI	metal-insulator
n	electronic density (per unit volume) (or real part of refractive index, Section 3.2 only)
N	complex refractive index
Q-state	quenched state
R	reflectance
R-state	relaxed state

SbF_6	hexafluoroantimonate
SDW	spin density waves
T	transmittance
T_c	superconducting transition temperature
t_i	transfer band integral (subscript indicate axis direction)
TMR	transverse magneto-resistance
TMTSF	tetramethyltetraselenafulvalene
TTF-TCNQ	tetrathiafulvalene-tetracyanoquinodimethane
$\alpha_{\text{tr}}^2(\omega)F(\omega)$ or α^2_F	phonon density of states weighted by the square of electron-phonon coupling for transport
$\epsilon(\omega)$	complex dielectric constant
κ	thermal conductivity
λ	electron-phonon coupling constant (or wavelength of electric field, Section 2.5 only)
λ_{tr}	electron-phonon coupling constant for transport
μ	electron/hole mobility
τ_c	lifetime of electrons in the zero frequency mode
τ_{sp}	single particle scattering lifetime
τ_p	scattering lifetime due to phonons
$\sigma(\omega)$	complex frequency dependent conductivity
$\sigma_1(\omega)$	real part of the conductivity
ω	frequency of electric field
ω_p	free electron plasma frequency
Ω_p	collective mode plasma frequency
1-D	one-dimensional
3-D	three-dimensional

CHAPTER I

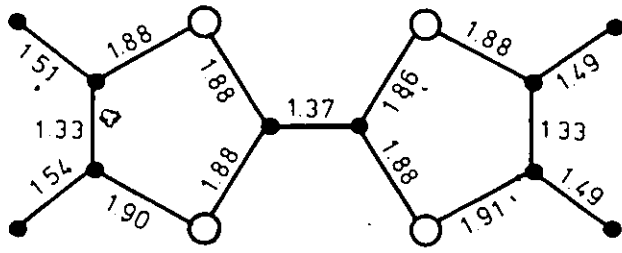
INTRODUCTION

The *bis-tetramethyltetraselenafulvalene-X* compounds, where X is any one of a number of inorganic anion e.g. PF_6 , AsF_6 , SbF_6 , NbF_6 , BF_4 , ClO_4 , ReO_4 , NO_3 , etc., form a novel family of charge transfer organic solids. These charge transfer salts have been of intense interest since they were first synthesized by K. Bechgaard [1] in 1979. Experimental measurements show that they exhibit diverse low temperature effects e.g. superconductivity [2-4], spin density waves (SDW) [5-7], anion ordering [8], quantized Hall effect [9,10], etc. Typically, under ambient pressure, the dc conductivity shows a metal-insulator (MI) transition in the range 12-40 K [1]. The insulating state has been identified as SDW [5,6] rather than the charge density wave (CDW) which occurs for other organic conducting salts e.g. TTF-TCNQ [11]. The SDW transition can be suppressed by the application of hydrostatic pressure above a critical value. In fact, this is how superconductivity was first observed in $(\text{TMTSF})_2\text{PF}_6$ by Jérôme et al. [2]. In this compound, the SDW transition occurs at 12 K. When pressure > 6.5 kbar is applied, the material remains metallic and undergoes a superconducting transition at ~ 1 K.

The planar TMTSF molecules stack together in a zig-zag fashion to form a linear chain (Fig. 1.1) [12]. The chain

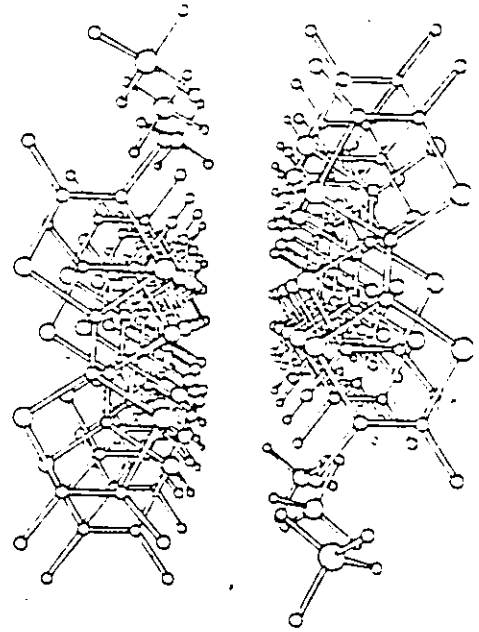
Figure 1.1

(a) A TMTSF molecule. [after N. Thorup, G. Rindorf, H. Soling, K. Bechgaard, Acta Cryst. B37,1236 (1981)] (b) View along the chain of $(\text{TMTSF})_2\text{ClO}_4$ crystal. [after J. Friedel and D. Jérôme, Comtemp. Phys. 23,583 (1983)] (c) Side-view of a chain of $(\text{TMTSF})_2\text{ClO}_4$ molecules. Note the slight dimerization as indicated by the Se-Se intermolecular distance (in Å). The anion is drawn for two ordering positions. The unit cell is triclinic with $a = 7.266 \text{ \AA}$, $b = 7.678 \text{ \AA}$, $c = 13.275 \text{ \AA}$ and $\alpha = 84.58$, $\beta = 86.73$, $\gamma = 70.43$. [after ref. 12]

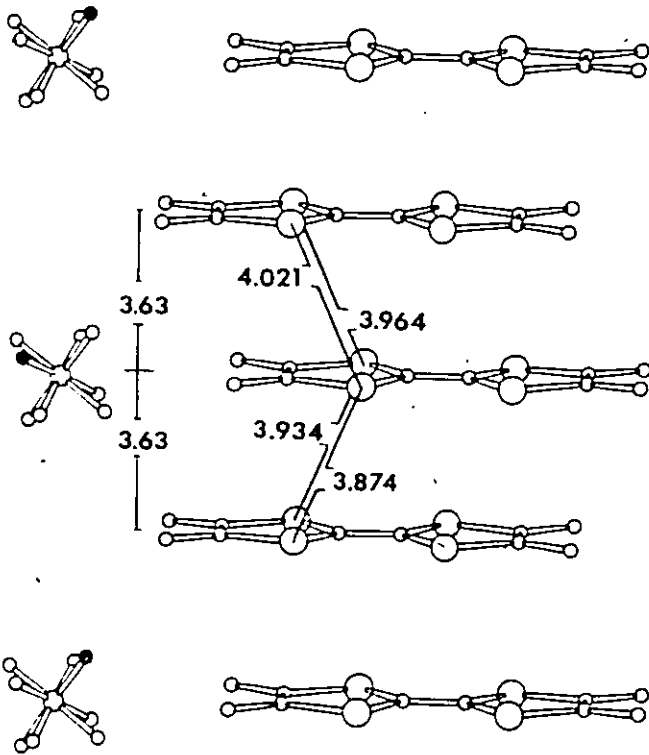


○ Se
● C

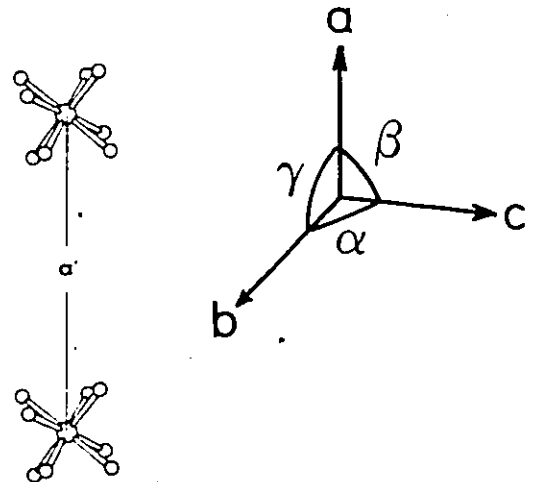
(a)



(b)



(c)



r.

direction is the a-axis, and the interchain direction (see figure) is the b-axis. Across the anion is the c-axis. There is a transfer of one electron from two TMTSF molecules to one anion giving a half-filled band if we take a' to be two molecular distances. The difference in anions does not affect the band structure parameters significantly [13]. Various methods [14-19] have been used to determine the bandwidth of the salts. They all give consistent results with $t_a \approx 200$ meV, $t_b \approx 13$ meV, and $t_c \approx 1$ meV where t is the transfer band integral. These values are important in determining the dimensionality of the materials. The criteria used to define the dimensionality have been discussed by Chaikin et al. [20]. One thing is clear, the materials are highly anisotropic no matter what the dimensionality is. The crossover temperature which determines a change in dimensionality is given by $\hbar/\tau_a = t_{\perp}$ [21] where τ_a is the scattering lifetime along the chain.

1.1 Mechanisms for High dc Conductivity

A striking property of these compounds is their high dc conductivity along the chain. At low temperatures, values greater than 10^5 ($\Omega\text{-cm}$)⁻¹ have been obtained [4]. The dc conductivity is highly anisotropic ($a:b:c \approx 10^5:400:1$) as indicated by the bandwidths. There are various mechanisms that can give rise to high dc conductivity. We will discuss three modes; namely, single particle transport, fluctuation superconductivity (FSC), and sliding CDW. Interpretation of experimental results in terms of these mechanisms will also be discussed.

In the single particle transport picture, the electrons act independently of each other. The conductivity is given by $\sigma = nev$ where n is the electronic density (1 electron per unit cell of volume $= 700 \text{ \AA}^3$), e the electron charge and μ the mobility. Using the above formula, μ for $(\text{TMTSF})_2\text{PF}_6$ is $> 10^4 \text{ cm}^2/\text{V}\cdot\text{sec}$ at 4.2 K and under 11 kbar [3]. A similar value was obtained using Hall measurements [22]. A mobility of this order of magnitude would imply a huge mean free path $\sim 3000 \text{ \AA}$ or ~ 350 lattice constants, if we assume free electron mass. As we will show, our far-infrared data imply an even larger mean free path.

Fluctuation superconductivity is normally discussed in the temperature regime $T_3 < T < T_1$ where below T_3 3-D behaviour predominates, and below T_1 1-D properties are strongly manifested [21]. The bulk superconducting transition temperature, T_c , is $< T_3$. A simple physical picture of FSC can be visualized in terms of small filaments in the crystal that are superconducting. The crux of this model, within the Ginzburg-Landau theory [23], is that interchain coupling must be weak, $t_{\perp} \ll t_a$ and $t_{\perp} < \hbar/\tau_a$. This gives an enhancement of the conductivity that is proportional to t_{\perp}^{-2} . As the temperature is decreased, more 'filaments' appear resulting in increased conductivity. The conductivity, however, is not infinite as in normal bulk superconductors.

There is also pairing of electrons in FSC within Ginzburg-Landau theory. Normal electrons form virtual Cooper pairs above

the Fermi surface in a time τ_N . They decay back to the normal state in time τ_S . Because of the formation of virtual Cooper pairs, there is a decrease in the density of states at the Fermi level given by $[N(\epsilon_F) - N_0]/N_0 = \tau_N/\tau_S$.

This reduction, but not complete removal, of the density of states is called a pseudo-gap. Since FSC is thought to occur below T_1 , this would imply a large pseudo-gap.

In Peierls instability there arise CDW [24]. The lattice distortion that signifies Peierl's distortion need not be static with a fixed phase but may be dynamic as pointed out by Bardeen [25], with the result that the CDW moves or slides along the lattice. In other words, the electrons 'surf-ride' on the CDW. Since scattering is inhibited by strong electron-phonon coupling, this movement of charge can carry a superconductive current as first shown by Fröhlich [26] for a 1-D system. In reality, no persistent current was ever observed in the Fröhlich mode as there cannot be long range order in a 1-D system. However, short-range order does give enhanced conductivity as observed for TTF-TCNQ [27,28] at temperatures \approx 68 K. As the temperature is lowered below 58 K for TTF-TCNQ, there is a decrease in conductivity. This is attributed to the CDW becoming pinned to charged impurities, lattice defects, and significant interchain coupling [29]. There is clear far-infrared evidence that this is the case for TTF-TCNQ [30], and KCP [31]. Sliding CDW cannot be responsible for the high dc conductivity in $(\text{TMTSF})_2\text{X}$ compounds since x-ray scattering

experiments [32] failed to detect any softening of the $2k_F$ phonons just above the MI transition temperature. This softening must be present if the materials undergo CDW transition.

1.2 Interpretations of Other Experimental Results in Terms of Single Particle Transport and/or Fluctuation Superconductivity

An attractive explanation for the observation of large transverse magnetoresistance (TMR) [2,20] is the breaking up of Cooper pairs in FSC. The huge TMR was observed for both $(\text{TMTSF})_2\text{PF}_6$ and ClO_4 , and also in another system, TMTSF-DMTCNQ [33]. It increases rapidly as the temperature is lowered below ≈ 30 K. Above this temperature, there is no significant difference. To explain the high TMR using a single carrier transport picture, one assumes that the scattering rate is wavevector dependent [20]. Thus, with the application of a magnetic field, the electrons are swept to those parts of the Fermi surface that have high scattering rates with a resulting increase in resistance. The temperature dependence of the TMR is accounted for by another scattering mechanism e.g. by phonons which becomes less dominant at low temperatures.

The huge mobility or mean free path obtained when single particle transport is used is objectionable. It requires high crystal quality which is unlikely to be met in the organic solids [34].

Perhaps, the strongest evidence for FSC was the observation of minima in $\frac{dV}{dI}$ characteristics as obtained by tunneling experiments [35-37]. The first reported measurements show two

clear minima 3.6 mV apart [35]. The sample was $(\text{TMTSF})_2\text{PF}_6$ which was under 11 kbar and at 50 mK. This value (3.6 mV) is far too large for bulk superconductivity $T_c \approx 1$ K. A Schottky junction N/Ga-Sb- $(\text{TMTSF})_2\text{PF}_6$ was used with a thin film of tin evaporated on N/Ga-Sb for electrical contact. Tin is superconducting with $2\Delta = 1.1$ mV. However, it is well known that thin films of superconducting materials have much bigger energy gaps than bulk materials. Later experiments [36,37] using different junctions and electrical contacts also show minima in $\frac{dV}{dI}$ characteristics but they are less conclusive. Tunneling experiments are difficult to interpret. It has been argued that the minima arise from band structure effects or possibly that the amorphous gallium or antimony become superconducting [38].

Pressure dependence studies of the bulk superconducting transition temperature T_c in $(\text{TMTSF})_2\text{PF}_6$ indicate a decrease in T_c as the pressure is increased [3]. If FSC were present before the material becomes superconducting, then increasing the pressure would increase T_c since one expects the coupling between filaments to increase. Theoretical calculations [39] for weakly coupled filaments show this to be the case.

The anisotropy in the superconducting critical fields, H_{c2i} ($i = a, b^*, c^*$) yields valuable information on the origin of pairbreaking [38,20]. The pairbreaking by the magnetic field can be either orbital or spin (or both). If the former is the case, then $H_{c2i}/H_{c2j} = (\sigma_i/\sigma_j)^{1/2}$. The ratio $b^* : c^*$ is in

excellent agreement but not the ratio of a to either of the perpendicular directions. The critical field ratio is much smaller than the conductivity ratio. The implication is that the pairbreaking is not due to orbital effects in the a direction. For the spin effect, in the Pauli limit, the critical field at $T=0$ is given by $H_{c2}(0) = 18.4 T_c$ [38]. The calculated value of H_{2ca} is very close to the measured value of the BCS T_c (1K) for both $(TMTSF)_2PF_6$ and ClO_4 salts. Now, since the Pauli critical field is a measure of the mean field transition temperature, T_{mf} , and not T_3 , there cannot be any fluctuations above T_{mf} . In other words, if there were any FSC, then H_{c2a} would be much larger.

For a normal BCS superconductor, the thermal conductivity, κ , decreases from T_c [40]. However, if FSC is present, then κ first increases before decreasing. This is due to the fact that in FSC, the pairing is above the Fermi surface and has higher energy and forms quasiparticles with longer mean free paths than in the normal state. When the pairing is destroyed by the magnetic field, then κ would be smaller than when FSC was present. This was found to be the case for fluctuation in filaments of Pb-5-at.% In [41]. The measured κ for $(TMTSF)_2ClO_4$ below 100 K shows contradictory results. Djurek et al, [42] on one hand, show a monotonic decrease in κ below ~ 50 K with an increase in κ below 40 K when a field of 50 K Gauss was applied while Kwak et al. [43] and Choi et al. [44] on the other hand show an increase in κ below 50 K with

no field dependence. This latter result is expected for a normal metal.

There are other experimental results e.g. thermopower [37,45] specific heat [18], Schubnikov-de Haas oscillations [17], linearity in resistance with increasing current above 2 K [20] etc. that do not necessitate the presence of, or would be difficult to explain if FSC were present over a wide temperature range.

1.3 Other Optical Experiments

The first optical measurements on the $(\text{TMTSF})_2\text{X}$ compounds were by Jacobsen et al. [14]. The reflectance along the chain and b directions show clear plasma edges in the near IR and mid-IR respectively for a number of salts; PF_6 , AsF_6 , ReO_4 and ClO_4 . Along the c direction, the reflectance is constant for the one compound studied, $(\text{TMTSF})_2\text{AsF}_6$.

~~From the reflectance, one can get the frequency dependent conductivity, $\sigma(\omega)$ (see Section 3.2). All of the results were for temperatures ≥ 25 K, and in the metallic state, except for $(\text{TMTSF})_2\text{ReO}_4$ which has $T_{\text{MI}} \approx 180$ K [1]. The principal results along the chain axis at 25 K for $(\text{TMTSF})_2\text{PF}_6$ were a large conductivity peak ($> 10^4 (\Omega \cdot \text{cm})^{-1}$) centred at $\sim 300 \text{ cm}^{-1}$ with threshold at $\sim 200 \text{ cm}^{-1}$, and extremely low conductivity ($\sim 300 (\Omega \cdot \text{cm})^{-1}$) at lower frequencies. There is no evidence of any rise in conductivity below 10 cm^{-1} to account for the known dc conductivity. The huge peak in $\sigma(\omega)$ is not well understood, and a similar peak was also observed in another~~

compound, TTF-TCNQ by the same experimental group [30]. However, Eldridge et al. [46] did not see any anomalous peak in the latter compound.

The low frequency data suggest that there is a narrow peak centred at $\omega = 0$, the zero frequency mode. Microwave data at 35 GHz and 300 K show a sharp decrease in conductivity from $\sigma(0)$ [1]. In the SDW state, the microwave measurements at 1 GHz show an increase in σ from dc [47]. This may be due to the zero frequency mode becoming pinned at a finite frequency in the SDW state (as in CDW) though no threshold depinning field was found in the dc conductivity [48]. If, in the SDW state, this mode does become pinned, then it should become visible at low frequencies and low temperatures.

The various instabilities (SDW, CDW etc.) have energy gaps that lie in the far-infrared. If the mechanism responsible for the high dc conductivity in the metallic state is due to FSC, then the frequency dependent conductivity would show low conductivity inside the pseudo-gap after which it would rise sharply to a normal metal response. On the other hand, one can also estimate the lifetime of the single particle transport optically. The zero frequency mode and the pinned mode would show signs of increasing conductivity as $\omega \rightarrow 0$. Our intention was to study the behaviour of the zero frequency mode as a function of temperature. We also wanted to measure the energy of the SDW gap, and to study the absorption process in the $30 - 400 \text{ cm}^{-1}$ range. Chapter 2 outlines the ex-

perimental techniques. The results for three compounds
(TMTSF)₂ClO₄, SbF₆, and AsF₆ are presented in Chapter 3. A
summary of the results will be given in Chapter 4.

CHAPTER 2

EXPERIMENTAL TECHNIQUES

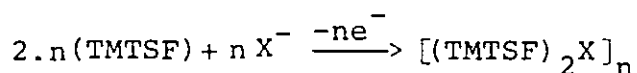
2.1 Introduction

Two types of experiments were done in the far-infrared. The first used grids as infrared absorbers, and the second was a reflectivity experiment on mosaics of crystals. The grid method was used since the original crystals were ≤ 0.1 mm wide and difficult to study using normal optical methods, i.e. absorption and reflection. In these experiments, the transmission through the grids was measured with the magnetic field off/on. The natural logarithm of the ratio gives the magneto-absorption. Transmission experiments on thin films were ruled out since the properties of the compounds are destroyed by sublimation. Later crystals were much bigger making the reflectivity experiments possible. The reflectivity measurements form the bulk of this report.

2.2 Sample Preparation

The compounds studied in our experiments were grown by Klaus Bechgaard [1]. The crystals are fairly soft and fragile. A constituent of these compounds, TMTSF, is stable when stored under argon and in the dark, but decomposes when exposed to air. By electrochemical oxidation under a constant current of 5-10 μA , 2 TMTSF molecules combine with a radical anion in a solution of 10^{-3} molar TMTSF in CH_2Cl_2 containing n-butylammonium - X

(0.1 mole) to give:



The end product, the $(\text{TMTSF})_2\text{X}$ compounds, appear as single shiny black crystals of typical dimension $50 \text{ mm} \times 0.3 \text{ mm} \times 0.1 \text{ mm}$.

2.3 a. Sample Mounting-Grids as Infrared Absorbers

For these experiments, the $(\text{TMTSF})_2\text{ClO}_4$ crystals were glued perpendicular to thin gold strips (1000/inch) on Mylar, using strain-free glue. This arrangement results in an E-field polarized along the highly conducting a-axis. The width, $2a$, and spacing, g , of the crystals were $80 \pm 40 \text{ } \mu\text{m}$ and $180 \pm 50 \text{ } \mu\text{m}$ respectively. The grids covered an area of $\approx 4 \text{ mm square}$. Four such grids were studied, with one batch of crystals from the group of Fabre, Montpellier (France), and the rest from Klaus Bechgaard, Copenhagen.

The grids as absorbers were also studied for two ordinary superconductors, lead and niobium with $T_c = 7.2 \text{ K}$ and 9.25 K respectively. The grids for these materials were made in the following way. A brass plate measuring $1/4''$ wide by $1/16''$ deep was centred on a lathe. Using a sharp pointed bit, grooves were cut $200 \text{ } \mu\text{m}$ apart on both sides of the plate. Then a 2 mil brass shim with a circular hole $\geq 3 \text{ mm}$ was placed on top of the plate. Lead or niobium wires were wound around the plate with the grooves as guides. The wires were then glued to the brass shim with GE-7201. When it had dried, the wires were cut at the side of the plate, and the grid was formed by the regular-

ly spaced wires across the hole on the brass shim. The lead and niobium wires had diameters, $2a$ of 80 and 51 μm respectively. Normally two grids were placed perpendicular to each other to form a mesh in our experiments. This increased the signal in our studies.

b. Sample Mounting - Reflectivity

The samples required to do the far-infrared reflectance experiments need to be large enough to cover ~ 3 mm circular area. Since the largest crystals had widths of 0.5 - 1 mm, it became necessary to form a mosaic of crystals. Initial experiments on $(\text{TMTSF})_2\text{ClO}_4$ were done with about 8 single crystals glued to a brass plate. Because the crystals were of different sizes, this gave an uneven optical surface. This unevenness gave rise to diffraction peaks in the reflectivity when the wavelength was of the order of the scale of the unevenness. Significant improvements were made when the crystals were glued to a mica ring of inner diameter 3 mm. This gives an exposed flat surface required for optical studies. The geometry of this arrangement is illustrated in the inset of Fig. 2.2. This arrangement was used on both the SbF_6 and AsF_6 compounds, and also on one mosaic of ClO_4 compounds.

2.4 a. Apparatus - Michelson Interferometers

The far-infrared measurements were made using two Michelson interferometers; a Martin-Puplett type polarizing Michelson interferometer [49], and a rapid scan Michelson interfero-

meter. The former utilizes an input polarizer, a wire grid with grid constant $9.5 \mu\text{m}$ as a beam splitter, a chopping polarizer, and roof-top mirrors. The advantage of this type of interferometer over the conventional interferometer is its almost ideal performance at low frequencies, the intensity being limited only by the lamp. An additional advantage is the suppression of the background level which can give rise to spurious modulation.

Briefly, the system works as follows. The movable mirror is driven by a Slo-Syn HS25V stepping motor which is controlled by commands from the computer (Nova II, Data General Co.). At each discrete position, the signal from the bolometer was sent to an Ithaco Dynatrac 3 lock-in amplifier with the reference being provided by the chopping polarizer. Each point was normally integrated for 2 seconds. The amplified signal was then sent to a V/F converter which was set at a convenient level so that the computer could read it as an integer into a 16 bit memory. The whole intensity versus scanning path is called an interferogram.

An RIIC FS720 Michelson interferometer was modified for rapid scan operation. Instead of a stepping motor, the moving mirror was driven by a linear magnetic motor. To ensure smooth scanning, the mirror is supported by hydrostatic pump oil chopper was used. The scan was fast enough for the interferogram to be detected as an AC signal. This suppresses the background level. A He-Ne laser emitting a line at 6348 \AA was used

in the same optical path. The interference of this laser line produced fringes, and the number of fringes was used to calculate the scanning path. A white light interferometer was also used to locate the zero path of the far-infrared interferogram. A more complete description can be found in Timusk and Lin [50].

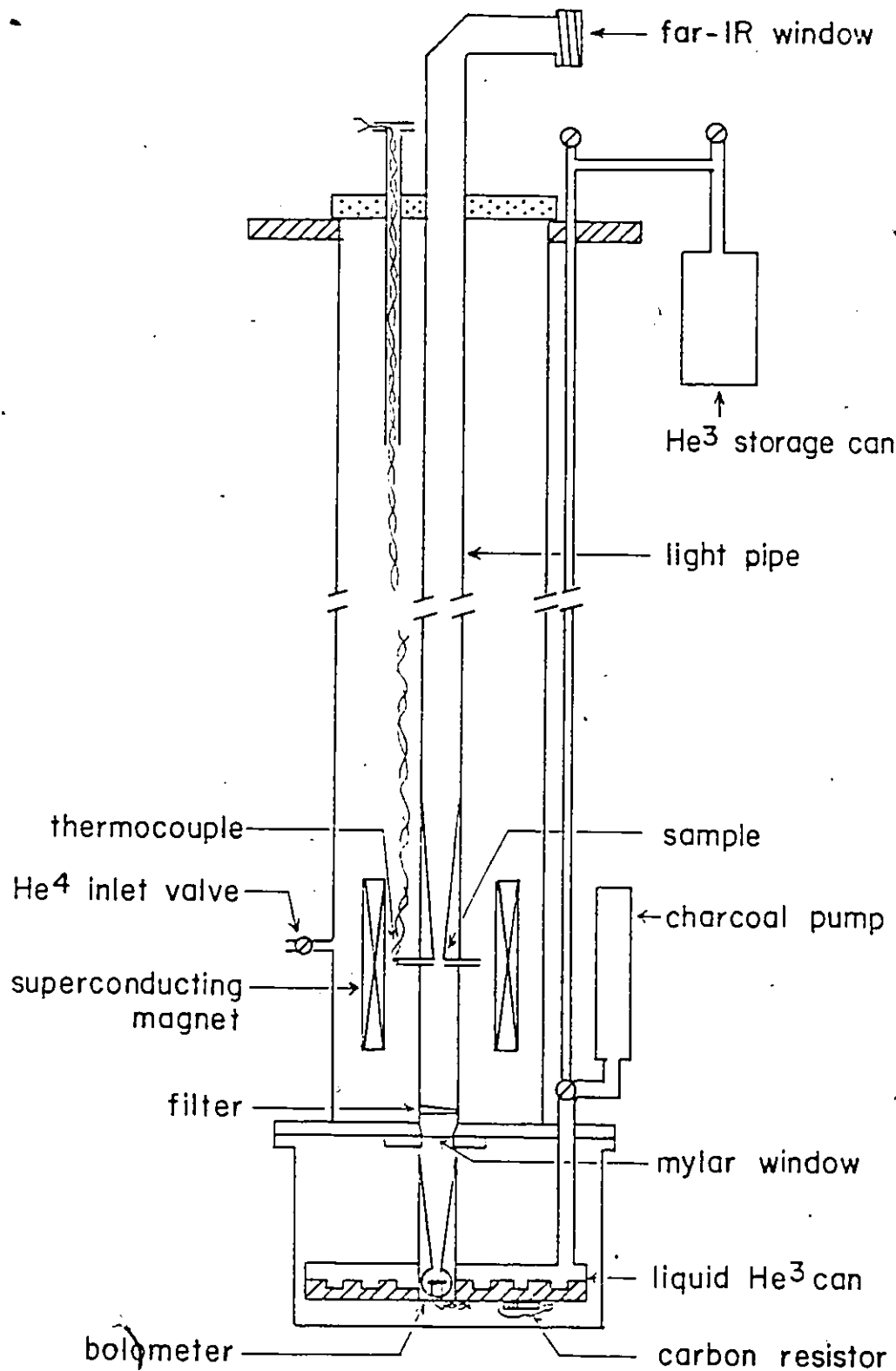
Interferograms so produced should ideally be symmetric functions. Fourteen points were taken to the left of the zero path position. These points were used to check the symmetry of the interferograms, and to make any phase corrections, if necessary, to produce a mathematically symmetric function. The number of points to the right was determined by the resolution and cutoff frequency. Before the computer calculated the Fourier transform, it multiplied the interferogram by an apodizing function. The intensity versus frequency spectrum was then stored on floppy disk, and could be displayed on an oscilloscope. Normally, about three scans were taken and averaged. The Martin-Puplett type interferometer gave good intensity from $\sim 10 - 120 \text{ cm}^{-1}$ while the fast scanning Michelson interferometer was good from $50 - 500 \text{ cm}^{-1}$ when a 1/4 mil mylar beam-splitter was used.

b. Apparatus - Probes

The probes used to measure the magneto-absorption of grids and the reflectivity of mosaics were all designed to fit into a common insert, Fig. 2.1. This insert housed a heavily doped composite germanium bolometer [51] that operated at $\sim 0.34 \text{ K}$. This temperature was attained by a hermetically sealed He^3

Figure 2.1

Schematic view of the common insert and probe used in magneto-absorption experiments. The detector chamber has a few torr of hydrogen for cooling by conduction to ≈ 20 K. However, below 20 K hydrogen condenses and the chamber was then under vacuum. The mylar window leading to the bolometer is 1/2 mil thick. For most experiments, the far-infrared window was a ≈ 50 mil white polyethylene sheet.



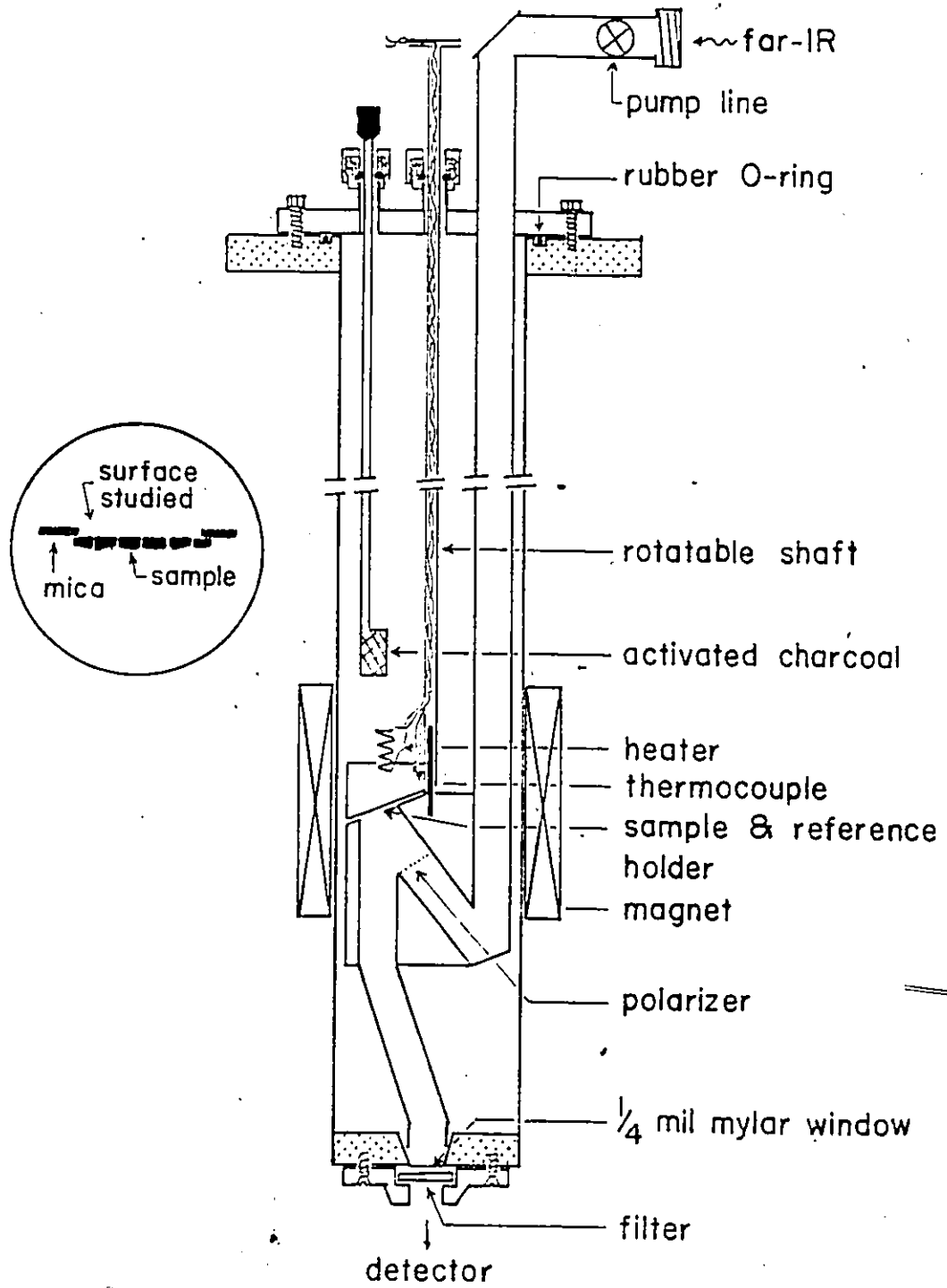
refrigeration system and was measured by a calibrated Speer 470 Ω carbon resistor. Far-infrared radiation was admitted to the detector via a 1/4" diameter mylar window of 1/2 mil thickness. The whole insert was screwed down inside a He⁴ dewar. The insert can be filled with liquid He⁴ by opening the He⁴ valve which can be operated from the outside. For more details, the reader may consult Navarro-Contreras [52].

The probe used in the magneto-absorption experiments is also shown in Fig. 2.1. It consisted of a half-inch inner diameter thin walled brass light pipe which narrows down to a one-eighth inch diameter pipe through the use of a cone. The grid sample was placed across the light pipe, and was surrounded centrally by a superconducting magnet. A Cu-Au (7% Fe) thermocouple was used to measure the sample temperature. A soot-coated KI filter at the end of the probe cuts off any radiation above $\sim 100 \text{ cm}^{-1}$ from reaching the detector.

Fig. 2.2 shows the probe and secondary insert used for the reflectivity experiments. The secondary insert was designed as an anti-cryostat so that temperatures up to 60 K could be maintained without putting an undue load on the bolometer, and it could be fitted inside the (primary) insert shown in Fig. 2.1. The mosaic arrangement of crystals was placed on the sample holder which also had a gold on brass reference plate. This holder could be rotated from the outside to bring the sample/reference into the light path. Far-infrared radiation

Figure 2.2

A longitudinal cross-section of the secondary insert and probe used in the reflectivity experiments. The system was designed as an anti-cryostat, and can be fitted into the (primary) insert shown in Fig. 2.1. When high temperatures were required, the bag of activated charcoal was lowered to adsorb He⁴ gas. The heater was then turned on to bring the sample to the desired temperature. The sample/reference can be rotated from the outside to bring the sample/reference into the far-infrared beam. The direction of polarization was aligned by eye and has an estimated uncertainty of $\pm 5^\circ$. Inset shows the mosaic arrangement of the crystals.



from the interferometer was passed along the light pipe. It was polarized by a 3.8 μm grid constant copper strip on 8G mylar before reflecting off the sample/reference. This polarizer was effective up to 700 cm^{-1} [53], and was placed 1 cm away from the sample. After a single reflection, the beam was diverted to the detector through a 1/4 mil mylar window. In most experiments, a 2 mil black polyethylene filter was used to cut off radiation above $\sim 700\text{ cm}^{-1}$.

The temperature in this setup was monitored using a thermocouple identical to that used in the magneto-absorption experiments. For low temperatures, below $\leq 4\text{ K}$, the bag of activated charcoal was lifted up. When higher temperatures were desired, this bag was lowered to just above the sample holder. The purpose of this was to adsorb any He^4 gas in the (secondary) insert. After 3 - 4 minutes, the heater was turned on, and the sample brought up to the required temperature. Usually about 300 mW was needed to bring the temperature to 20 K.

2.5 Magneto-Absorption: Results and Discussion

The magneto-absorption of a grid was measured in the following way. Spectra of transmission through the grid with magnetic field off were taken. These were called numerators. Then a static magnetic field was applied at a right angle to the a-axis of the crystals, and the spectra taken were called denominators. For the two ordinary superconductors studied, the field applied exceeded the critical field. Taking the natural

logarithm of the ratio of numerator over denominator gives the magneto-absorption.

There are several advantages in using grids to measure any change in absorption brought on by the application of a magnetic field. (1) The shape of the sample required was ideally met by the small, needle-like $(\text{TMTSF})_2\text{ClO}_4$ crystals. (2) The E-field was polarized along the highly conducting a-axis; the axis we were interested in. (3) The grids, normally called inductive grids, are well known to be more lossy than calculated from surface impedance. (4) Any absorption can easily be magnified by placing two grids, one after the other, and tilted to avoid Fabry-Perot interferences. Two disadvantages of this method are; (1) the spectral range studied is limited to $\lambda < g$. (2) There is a lack of absolute calibration i.e. we do not know by how much the conductivity actually changes.

The reflectance (R), transmittance (T) and absorbance (A) of a grid of regularly spaced wires have been treated theoretically by Ulrich [54], and Lewis and Casey [55]. The former author used an analogue of the transmission line theory. A detailed description of this theory can also be found in Chapter 3 of Moeller and Rotschild [56]. Both Ulrich, and Lewis and Casey solved the problem for light polarized parallel to the wire (the grid is transparent to light polarized perpendicular to the wire) and in the limit of the wavelength $\lambda > 2g$. An additional restriction is that the skin depth be much less than the wire diameter, $2a$. Under these limits, the following

expressions were obtained by Lewis and Casey:

$$\begin{aligned}
 R &= 1 - \left(\frac{2g}{\lambda} \ln \frac{g}{2\pi a} \right)^2 \\
 T &= 1 - R - A \approx \left(\frac{2g}{\lambda} \ln \frac{g}{2\pi a} \right)^2 \\
 A &= \frac{g}{\pi a} \left(\frac{c}{\sigma \lambda} \right)^{1/2} R
 \end{aligned}
 \tag{2.1}$$

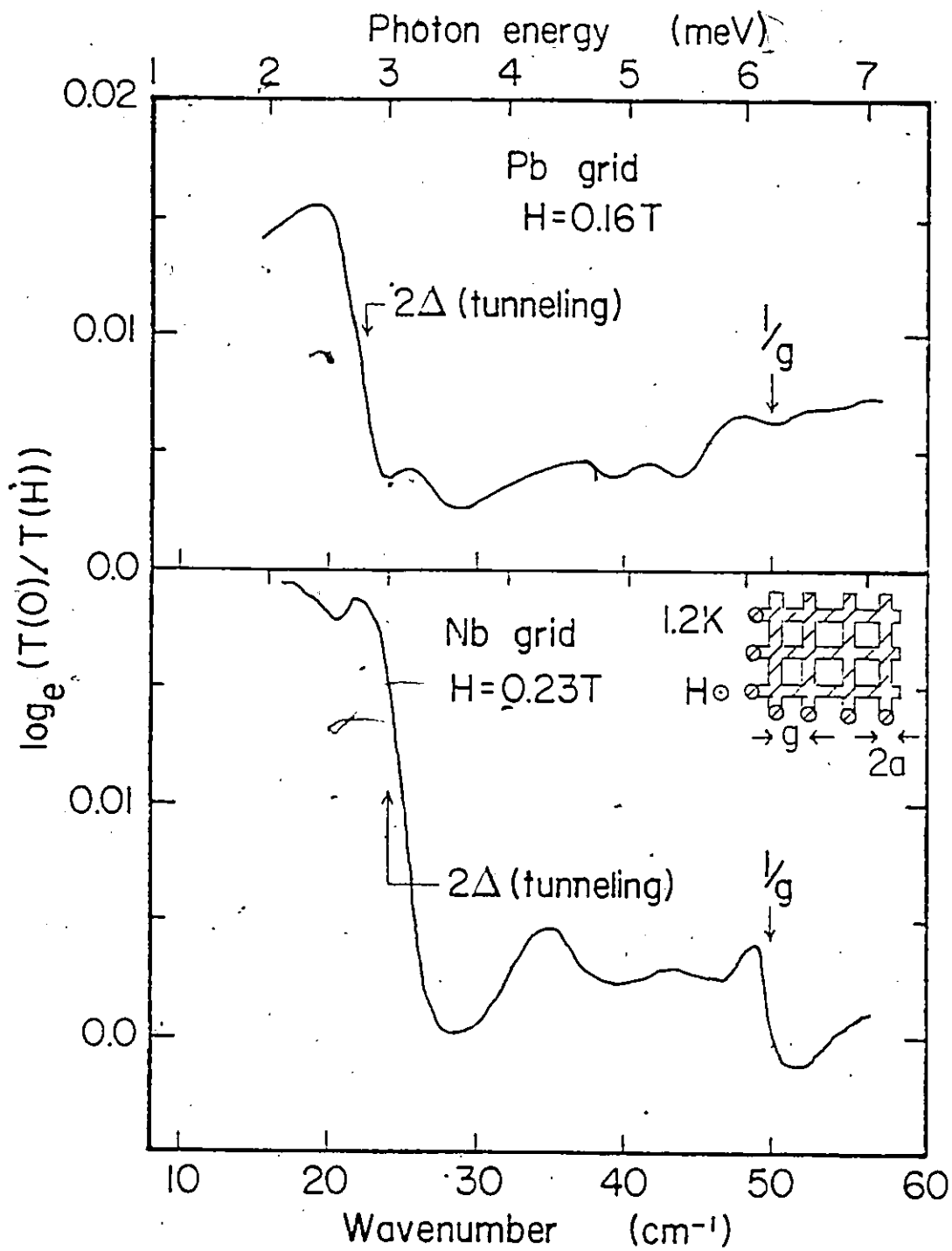
where c is the speed of light and σ is the conductivity of the wire. The absorbance of a conducting material is normally less than one percent in the far-infrared. Thus the quantity R in the expression for A can be replaced by $1-T$.

Fig. 2.3 shows increased absorption at 1.2 K for lead, and niobium below the energy gap 2Δ brought on by the application of the magnetic field. Above the gap, the normal and superconducting states have the same surface impedance, and the magneto-absorption is zero. The energy range where there is an increase in absorption is in excellent agreement with tunneling results. The uncertainty in the position of the baseline is 0.01, and that of the amplitude of the signal is 0.005.

A theoretical estimate of the increase in absorption can be obtained using the above equations for A and R . For Pb, using a dc resistivity of $1.0 \mu\Omega\text{.cm}$, and assuming Drude normal state absorption, $A \approx 0.0013$. Our measured value is ~ 0.012 . Similarly, for Nb with a measured dc resistivity value of $1.3 \mu\Omega\text{.cm}$ using four probe technique, $A \approx 0.0025$ whereas the observed was ~ 0.02 . This enhanced effect can be attributed to

Figure 2.3

Magneto-absorption of Nb and Pb grids. The \log_e of the ratio of the transmission in the superconducting state to the normal state is plotted as a function of frequency. In both cases there is an onset of magneto-absorption below the energy gap as the superconductivity is destroyed by the magnetic field. The arrow marked $1/g$ denotes the position of grid spacing frequency.



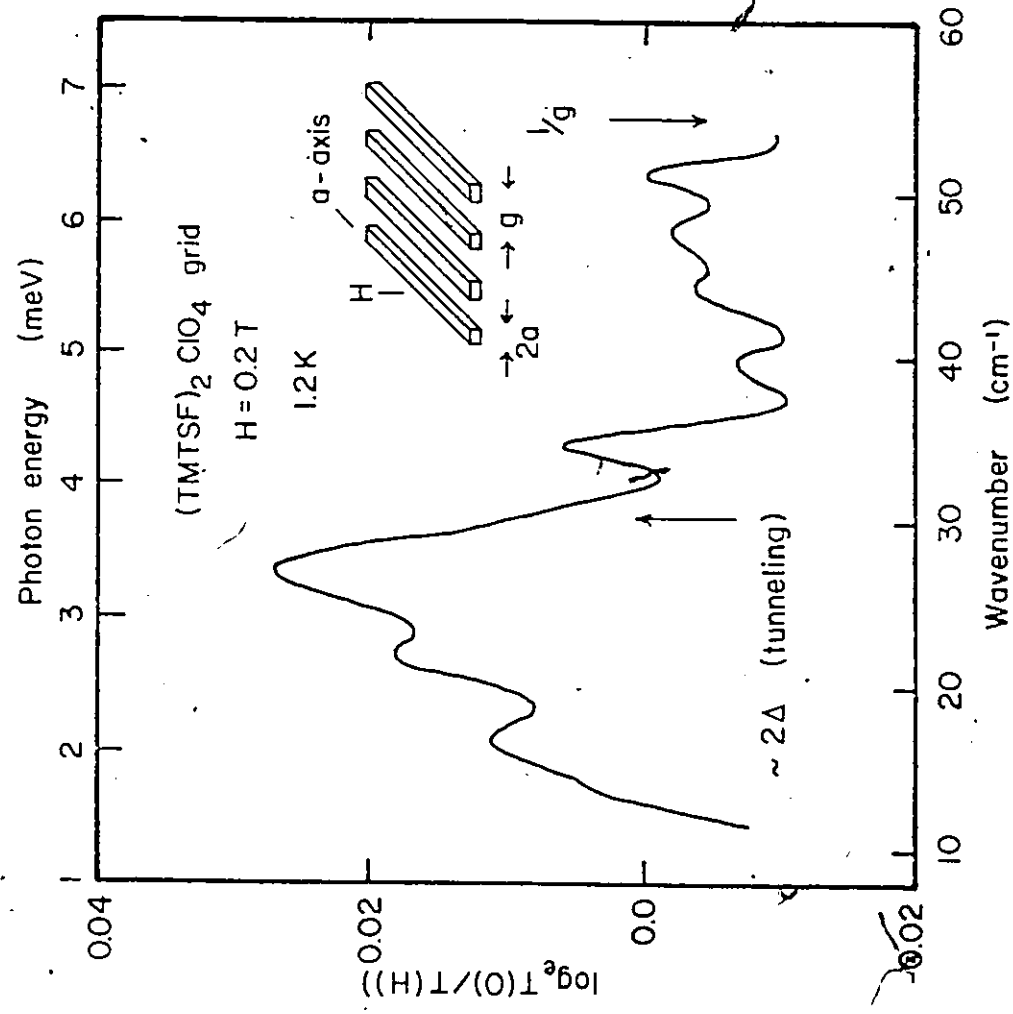
two physical causes. First, geometrical surface irregularities on the Pb and Nb wires increase the absorption. Second, a high surface impedance in the normal state can be related to impurities on the surface such as nitrogen, and oxygen in the case of Nb. Runs on etched wires give a much weaker signal, in accord with these ideas.

The method outlined above was applied to $(\text{TMTSF})_2\text{ClO}_4$. Fig. 2.4 shows the results obtained for one of the grids. Similar results were obtained for the other grids. The energy where there was an increase in magneto-absorption agreed with those obtained by tunneling results [36,37]. The increase in the absorption is $\sim 0.03 \pm 0.005$.

The spectra shown in Figs. 2.3 and 2.4 have several similar features. They all have the same sign in magneto-absorption, they are all of the same order of magnitude (0.01 - 0.03), and the energy where the absorption starts is in the same range (3 to 4 meV). Also the magnetic fields applied were all about 0.2 Tesla. However, there are two important differences. First, the ratio of the energy of the absorption onset to $k_B T_C$ in Pb & Nb is close to the BCS ratio i.e. 3.5 whereas in $(\text{TMTSF})_2\text{ClO}_4$ this ratio would be ~ 30 since $T_C \approx 1.3$ K [4]. This ratio would not be in agreement with specific heat measurements [18] below T_C where a ratio of 4 was obtained, a value more in line with strong coupling superconductors. Second, the temperature at which the anomaly was observed is so close to T_C that a conventional superconductor would give a very small amplitude. Therefore, the

Figure 2.4

Magneto-absorption of a grid of $(\text{TMTSF})_2 \text{ClO}_4$. The electromagnetic radiation is polarized along the a-axis of the crystals, and the static magnetic field is normal to this axis. There is a pronounced onset of magneto-absorption below 3.8 meV.



observed anomaly in $(\text{TMTSF})_2\text{ClO}_4$ cannot be ascribed to a conventional BCS superconductor.

The observed feature in $(\text{TMTSF})_2\text{ClO}_4$ cannot be due directly to phonons or librational modes. However, if phonons are coupled to a collective mode, e.g. CDW or SDW, then it can have field dependence via the collective mode. For example, it has been suggested that the magneto-absorption is due to phase phonons. Phase phonons [57,58] are the excitation of symmetric phonon modes via the condensed electrons in the CDW state. (A more complete description will be given in the next chapter.) However, group theory calculations by Challener [59] show that there are no symmetric modes in this frequency range. This does not rule out the possibility of some other mechanism which couples phonons with a collective mode.

When these experiments were done, the role the anions play was not understood. It was shown later [60] that the tetrahedral ClO_4 anion can be ordered if cooled slowly (~ 0.1 - 0.2 K/min) from ~ 30 K, and disordered otherwise i.e. when cooled rapidly > 70 K/min. These order/disorder states were called relaxed or R-states and quenched or Q-state respectively. In the R-state, superconductivity was observed; whereas, in the Q-state the instability was a SDW state with transition temperature $T_{\text{SDW}} \approx 3.5 - 6.5$ K. The transition temperature varies with the cooling rate. It is not clear under what conditions the magneto-absorption was observed. However, we will assume first that it was in the Q-state with $T_{\text{SDW}} = 5$ K. Following the argu-

ment of Ng et al. [61], the increase in magneto-absorption should be around 0.3 meV, an order of magnitude less than our observation. Moreover, careful reflectivity studies later in the Q-state (Chapter 3) revealed a gap in the conductivity in the 2.5 meV region, and did not show any observable field dependence up to 0.7 T. Thus, we can conclude that the magneto-absorption was not due to the presence of a SDW gap.

In the R-state, the dc conductivity did not show any decrease as the temperature was lowered below 10 K [62], but continued to increase to $> 10^5 (\Omega\text{-cm})^{-1}$ before it underwent a superconducting transition at 1.3 K. This is not like normal metals, where the conductivity would be limited by impurities in this temperature range. It was proposed [2,63] that this may be due to fluctuation superconductivity. In this model, within the Ginzburg-Landau theory [23], it was thought that the normal electrons form virtually-bound Cooper pairs, creating a pseudo-gap (see Section 1.1). Virtual Cooper pairs form gradually below $\hbar/\tau_a \sim t_b$. Initial analysis of the optical measurements by Jacobsen et al. [15] gave $t_b \sim 3.5$ meV. This could possibly explain our observation of the magneto-absorption as being due to the destruction of the virtual Cooper pairs by the magnetic field. However, a re-analysis of Jacobsen's results by Kwak [64] gave t_b an order of magnitude bigger. Thus our result is not consistent with the fluctuation superconductivity pseudo-gap.

It should be pointed out that a parallel study by

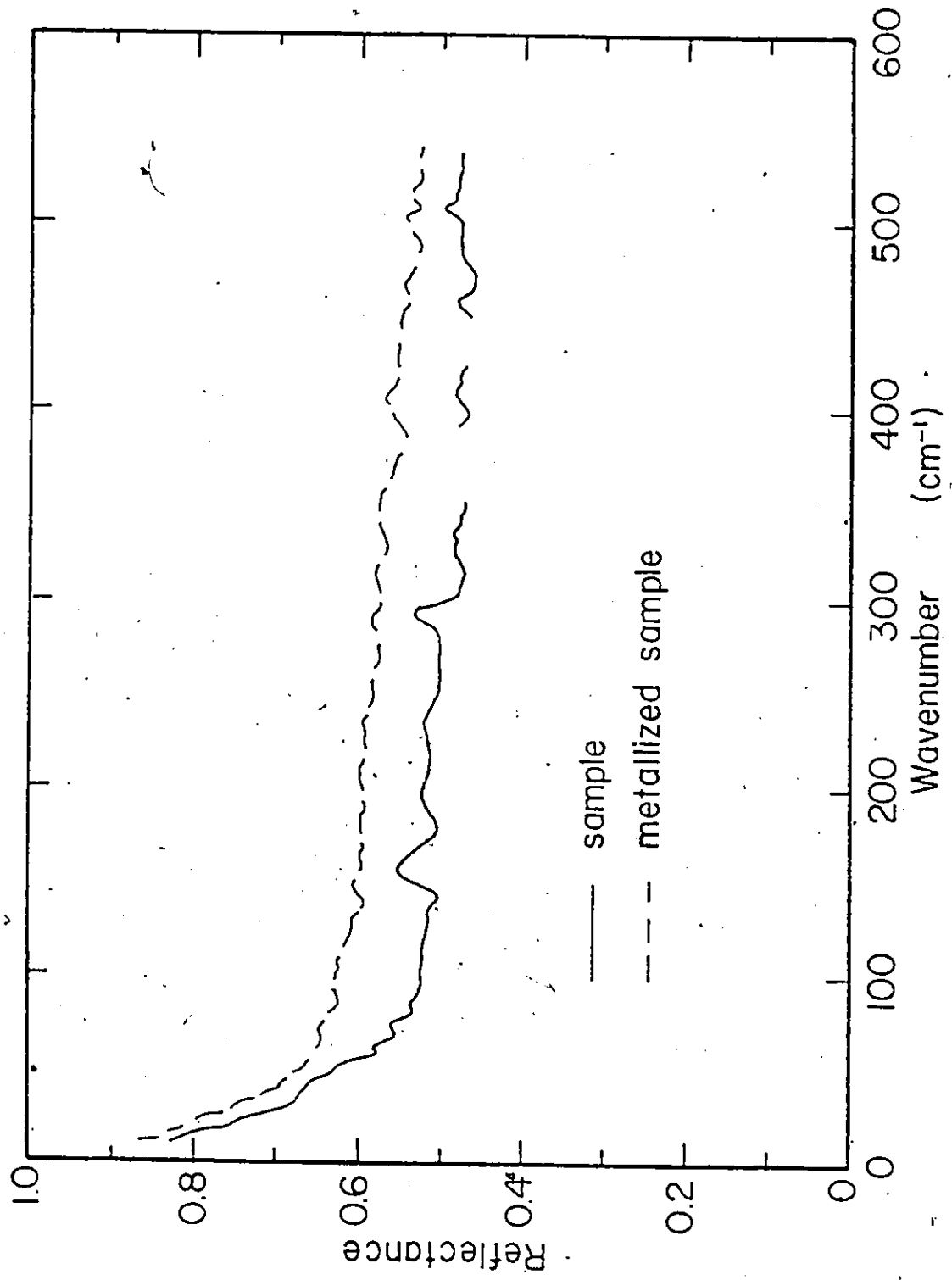
Challener [59] failed to observe any magnetic field dependence in this energy range. It should, however, be emphasized that there are several differences in the experimental conditions. First, instead of our grid arrangement, Challener used closely packed $(\text{TMTSF})_2\text{ClO}_4$ crystals. Second, the temperature below which our magneto-absorption was observed was lower (1.2 K) than Challener's (2.3 K). Third, the samples were from different sources. However, this (i.e., sample origin) is not expected to cause any significant difference since other measurements show similar results.

2.6 Reflectivity - Raw Data

In a typical reflectivity study of a compound, a spectrum of the sample was first taken using the Martin-Puplett type interferometer with a resolution of 2 cm^{-1} . This spectrum was not corrected for instrumental response. By taking the ratio with respect to a spectrum obtained from a gold coated brass plate one gets the reflectance for the sample. The reflectance is not the absolute reflectance since the mosaic arrangement scatters light. Fig. 2.5 (solid line) shows an example of such a spectrum. Normally four such spectra were taken for a single temperature, a given frequency range, and for a given E-polarization. After taking spectra over a range of temperatures, the dewar was moved over to the fast-scanning Michelson interferometer for studies in a higher frequency range ($50 - 500 \text{ cm}^{-1}$). In this part, the resolution was 4 cm^{-1} . The changeover to the Michelson interferometer was done without warming up the sample to room temperature, or if done on the following day, re-trans-

Figure 2.5

An example of the uncorrected reflectance from a mosaic of crystals and after evaporating with gold. The blank frequency region in the $350 - 450 \text{ cm}^{-1}$ is due to strong mylar absorption lines.

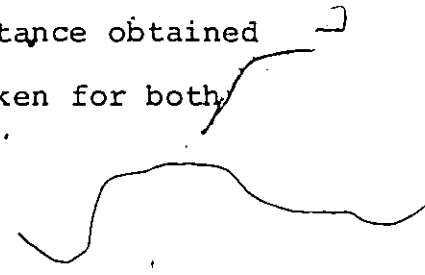


ferred with liquid He⁴. The sample temperature would usually be about 60 K the next day. The experiment was then repeated for the different frequency range using the same set of temperatures.

In magnetic field experiments, the sample was usually kept at 2 K. Then ratios of spectra were taken for the sample with field on and field off. This was preferable to the field on for sample and reference since any slight geometric diffraction effect cancelled out. Also, it is much easier to observe any small magnetic changes. Normally, the compound was checked for any magnetic field dependence in the same cryogenic run i.e. without bringing the sample to room temperature.

The present system (Fig. 2.2) does not allow us to change the E-field polarization without first warming up the sample to room temperature. The polarization was changed by rotating the polarizer by 90°. The system was then re-cooled, and the whole procedure repeated for the perpendicular direction.

After taking the spectra for the two polarizations, the sample was again warmed up to room temperature. Then gold was evaporated on the sample in a vacuum of 10^{-5} - 10^{-6} torr. The metallized sample was then placed back on the sample holder, and the system re-cooled. Spectra of metallized sample over gold on brass were taken, usually at 2 K. There was no observable difference in spectra taken at much higher temperatures. This ratio forms the unit reflectance for the reflectance obtained in the first part. The unit reflectance was taken for both



polarizations. Fig. 2.5 (dashed line) shows an example of the unit reflectance. To summarize, the absolute reflectance was obtained by first taking $R(\text{sample})/R(\text{gold})$. Then ratios of $R(\text{gold on sample})/R(\text{gold})$ were taken. The absolute reflectance was then the first ratio over the second.

The spectra were stored on floppy disk and later transferred to a LSI-11/23 (Digital Equipment Corp.) computer for analysis and plotting on hardcopy.

The spectra taken using the two interferometers overlap in the $\approx 50\text{-}120\text{ cm}^{-1}$ range. There is good agreement in the level of reflectance in this region, usually within one percent. In the analysis, an average of the overlap was taken rather than choosing the spectra from either of the interferometers. This procedure was followed for both the sample and the metallized sample. However, the level of the unit reflectance from the metallized sample was taken to be a smooth curve drawn across the (one percent) statistical noise. A smoothing procedure is commonly used when doing Kramers-Kronig transformations.

CHAPTER 3

REFLECTIVITY MEASUREMENTS AND ANALYSIS

3.1 Introduction

Detailed far-infrared reflectivity measurements were performed on three compounds: *bis*-tetramethyltetraselenafulvalene perchlorate (ClO_4), hexafluoroantimonate (SbF_6) and hexafluoroarsenate (AsF_6). For simplicity in discussion, these compounds shall be referred to by the symbols of their anions. The results presented in this chapter are for E polarized along the a-axis and perpendicular to the a-axis. The morphology of the crystals is such that it is not certain that all of the crystals had their b-axes aligned without making detailed x-ray analysis. Depending on the experimental conditions, the compounds can either be in the metallic or semiconducting (SDW) state. For the ClO_4 salt, the two states are achieved independently via the cooling rate (Section 2.5). The two centrosymmetric anion compounds, on the other hand, have a MI transition at $\approx 12\text{K}$ at ambient pressure. The results for the compounds in their different states will be shown in Section 3.3.

There are various complex response functions that can describe the interaction of electromagnetic waves with matter. These functions, namely, complex refractive index N , complex dielectric constant $\epsilon(\omega)$, and conductivity $\sigma(\omega)$ are all re-

lated. We chose to present our results as the real part of the conductivity since this is the quantity measured at $\omega = 0$, and also most of the theoretical calculations have been done for $\sigma(\omega)$. The conductivity was obtained from the absolute reflectance via Kramers-Kronig transformations.

3.2 Kramers-Kronig Transformation

The causality condition imposes a general relation between the real and imaginary parts of any linear response function. The path followed in calculating $\sigma(\omega)$ will be outlined briefly. It is commonly used in optical experiments and can be found in most textbooks on optics e.g. Wooten [65] and Moss [66].

The absolute reflectance can be expressed as a complex function

$$R = r(\omega) r^*(\omega) \quad (3.1)$$

or

$$r(\omega) = \sqrt{R} e^{i\theta}$$

where r is the complex reflectivity amplitude and R is the actual measured reflectance. The Kramers-Kronig relation governing the real and imaginary part of equation (3.1) (appendix G ref. 65) is

$$\theta(\omega_0) = \frac{\omega_0}{\pi} \int_0^{\infty} \frac{\ln[R/R_0]}{\omega_0^2 - \omega^2} d\omega \quad (3.2)$$

There is no singularity at $\omega = \omega_0$ in equation (3.2) as can be easily checked using L'Hospital's rule. Note that to calculate the phase shift at ω_0 , one needs the reflectance from $\omega = 0 \rightarrow \infty$. Such complete data do not exist. Various extrapolations are employed at high frequencies e.g. ω^{-s} , ω^{-4} [65,67]. The extrapolation procedure used has an adjustable parameter, s , so that the calculated optical constants agreed with the measured value at a single frequency e.g. the dielectric constant ϵ_0 . Extreme care must be taken in the extrapolation if one wants reliable optical constants at frequencies close to the highest measured frequency. However, if the highest frequency at which the optical constants are needed is an order of magnitude or more less than the measured cutoff (as is in our case), then the discrepancy arising from different extrapolations is not serious. We use the following extrapolations. Above the cutoff frequency (25000 cm^{-1}), the reflectance was taken as a constant equal to $R(25000)$. For Ela , the near infrared and visible reflectance data were taken from Jacobsen et al. [15,68] and Kikuchi et al. [69]. In this frequency range, the reflectance can be fitted using Drude's model. We find that by extending the reflectance down to the mid-infrared using the Drude parameters, there is a good match to our highest measured reflectance (at $\approx 500 \text{ cm}^{-1}$). The agreement varies for different compounds. For example, in ClO_4 the discrepancy

is about 3%; whereas, in AsF_6 it is only about 1%. In the low frequency end, $< 10 \text{ cm}^{-1}$, the reflectance is extrapolated smoothly to unity. (A more systematic extrapolation in the low frequency end is to use the Hagen-Rubens relation i.e. $R = 1 - \sqrt{2\omega/\pi\sigma}$ applicable when $\omega\tau \ll 1$. The σ is the measured dc conductivity. This method was not used here since it produces a serious mismatch with measured reflectance at the lowest frequency.) Similar extrapolations were used for $E_{\parallel a}$. However, in this direction measurements of the mid-infrared reflectance do exist. While these extrapolations may appear arbitrary to some extent, the effect of an incorrect choice in the Kramers-Kronig integral is, primarily, to alter the magnitude of the optical constants derived. Any difference in reflectance in the extrapolated regions does not affect the structure significantly.

Once the phase shifts $\theta(\omega)$ are obtained, the complex refractive index $N = n - ik$ can be calculated. The expressions for n and k in terms of R and θ are [66]

$$n = \frac{1-R}{1+R-2r\cos\theta} \quad (3.3)$$

$$k = \frac{2r\sin\theta}{1+R-2r\cos\theta}$$

By definition, $\epsilon(\omega) = N^2$. Our desired conductivity can then be calculated from

$$\epsilon(\omega) = 1 + \frac{4\pi}{\omega} i\sigma(\omega) \quad (3.4)$$

There are other Kramers-Kronig relations that relate the real and imaginary parts of $\epsilon(\omega)$, $\sigma(\omega)$ and N . They can all be derived from the basic causality condition. Ref. [65] chapter 6 gives a good detailed account.

Often in the analysis of optical measurements one uses a sum rule for the conductivity or oscillator strength of solids. This sum rule is related to the f-rule in atomic physics i.e. $\sum_i f_i = 1$, and is given by

$$\int_0^{\infty} \sigma_1(\omega) d\omega = \frac{\omega_p^2}{8} \quad (3.5)$$

where ω_p is the free electron plasma frequency and the subscript 1 refers to the real part of $\sigma(\omega)$. Physically, the integral is a measure of the energy absorption at all frequencies. We shall, however, make use of equation (3.5) to estimate the fraction of oscillator strength of the zero frequency mode.

3.3 Absolute Far-Infrared Reflectance of (TMTSF)₂ClO₄, SbF₆ and AsF₆

In this section, the reflectivity measurements are presented in two spectral ranges, from 10 to $\sim 400 \text{ cm}^{-1}$ and < 10 to $\sim 70 \text{ cm}^{-1}$. We will point out the similarities in the metallic state and in the high frequency range $> 50 \text{ cm}^{-1}$.

The differences in the SDW state at low frequencies will be emphasized.

Figures 3.1, 3.2 and 3.3 show the absolute reflectance for $E||a$ and $E\perp a$ for ClO_4 , SbF_6 and AsF_6 salts, respectively. The error bars shown are the estimated uncertainty for $\omega > 350 \text{ cm}^{-1}$. This is due to low signals above 350 cm^{-1} since the mylar beamsplitter used has strong absorption lines in this frequency region. All three compounds in the metallic state, and for $E||a$, show kinship similarity in the high frequency range. The reflectance is in the 90% level and stays fairly constant. There is a slight rise in reflectance of about 2-3% at 173 cm^{-1} and $\approx 250 \text{ cm}^{-1}$. Line D in Fig. 3.2 is identified as an SbF_6 internal phonon line and is present in both polarizations. Anion lines for the other two compounds were not observed since the expected ClO_4 line was at a much higher frequency than our measurements, and the AsF_6 has a line at around 380 cm^{-1} , a region where we have low signals. It should be pointed out that the ClO_4 line has been seen at $\approx 630 \text{ cm}^{-1}$ by another experimental group [15].

In the $E\perp a$ direction at high frequencies the three compounds display some differences. The reflectance of the ClO_4 and SbF_6 salts decreases by about 20% over the spectral range presented. The overall reflectance for the AsF_6 salt, on the other hand, remains fairly constant with structures at

Figure 3.1

Absolute reflectance of $(\text{TMTSF})_2\text{ClO}_4$ at 2 K for $E||a$ and $E \perp a$. The polarizer used to study this compound loses its efficiency above 180 cm^{-1} . Thus, the results above this frequency are based on unpolarized data. The dotted line shows the reflectance obtained using the Drude parameters from ref. 69.

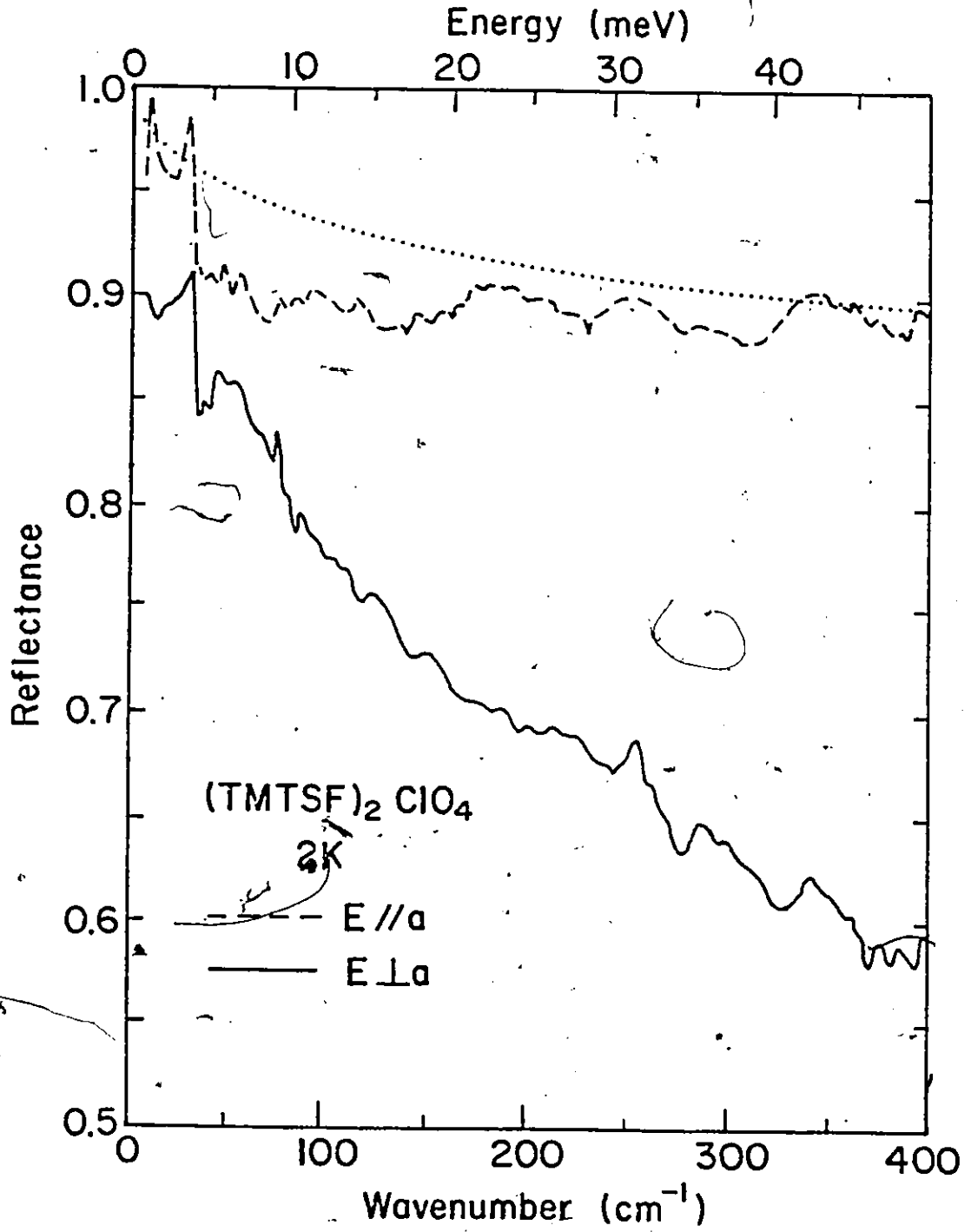


Figure 3.2

Polarized reflectance data of $(\text{TMTSF})_2\text{SbF}_6$ for the $E||a$ and $E \perp a$ directions. The polarizer used in this case, and henceforth, is effective up to 700 cm^{-1} . In going from 19 K to 2 K, three lines A, B and C appeared for $E||a$. Line D is identified as an internal SbF_6 phonon. In the $E \perp a$ direction, there is little observable change with temperature up to 30 K. Inset shows detailed reflectance below 45 cm^{-1} .

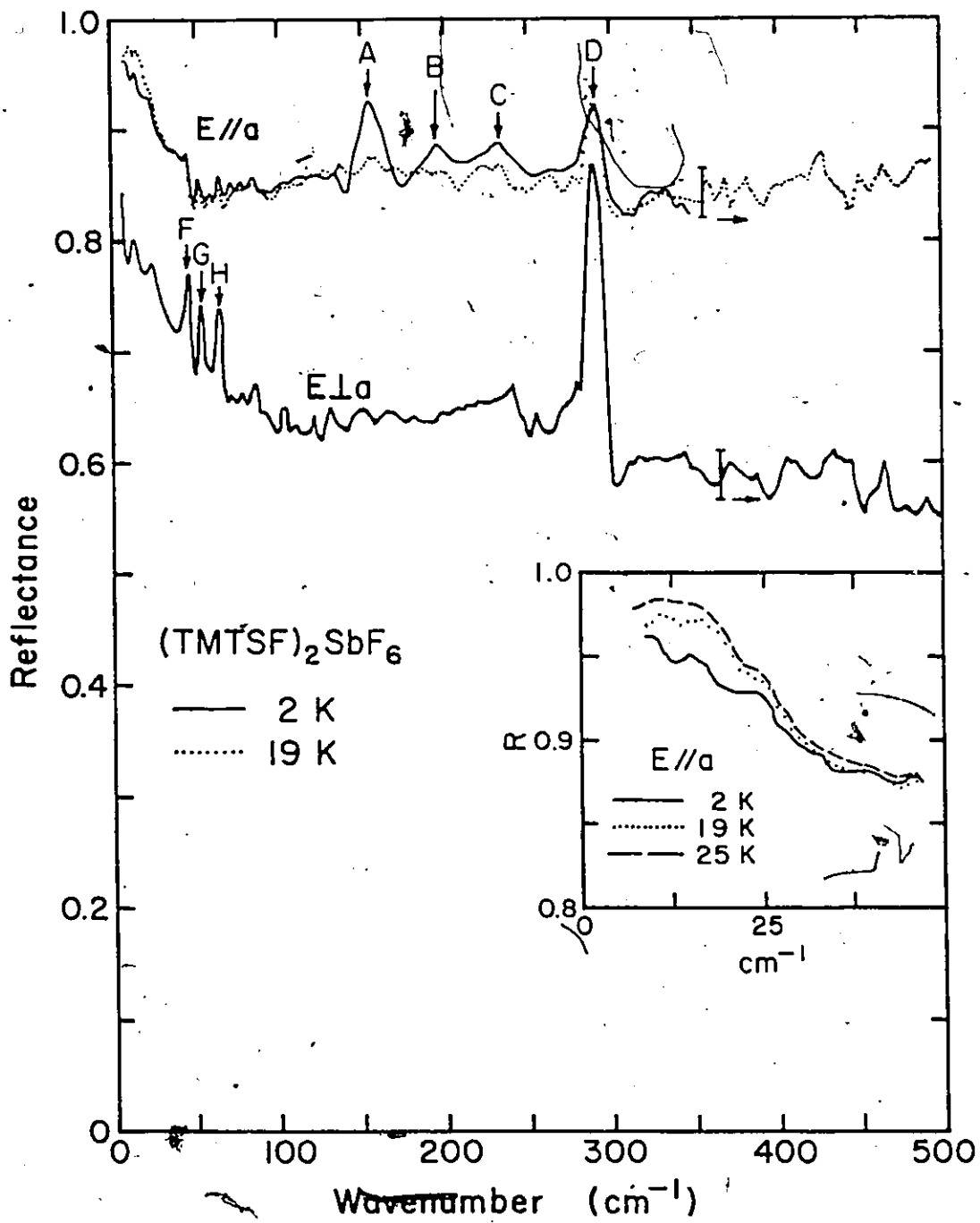
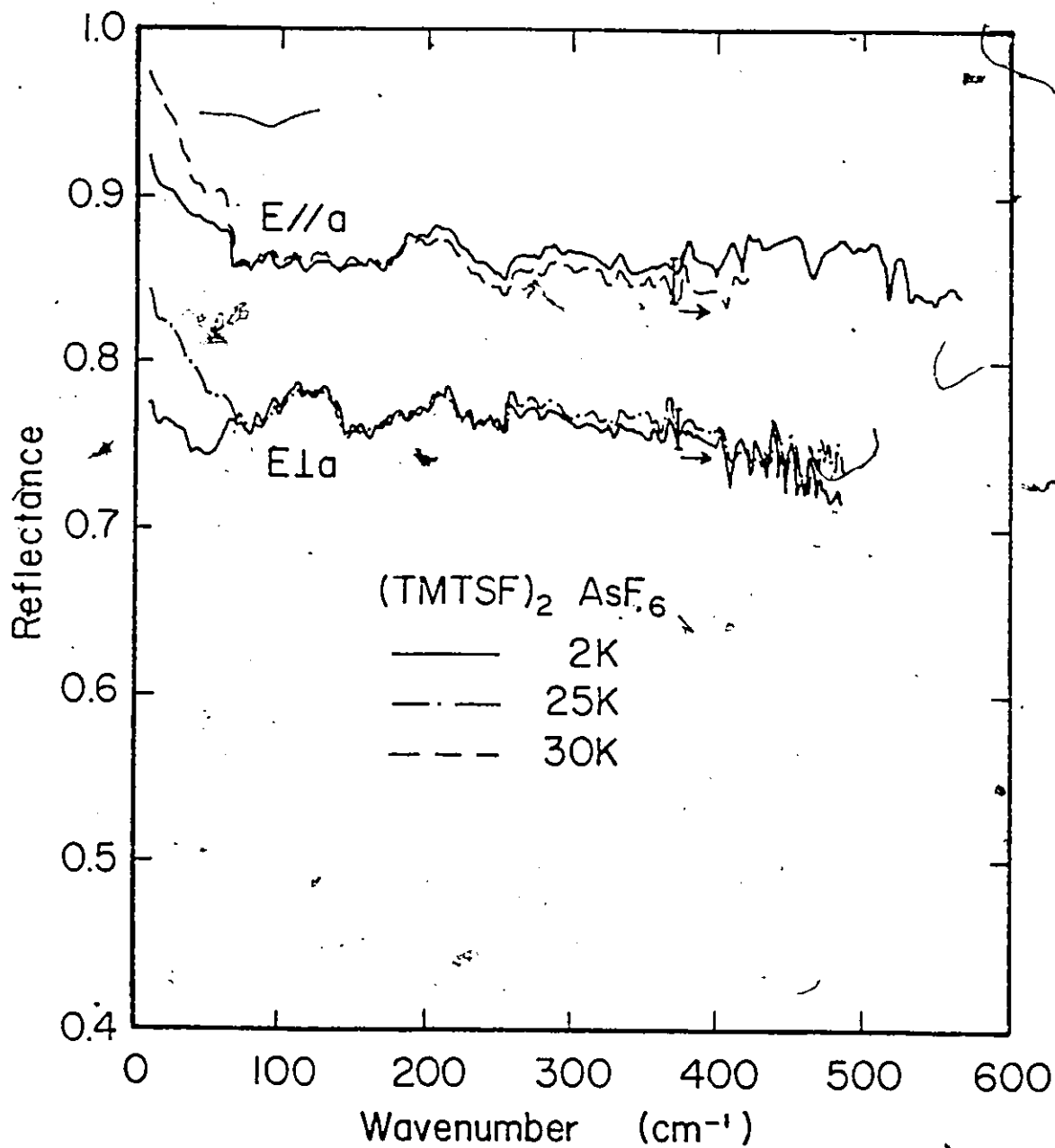


Figure 3.3

Reflectance measurements for $(\text{TMTSF})_2\text{AsF}_6$ in the $E \parallel a$ and $E \perp a$ directions. Note the change in reflectance for both polarizations below $\approx 65 \text{ cm}^{-1}$ as a function of temperature. The error bars indicate the level of uncertainty above 350 cm^{-1} .



120 cm^{-1} and 210 cm^{-1} . There are three relatively strong lines F, G and H in the SbF_6 salt. These lines are very weak in the $E||a$ direction and did not show any change with temperature up to 30K.

The reflectances presented so far do not follow that of a simple metal. We have shown for comparison in Fig. 3.1 (dotted line) the reflectance using the Drude parameters from ref. 69. It would appear that at high frequencies the compounds behave like a simple metal, whereas at low frequencies there is a marked difference.

For the SbF_6 compound, there was a pronounced change in reflectance as the temperature was lowered to 2K, i.e. in the SDW state (Fig. 3.2). Three lines A, B and C appeared. These lines have been studied in detail as a function of temperature. We will present these results as $\sigma_1(\omega)$ in the next section. It should be noted that the lines were only observed in the $E||a$ direction. We were not able to see any appearance of lines in the AsF_6 salt (Fig. 3.3). However, in this material the reflectance increased by about 2-3% at higher frequencies when the temperature was decreased from 30K to 2K. This is probably due to the optical relaxation time becoming longer.

At low frequencies, the three salts display diverse results. We will present these results for each compound separately.

Figs. 3.4 and 3.5 show the temperature dependence in the R-state of the ClO_4 salt for $E||a$ and $E\perp a$ respectively. In the parallel direction there are two peaks at 8 cm^{-1} and 29 cm^{-1} . The lower frequency peak decreases gradually with increasing temperature. However, the 29 cm^{-1} peak displays a two-step change. Going from 2K to 20K, the reflectance drops by about 2%. At 24K, there is an abrupt shift to lower frequency by 2 cm^{-1} . This shift can also be monitored by scanning the reflectance of the sample as a function of temperature with the interferometer set at the zero path position*. The inset in Fig. 3.4 shows a sudden change in reflectance as the temperature was increased above 24K. The 24K change has been associated with an anion order/disorder temperature [8]. There is a similar change for $E\perp a$ (Fig. 3.5). Due to the geometry of the sample arrangement, we were not able to go below 10 cm^{-1} . Thus, it is not clear whether there is a lower frequency peak in this direction. The overall reflectance decreases with increasing temperature.

In the inset of Fig. 3.2 we have plotted the reflectance of the SbF_6 salt below 45 cm^{-1} for $E||a$ at three temperatures. As the temperature was decreased there was a

* A $150\text{ }\mu\text{m}$ soot-coated glass slide filter was used to cut off radiation above $\approx 40\text{ cm}^{-1}$.

Figure 3.4

A detailed reflectance measurement for $E||a$ in the R-state for $(\text{TMTSF})_2\text{ClO}_4$ at low frequencies as a function of temperature. Inset illustrates the change in reflectance as the sample was heated above 24 K.

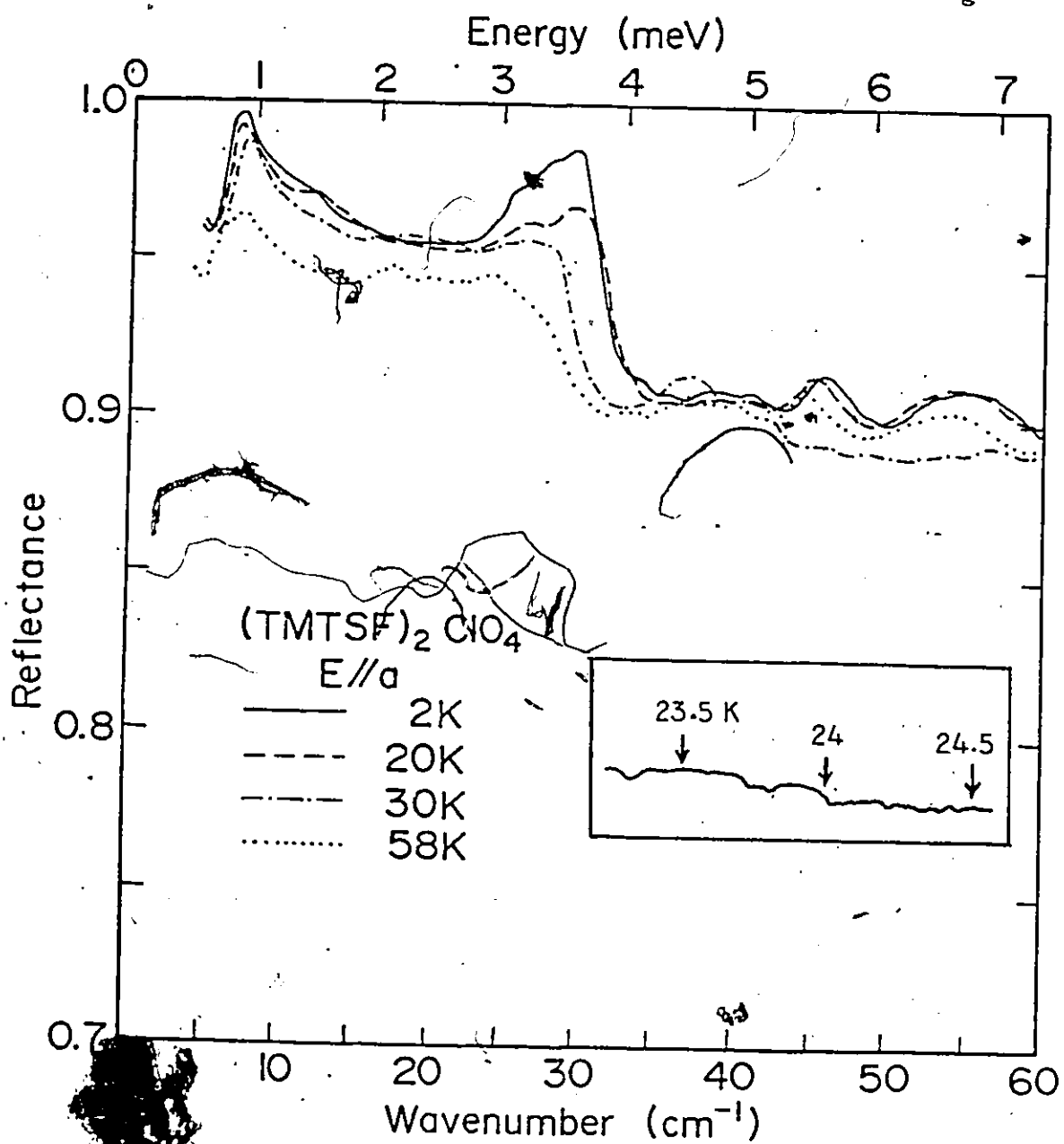
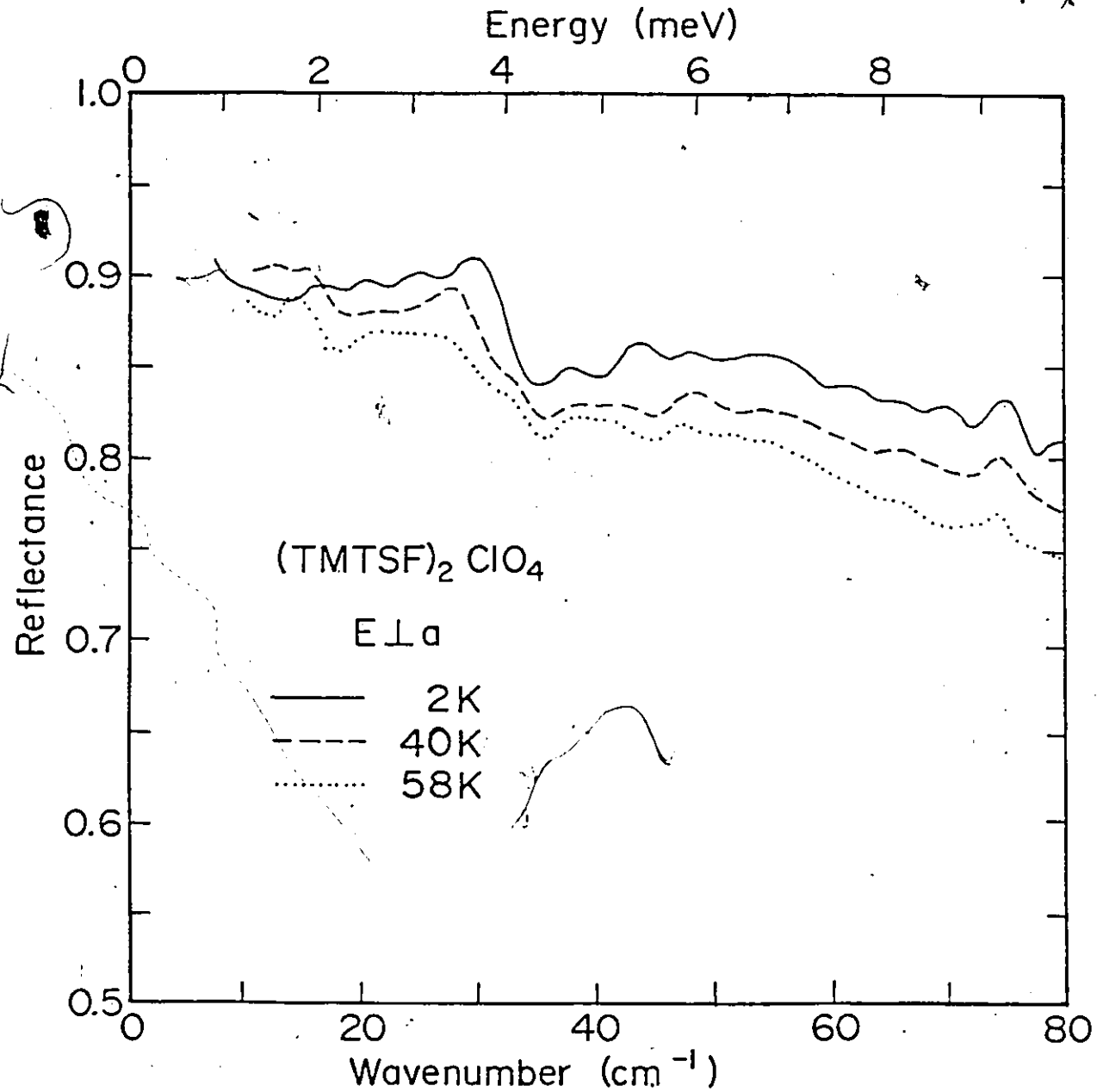


Figure 3.5

A corresponding measurement for $(\text{TMTSF})_2\text{ClO}_4$ in the perpendicular to a-axis polarization. The decrease in overall reflectance as the temperature increases is more evident than for $E||a$.



gradual decrease in reflectance below $\approx 40 \text{ cm}^{-1}$. This change in reflectance occurs above the MI transition temperature ($\approx 12 - 14\text{K}$). We were not able to observe any corresponding change in the $E_{\perp a}$ direction.

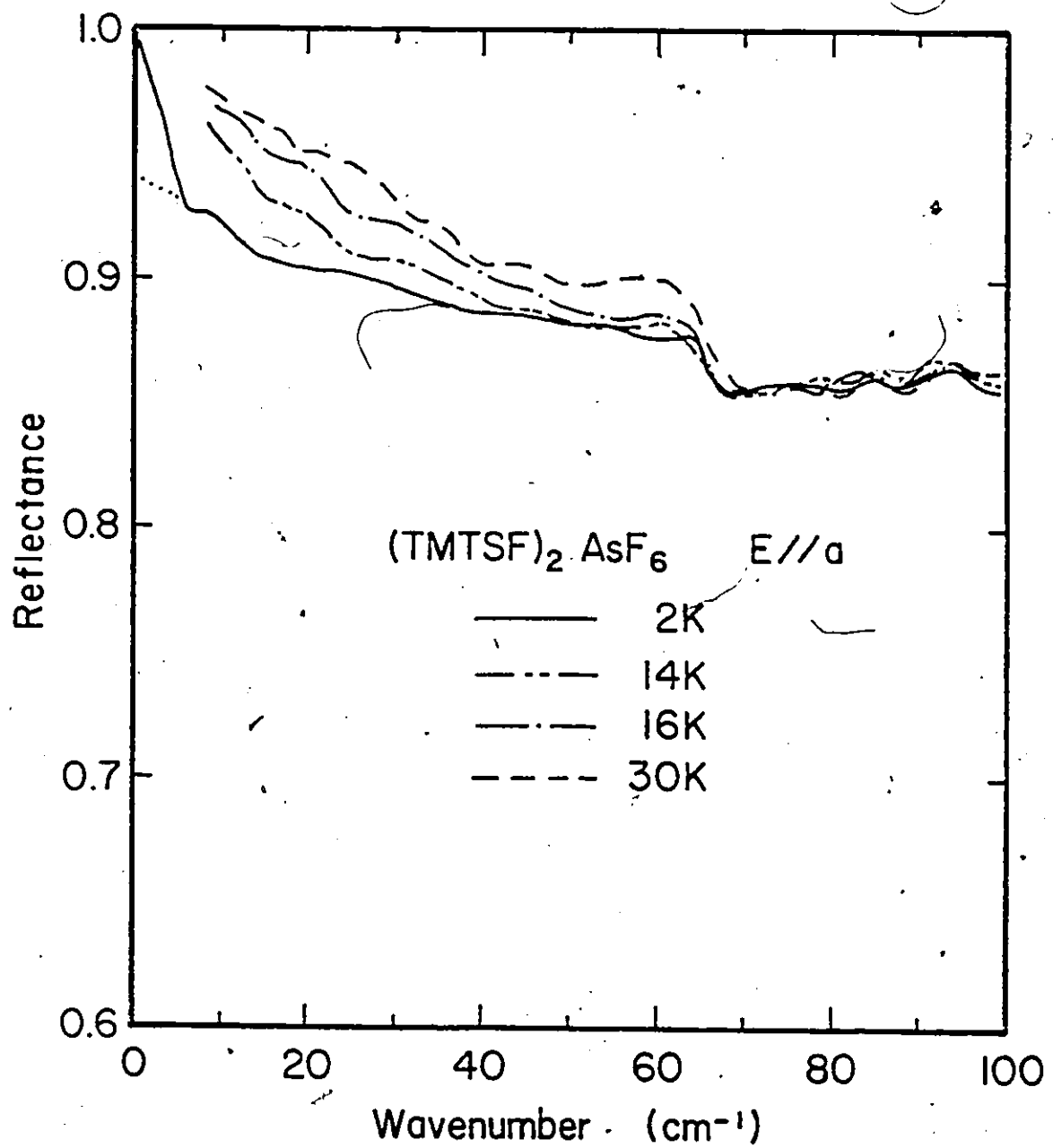
We have already shown in Fig. 3.3 the reflectance for two temperatures in the low frequency end for the AsF_6 salt for both polarizations. The details as a function of temperature for $E_{\parallel a}$ are illustrated in Fig. 3.6. The change in reflectance with respect to temperature is similar to the SbF_6 salt except that the variation is more abrupt and starts from higher frequencies. However, in the AsF_6 salt, there are also changes in the $E_{\perp a}$; whereas, none were observed in the SbF_6 salt. At the lowest temperature measured, 2K, the reflectance at $\approx 7 \text{ cm}^{-1}$ is about 93%. Two choices of extrapolation to $\omega = 0$ were employed, one to unity (continuous solid line), the other to about 94% (dotted line).

3.4 Discussion

The results presented in the last section show clearly that there are similarities and diverse behaviours in the three compounds. The similarities were in the metallic state and at high frequencies while the differences were in the SDW state and at low frequencies. Kramers-Kronig transformations were done for all the reflectivity data. This section will be divided into three sub-sections. First, we will discuss the common features observed and suggest pos-

Figure 3.6

Reflectance measurements for the $(\text{TMTSF})_2\text{AsF}_6$ compound for $E||a$ as a function of temperature. There is a decrease in reflectance below $\approx 62 \text{ cm}^{-1}$ as the sample changes to a SDW state. The dotted line and the continuous line to unity at $\omega=0$ represent two choices in the extrapolation.



sible explanations. Next, we will present the unique features seen in the individual compounds. The effect of a magnetic field will also be discussed. The changes due to thermal cycling will be shown in the last sub-section. The interpretations will be based on $\sigma_1(\omega)$.

a. Common Features

The frequency dependent conductivity of ClO_4 , SbF_6 and AsF_6 salts are shown in Figs. 3.7, 3.8 and 3.9 respectively for the frequency range indicated. There are two obvious features in the $E \parallel a$ direction. First, the high dc conductivity in the a direction is not reproduced in the metallic state. From our measurements to less than 10 cm^{-1} , we did not observe a rise in conductivity as $\omega \rightarrow 0$ (Fig. 3.7) to account for the dc value. (The SbF_6 and AsF_6 salts do show some increase in $\sigma_1(\omega)$ as $\omega \rightarrow 0$.) This suggests that there is a zero frequency mode with a very narrow linewidth. We will discuss this mode more fully later. The second common feature is the increasing conductivity as a function of frequency before it levels off at about 200 cm^{-1} . There are broad peaks in $\sigma_1(\omega)$ of which the most pronounced is found in the AsF_6 salt (Fig. 3.9).

The increase and levelling off in $\sigma_1(\omega)$ can be most simply interpreted as being due to the Holstein process [70, 71]. There are two types of Holstein mechanisms; one is a surface absorption, and the second is a volume absorption.

Figure 3.7

The frequency dependent conductivity $\sigma_1(\omega)$ of the $(\text{TMTSF})_2\text{ClO}_4$ compound. This result corresponds to the Kramers-Kronig transforms of Fig. 3.1. Note the increase in $\sigma_1(\omega)$ as ω increases for $E||a$. The rise in $\sigma_1(\omega)$ at about 167 cm^{-1} is identified as being due to the $a_g v_{12}$ TMTSF mode. The dotted curve is the Holstein conductivity using equation 3.6 and Fig. 3.10. The dashed line is the Drude conductivity with half-width of 3.5 cm^{-1} (see text).

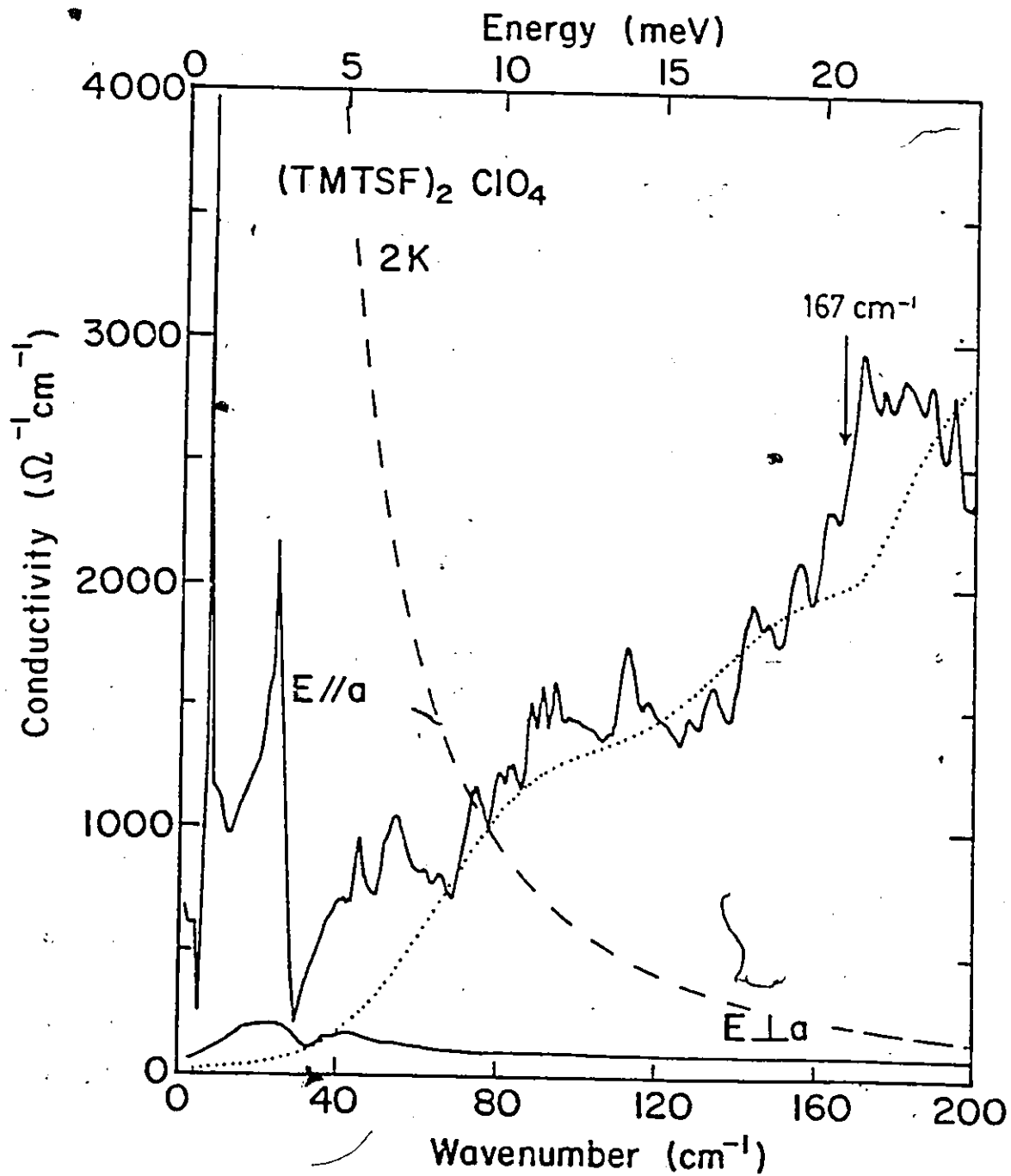


Figure 3.8

Conductivity for $(\text{TMTSF})_2\text{SbF}_6$ crystal in the $E \parallel a$ direction at 2 K and 19 K. The sharp lines at 2 K are identified as phase phonons. (Dashed line is the Holstein fit similar to the previous figure.) The inset illustrates the presence of a zero frequency mode at 25 K that appears to become pinned by a spectrum of low lying pinning states at low temperatures.

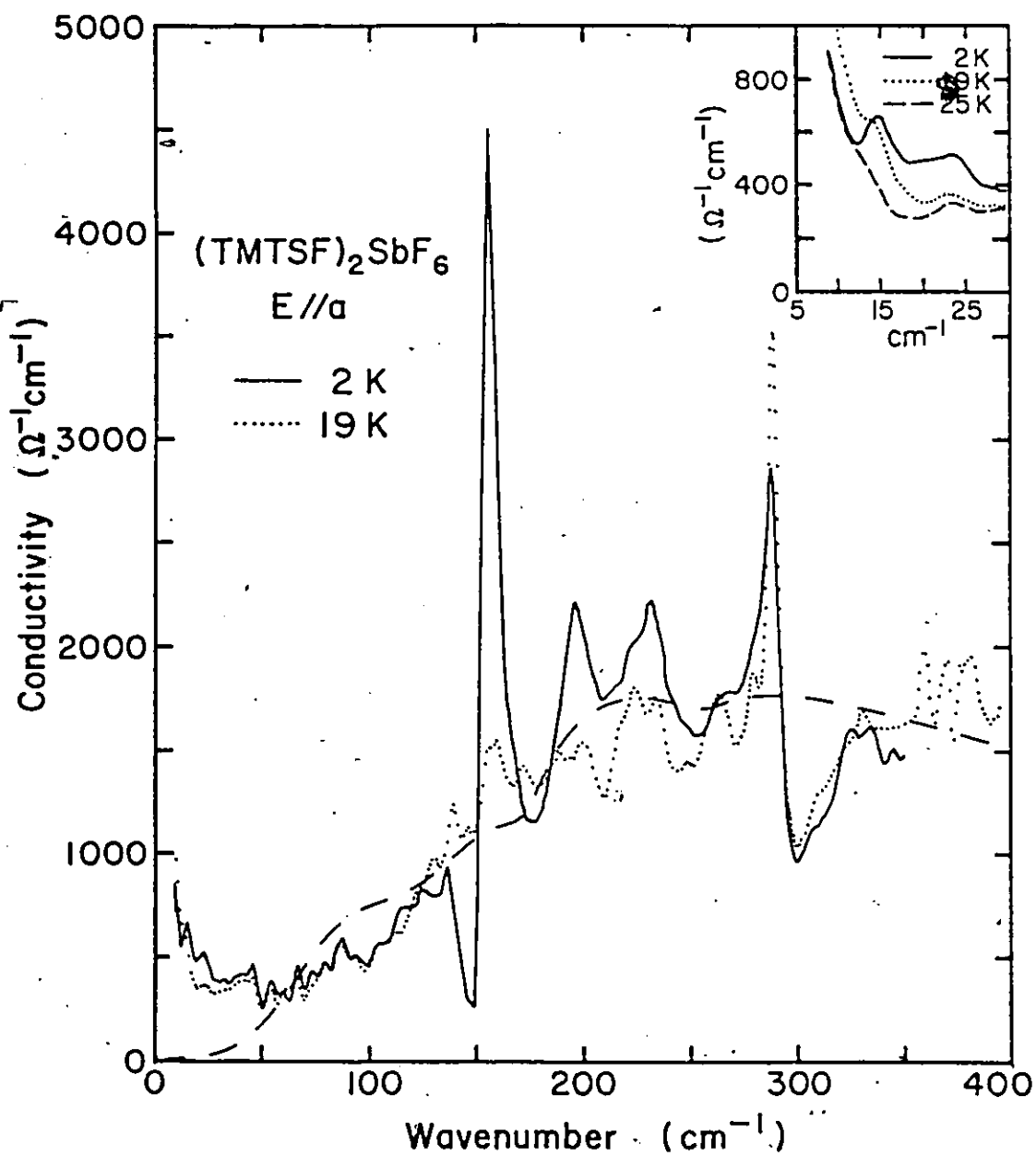
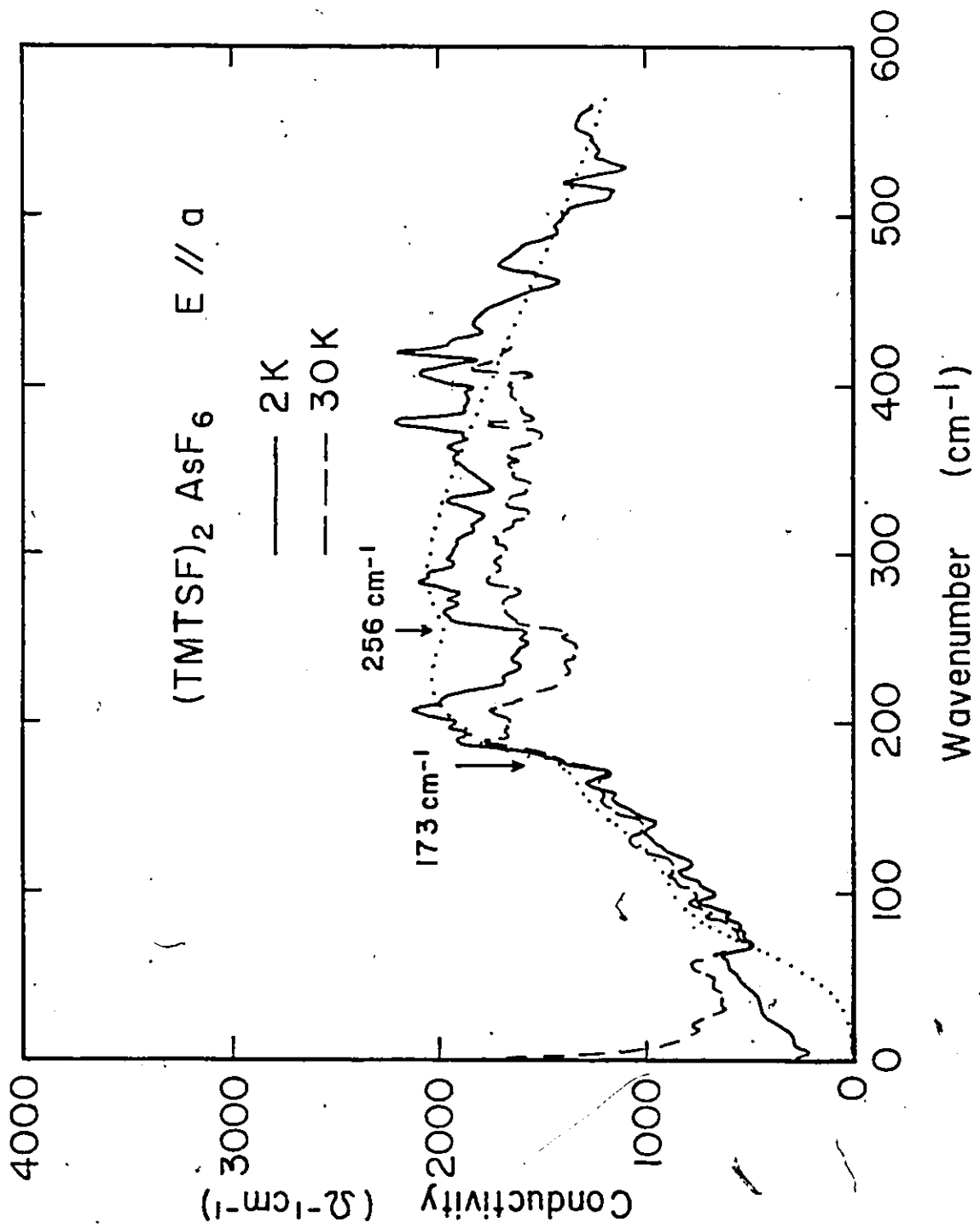


Figure 3.9

Overall conductivity for $(\text{TMTSF})_2\text{AsF}_6$ in the $E \parallel a$ direction at 2 K and 30 K. The dotted line is a fitted Holstein conductivity using equation 3.6 and the α^2_F shown in Fig. 3.10 for 2 K. The α^2_F was adjusted to fit this compound (see text). The arrows show the positions of the $a_g \nu_{11}$ (256 cm^{-1}) and $a_g \nu_{12}$ (173 cm^{-1}) TMTSF modes.



For the former to be dominant the electronic mean free path must be greater than the penetration depth. Here, the collision is with the surface which takes up the change in momentum. For $E \parallel a$, Holstein surface absorption is not expected to be important in our case. The conductivity σ_a is small and the Fermi velocity normal to the surface is also small. Thus, there cannot be an anomalous skin effect in these materials. However, Holstein volume absorption can take place since a mean free path less than the skin depth implies that the momentum balance can be taken up by collisions. By this (volume) process, a photon is absorbed with the simultaneous creation of an electron-hole pair and a phonon. The threshold energy is the phonon energy. It is clear then that as more phonons become available, the conductivity will increase. Another way of putting it is that the electron-hole pairs created cannot interact with all the phonons unless the incident photon energy is greater than or equal to the highest phonon energy. We thus expect the collision time τ_p to be frequency dependent. We will attempt to fit our observed conductivity following the procedure described by P.B. Allen [72].

In Allen's formalism in the local approximation, the electron-phonon (e-p) interaction was accounted for by using the second order golden rule. The summation in the second order golden rule is over all of the allowed intermediate

states. The final states of an electron-hole pair have a non-zero momentum, the balance in momentum being taken up by phonon creation or elastic collisions with impurities. In our fit, we shall ignore scattering by impurities. The conductivity due to e-p interactions is given by

$$\sigma_1(\omega) = \frac{\omega_p^2}{4\pi\omega} \left(\frac{1}{\omega\tau_p} \right) \quad (3.6)$$

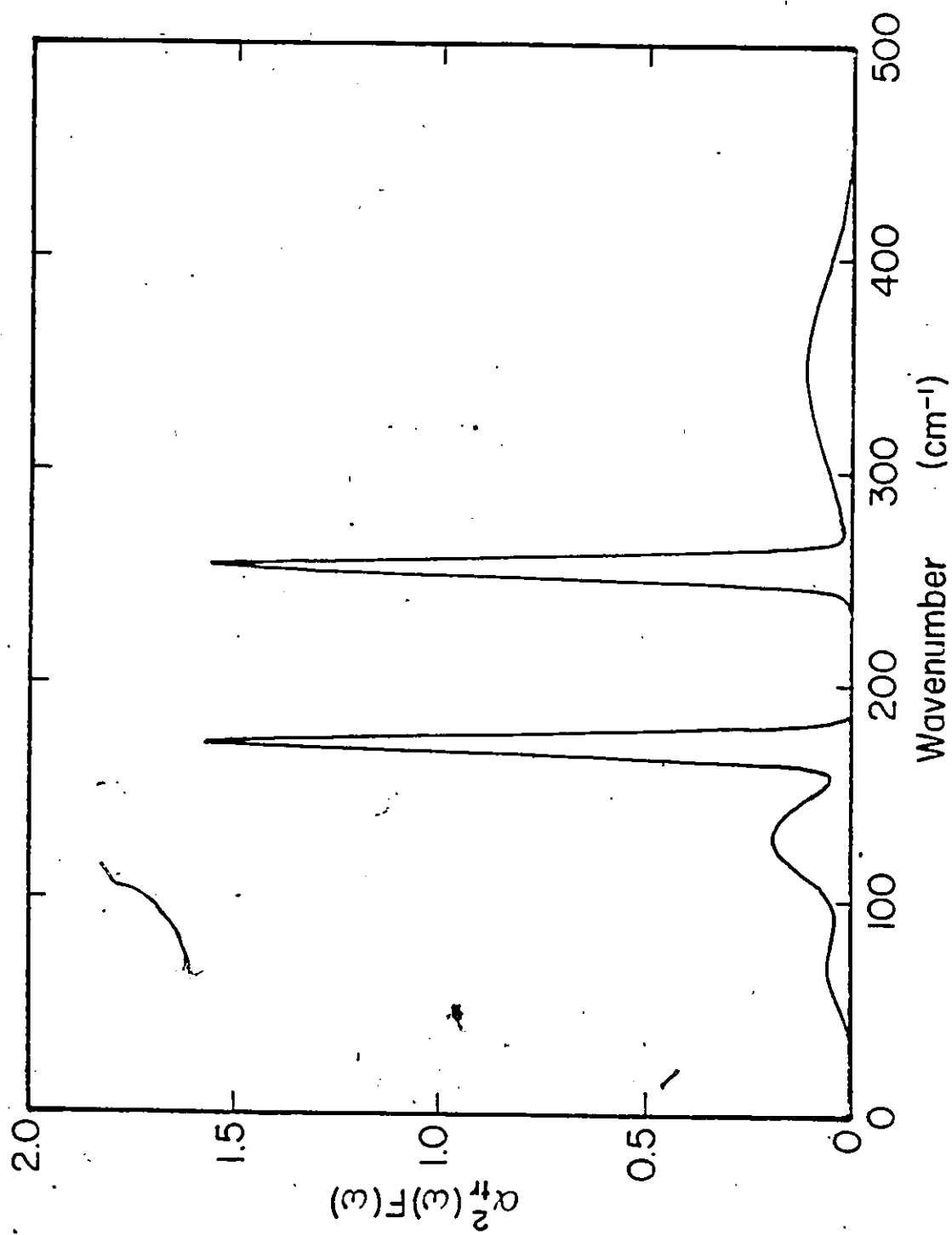
where,

$$\frac{1}{\tau_p} = \frac{2\pi}{\omega_0} \int_0^{\omega_0} d\omega (\omega_0 - \omega) \alpha_{tr}^2(\omega) F(\omega) \quad (3.7)$$

The function $\alpha_{tr}^2(\omega)F(\omega)$ is the phonon density of states weighted by the square of the e-p coupling for transport. For brevity, $\alpha_{tr}^2(\omega)F(\omega)$ shall simply be referred to as α^2F henceforth. In our calculations, we shall model α^2F by gaussian peaks. Three broad peaks centred at 70, 130 and 350 cm^{-1} with full width at half-maximum (FWHM) of 40, 40 and 100 cm^{-1} respectively were taken (Fig. 3.10). These peaks were chosen to represent the librational, bending and stretching modes that must be present in these materials [73]. The sharp peaks at 173 and 256 cm^{-1} were used to simulate the internal TMTSF phonon modes [74,75]. These peaks were assigned a FWHM of 10 cm^{-1} . The assumed α^2F was first used to fit $\sigma_1(\omega)$ of the AsF_6 salts at 2K since the $\sigma_1(\omega)$ data is over the widest frequency range. The heights of the peaks were adjusted to give the correct sum rule

Figure 3.10

Assumed form of $\alpha_{\text{tr}}^2(\omega)F(\omega)$ used to fit $\sigma_1(\omega)$ of $(\text{TMTSF})_2\text{AsF}_6$. The three broad peaks were chosen to represent librational, bending and stretching modes that must be present in these materials. The sharp lines were to simulate the internal TMTSF phonon modes. Apart from a constant scale factor, the assumed $\alpha^2 F$ can also be used to fit the other two compounds.



(equation (3.5)). Fig. 3.9 (dotted line) shows that the overall fit to the AsF_6 salt is very satisfactory. This good fit supports our interpretation that the observed conductivity profile is due to the Holstein volume mechanism. We were able to fit the $\sigma_1(\omega)$ for the other two salts using the same α^2_F except for the absolute magnitude. The factors required to give the correct magnitude in α^2_F for ClO_4 and SbF_6 salts can be derived by taking ratios of λ listed in Table I. The results of the fit can be seen in Figs. 3.7 and 3.8.

One can estimate the total strength of the e-p coupling for transport via

$$\lambda_{\text{tr}} = 2 \int \frac{d\omega}{\omega} \alpha^2_F \quad (3.8)$$

Table I lists the values of λ_{tr} for the three compounds, and also some of the other superconducting elements. The values of λ_{tr} are very reasonable and give additional support to the Holstein process. The values depend on the accuracy of the fit and on the shape of the assumed α^2_F . We estimate the uncertainty to be ± 0.05 .

An alternative way of estimating the strength of the e-p coupling without any direct reference to α^2_F is to use

$$\lambda_{\text{tr}} = \frac{1}{\pi \langle \omega \rangle \tau_{p,l}} \quad (3.9)$$

Table 1

Material	λ_{tr}	ω_p^* (cm^{-1})
$(\text{TMTSF})_2\text{AsF}_6$	0.6	10470
$(\text{TMTSF})_2\text{SbF}_6$	0.55	10200
$(\text{TMTSF})_2\text{ClO}_4$	0.95	10170
Pb	1.55	7.5 eV
Al	0.46	14.7 eV
In	0.834	

*The plasma frequencies for the three compounds were from refs. 68 and 69 and the λ_{tr} for the three elements were from ref. 76.

where $\tau_{p,l}$ is a constant, phonon limited scattering time, and is given by $1/\tau_{p,l} = \omega_p^2 / [(1+\lambda_{tr})4\pi\sigma]$. Here σ is the maximum or saturation Holstein conductivity. The symbol $\langle\omega\rangle$ denotes the average phonon frequency and can be taken to be equal to the Debye frequency ω_D . From specific heat measurements of $(TMTSF)_2ClO_4$, ω_D is found to be 148 cm^{-1} [18]. The calculated λ_{tr} using equation (3.9) is in agreement with that listed in Table 1. Debye frequencies for the other two compounds are not known. However, if we use the value for the ClO_4 salt, there is a disagreement in λ_{tr} by a factor of two. This discrepancy is also a measure of the uncertainty in using $\langle\omega\rangle$ from the ClO_4 salt. The Holstein conductivity contributes more than 95% of the oscillator strength. (Above the measured conductivity a Drude model was assumed.)

It should be emphasized that the Holstein conductivity derived by Allen is for a 3-dimensional conductor. This implies that the scattering of electrons by phonons is isotropic. In our system, a quasi-1-dimensional (or 2-dimensional) model would be more applicable where the anisotropy in the scattering should be taken into account. The Holstein volume generation of phonons has been suggested by Gor'kov and Kasha [77] as a model for linear organic materials in the metallic state. A similar process, where an electron first absorbs a photon with the creation of optic

and acoustic phonons, can produce sharp peaks in the conductivity [77]. This process may be required to explain the finer details (broad peaks) in $\sigma_1(\omega)$ of the AsF_6 compound (Fig. 3.9).

To extend the interpretation of Holstein emission of phonons to $\sigma_1(\omega)$ of the $(\text{TMTSF})_2 \text{PF}_6$ salt as measured by Jacobsen et al. [15] would be difficult. What would be required is a single strong peak at $\approx 200 \text{ cm}^{-1}$ in $\alpha^2 F$, and for this peak to dominate the e-p interaction. Preliminary reflectivity measurements by D. Bonn [78] on the PF_6 compound show a much weaker peak, and overall $\sigma_1(\omega)$ that would be in agreement with the results obtained in the present study.

We now turn our attention to the zero frequency mode. In Fig. 3.7 we saw no evidence of any rise in $\sigma_1(\omega)$ as $\omega \rightarrow 0$. If the observed dc conductivity follows Drude's model, then $\tau_{\text{sp}} = 1.5 \times 10^{-12} \text{ sec}$ ($\Gamma_{\text{sp}} = 3.5 \text{ cm}^{-1}$) for a typical $\sigma_{\text{dc}} = 500000 (\Omega\text{-cm})^{-1}$ (see Appendix for unit conversion) [4]. What this would imply is that ω^{-2} dependence in $\sigma_1(\omega)$ would fall in the $10 \text{--} 100 \text{ cm}^{-1}$ region (Fig. 3.7 dashed line). A purely Drude mechanism of conductivity would certainly be observable. The fact that we do not see any ω^{-2} dependence suggests some other mechanism, possibly a collective mode [79]. For both the SbF_6 and AsF_6 salts, there is a slight rise in $\sigma_1(\omega)$ as $\omega \rightarrow 0$ in the metallic state. This is taken as evi-

dence of a zero frequency mode. That it should become visible in the $10 - 15 \text{ cm}^{-1}$ range (see inset Fig. 3.8 for 25K) may be due to the fact that these two compounds, especially the AsF_6 salt, are less pure [80]. However, we were not able to obtain the correct dc value by extrapolating the reflectance to unity at $\omega = 0$.

The zero frequency mode of the SbF_6 material broadens as the temperature is lowered, inset Fig. 3.8. This is probably due to pinning by a spectrum of low lying pinning states [30,31].

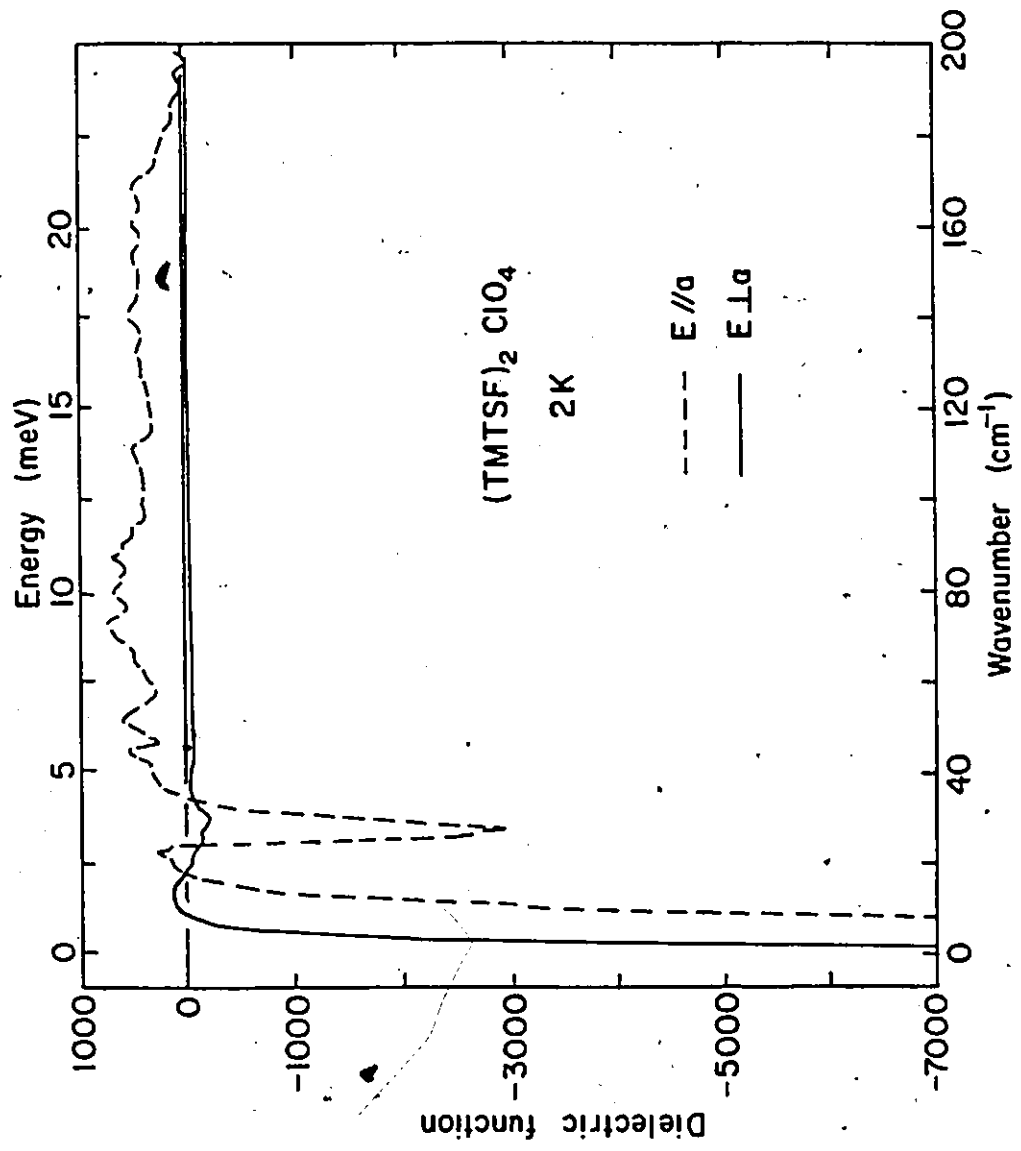
The Drude model clearly gives a half-width that is too wide to fit into our observations. An estimate of the zero frequency mode lifetime τ_c for the ClO_4 salt at 2K can be made from the measured dc conductivity [1,88] and the zero frequency mode oscillator strength Ω_p^2 , since $\sigma_{dc} = \frac{1}{4\pi} \Omega_p^2 \tau_c$. A value for Ω_p can be obtained from $\epsilon_1(\omega)$. Fig. 3.11 shows that $\epsilon_1(\omega)$ crosses zero at 18 cm^{-1} and levels off at about $\epsilon_H = 500$. Now, since $\epsilon_1(\omega) = 500 - (\Omega_p/\omega)^2 = 0$ at 18 cm^{-1} , $\Omega_p = 400 \text{ cm}^{-1}$, a reasonable value. Hence $\tau_c = 1.0 \times 10^{-9} \text{ s}$ ($\Gamma_c = 0.005 \text{ cm}^{-1}$). This value is to be compared to the single particle lifetime $\tau_{sp} = 7.83 \times 10^{-15} \text{ s}$ [69].

One can also estimate the effective mass M^* of the zero frequency mode from

$$\Omega_p^2 = \frac{4\pi n e^2}{M^*} \approx \omega_p^2 \frac{m^*}{M^*} \quad (3.11)$$

Figure 3.11

The real part of the dielectric constant for $(\text{TMTSF})_2\text{ClO}_4$ at 2 K. For $E \parallel a$, ϵ_1 first crosses zero at 18 cm^{-1} . Between 50 and 160 cm^{-1} , $\epsilon_1 = 500$.



This gives $M^* = 646 m^*$ ($m^* = 1.3 m$ where m is the free electron mass) for the zero frequency mode. A similar effective mass was obtained for the pinned mode of the TTF-TCNQ salt [11]. Table 2 lists the values of τ_c and M^* for the three compounds in the metallic state. The value of τ_c for the ClO_4 salt at 25K is $\approx 6 \times 10^{-11}$ s (0.09 cm^{-1}), more than five times longer than the two centrosymmetric salts. This may explain why the high frequency 'tail' of the zero frequency mode is visible in the AsF_6 and SbF_6 salts, and not in the ClO_4 compound.

We have shown in this sub-section that $\sigma_1(\omega)$ in the metallic state can be divided into two regions: a very narrow mode centred at $\omega = 0$, and an overall conductivity due to Holstein emission of phonons. The Holstein conductivity is thus in the relaxation region of the zero frequency mode. The zero frequency mode has a half-width of $\approx 0.3 \text{ cm}^{-1}$ while the Holstein phonon limited scattering half-width is $\approx 500\text{--}650 \text{ cm}^{-1}$.

For $E \perp a$, the overall conductivity is about an order of magnitude smaller than $E \parallel a$, Figs. 3.7, 3.12 and 3.13. The accuracy in this direction is not good for two reasons. First, not all of the crystals were arranged along the b direction. This is reflected in the oscillator strength, which is not conserved for all three compounds. Second, due to the geometry of the sample arrangement, diffraction

Table 2

Material	T(K)	ω (cm^{-1}) at $\epsilon_1=0$	ϵ_H	Ω_p (cm^{-1})	τ (s)	$[\Gamma(\text{cm}^{-1})]^\dagger$	M*
(TMTSF) ₂ ClO ₄	2	18	500	400	1.0×10^{-9}	[0.005]	646
(TMTSF) ₂ SbF ₆	25	33	350	617	1.7×10^{-11}	[0.32]	273
(TMTSF) ₂ AsF ₆	30	37	300	640	1.6×10^{-11}	[0.34]	268

[†] The dc conductivities used in the calculations were from refs. 1, 4 and 88.

Figure 3.12

The conductivity for $E \perp a$ of $(\text{TMTSF})_2\text{SbF}_6$. In this polarization direction we were not able to observe any change up to 30 K. The sharp dispersive line at 288 cm^{-1} is the internal SbF_6 phonon. The origin of the three narrow lines at low frequency is not known.

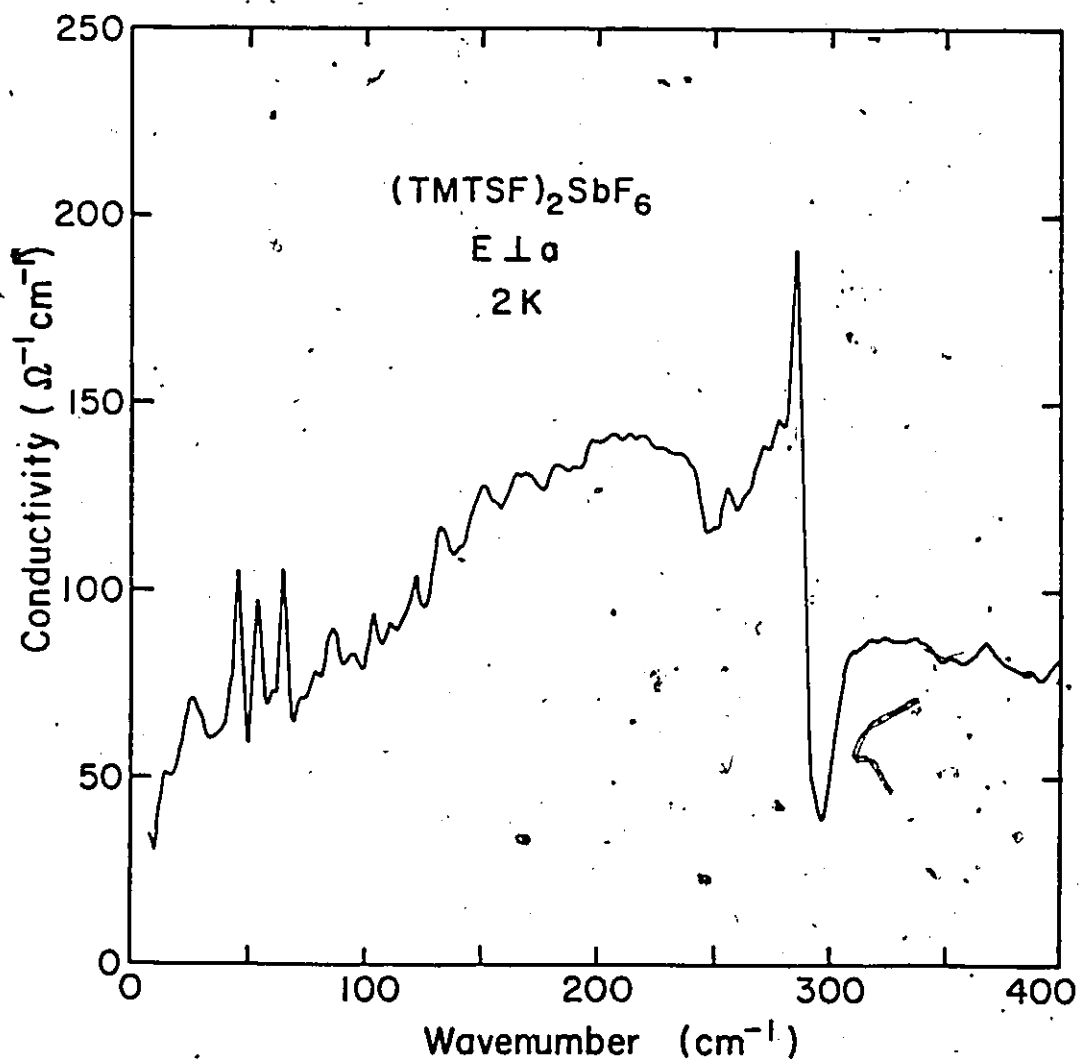
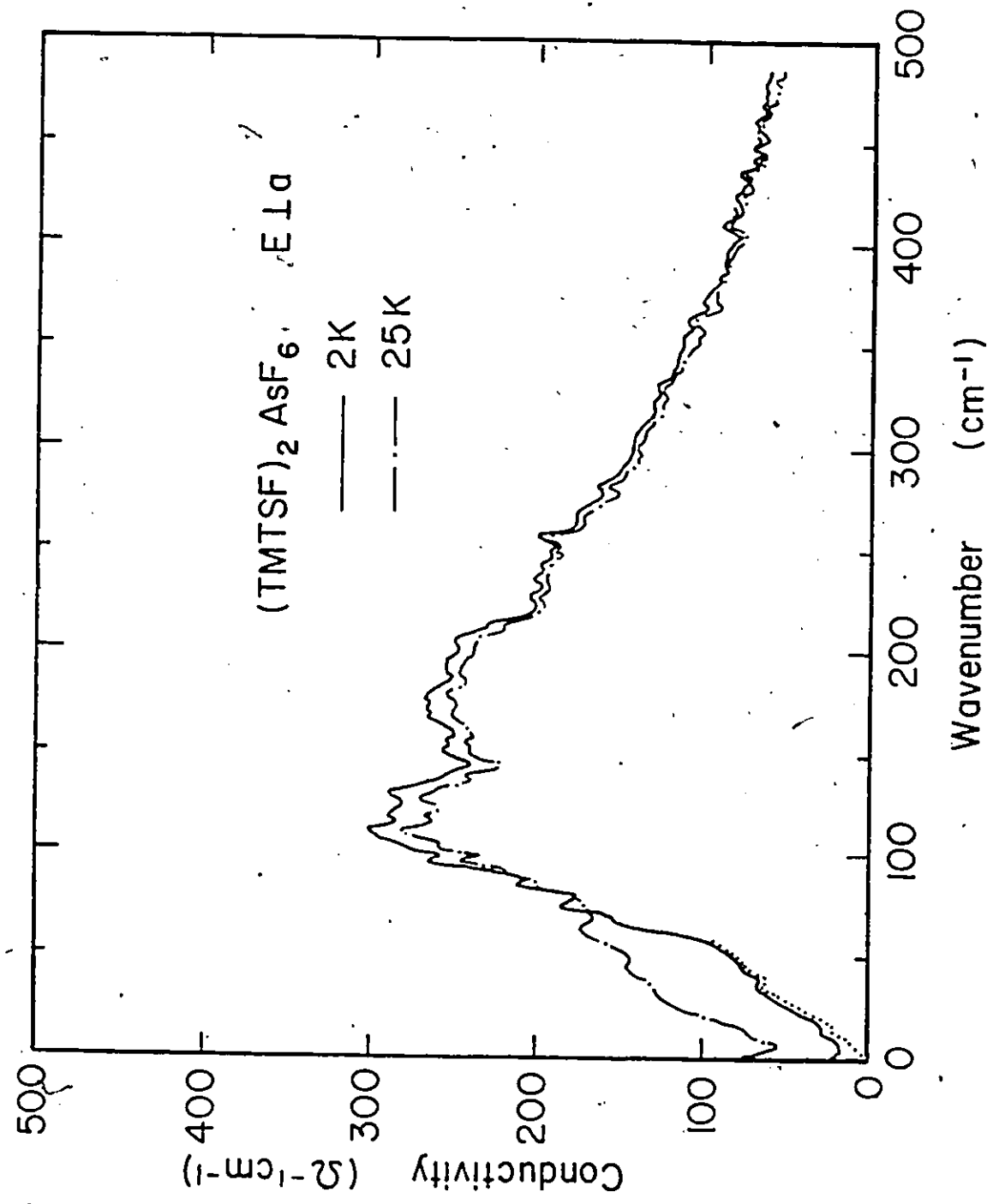


Figure 3.13

The conductivity for $(\text{TMTSF})_2\text{AsF}_6$ in the $E \perp a$ direction.
Note the change in $\sigma_1(\omega)$ below $\approx 67 \text{ cm}^{-1}$ as the temperature
was decreased from 25 K to 2 K. The dotted line was obtained
when the reflectance was extrapolated to $\approx 78\%$ at $\omega = 0$
(similar to that shown in Fig. 3.6).



is more pronounced in the $\perp a$ direction.

The conductivity in the $E \parallel a$ direction is probably better described using a diffusive model. That is to say, the electrons are more likely to be confined to the chain, and the interchain conductivity occurs by hopping across chains. The extrapolated dc value for the three materials is between 50 - 100 $(\Omega\text{-cm})^{-1}$, and is in good agreement with the $(\text{TMTSF})_2\text{PF}_6$ data [15] and direct dc measurements.

In the high frequency region $\geq 70 \text{ cm}^{-1}$, $\sigma_1(\omega)$ for $E \parallel a$ and for all three compounds does not change much with temperature up to 30K (58K for the ClO_4 salt). However, below 70 cm^{-1} , both the ClO_4 and AsF_6 materials show similar changes with temperature as for $E \parallel a$. The SbF_6 compound, on the other hand, did not show any change up to 30K. We will try to explain these observations in the next subsection.

A puzzling observation in the SbF_6 compound is the strong dispersive SbF_6 line in the high temperature conducting state (Fig. 3.14 line D'). Using the theory of Ipatova et al. [81] we estimate the strength of an optic phonon in this material to be several orders of magnitude lower than what is observed. The presence of the anion lines, however, is not confined to this material but can also be seen in the $(\text{TMTSF})_2\text{PF}_6$ and ClO_4 salts [15].

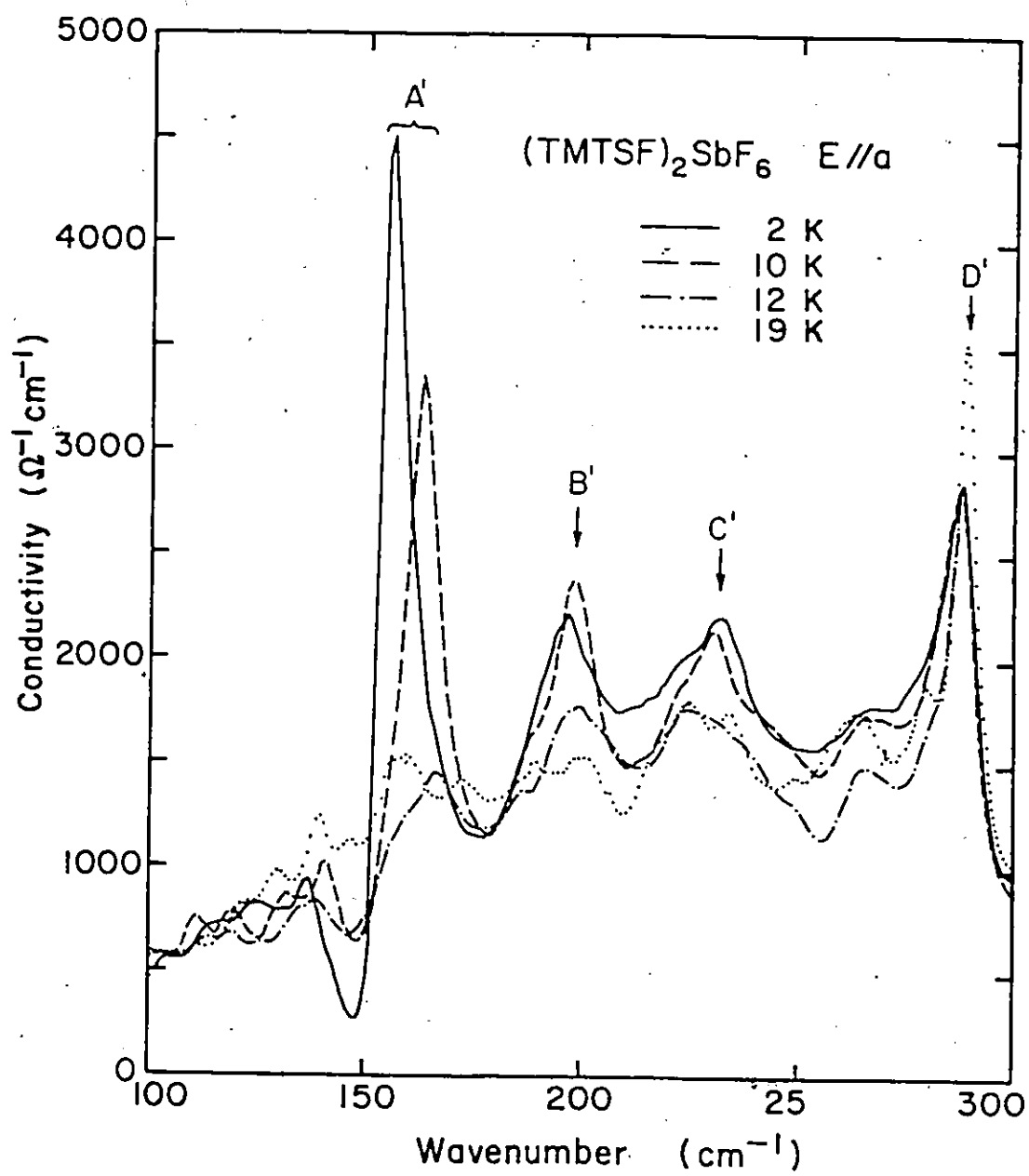
b. Unique Features

In our discussion in the previous sub-section, we had ignored the sharp lines at low frequencies in Fig. 3.7, and also the differences in the SDW state for the other two salts. We will now discuss the features that are unique to each compound. As in the case of the reflectance data, each compound will be discussed separately. Additional results for the ClO_4 material in the Q-state will also be given. However, we will first discuss the SbF_6 salt in the SDW state since the explanation used to interpret the sharp lines in this material (Fig. 3.8) may throw light on the structure observed in the ClO_4 salt.

The most dramatic feature in the SbF_6 compound is the appearance of three peaks (A', B', and C') as the temperature was decreased to 2K (Fig. 3.8). In Fig. 3.14, we show the temperature dependence of the conductivity in the frequency range $100 - 300 \text{ cm}^{-1}$. We first note a decrease in intensity as the temperature increases and also a shift to higher frequencies of the lowest frequency peak A'. From Raman scattering [74] of TMTSF molecules, the peak was assigned to the $a_g \nu_7$ mode with frequency 173 cm^{-1} that has been shifted down due to e-p coupling. (Bozio et al. [15] assigned this mode to $a_g \nu_{12}$ with a value of 146 cm^{-1} .) Peak C' will then be $a_g \nu_{11}$ with calculated frequency 240 cm^{-1} . However, to be consistent with the data on Fig. 3.9,

Figure 3.14

Detailed temperature dependence of the conductivity along the a direction of $(\text{TMTSF})_2\text{SbF}_6$. Note the shift and weakening in intensity of peak A' as the temperature is increased.

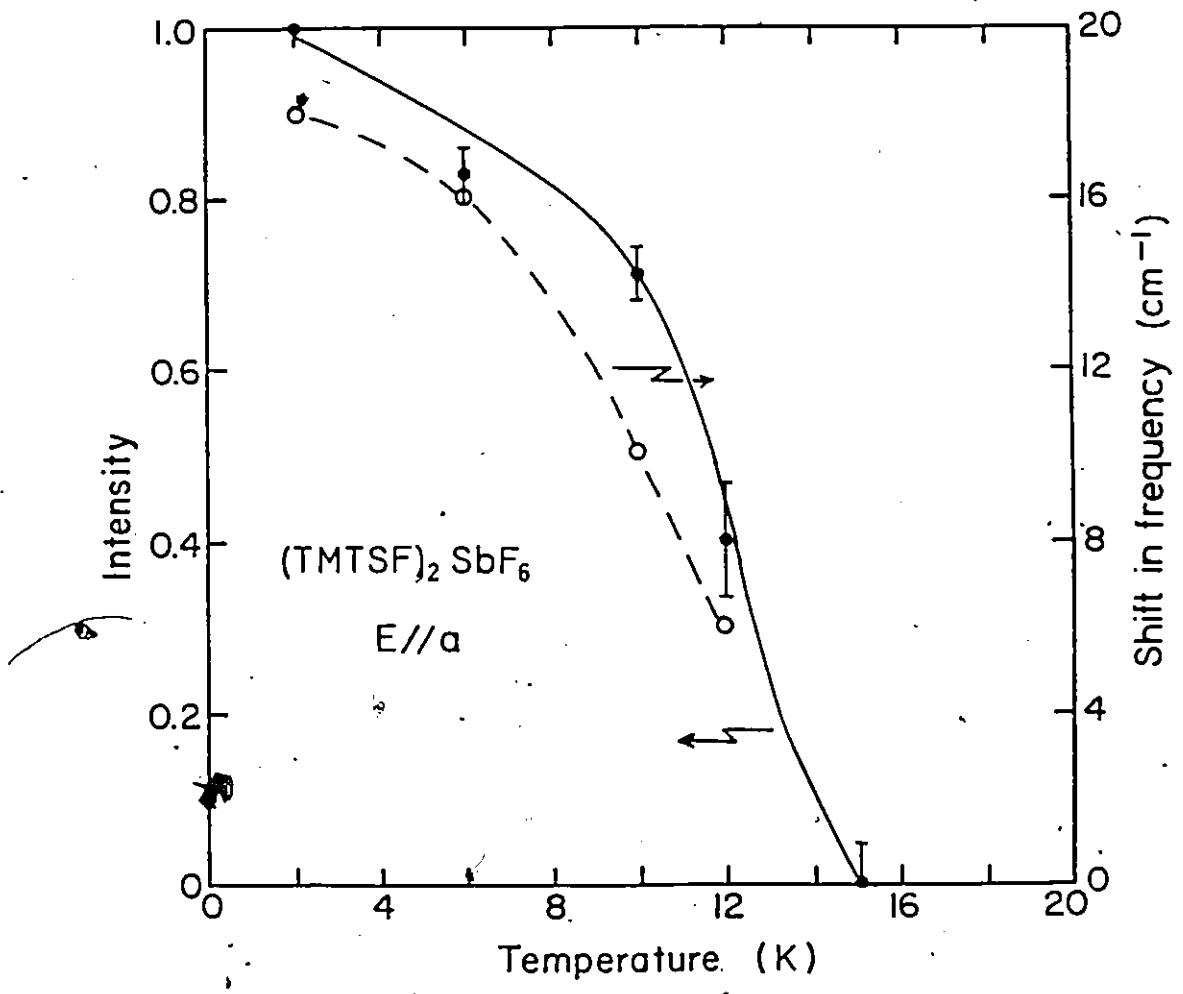


$a_g \nu_{11}$ is assigned an experimental value of 256 cm^{-1} . A plot of the integrated normalized intensity of peak A' versus temperature is shown in Fig. 3.15 (solid circles). It shows an abrupt rise in intensity for $T < 14\text{K}$. The shift in frequency of peak A' (open circles) versus temperature also changes rapidly below 14 K. Thus our measurements indicate a phase transition with $T_{\text{SDW}} \approx 12 - 14\text{K}$.

In the absence of a complete theory of SDW induced phonon absorption we will apply the theory of Rice for a one-dimensional semiconductor with a gap [57,58]. A SDW theory does exist [81] but is not applicable since it predicts the wrong sign in the shifts of the phonon frequency. Since SDW cannot interact with phonons directly a mechanism of the type proposed by Rice may still operate via the second harmonic CDW that in general accompanies a SDW [83]. Our observation of the persistence of the high conductivity in the frequency range below 200 cm^{-1} implies a partial presence of a metallic state. In $(\text{TMTSF})_2\text{PF}_6$, it was demonstrated that SDW coexists [84] with a metallic state. The background free-electron conductivity must be subtracted first. The free conductivity is non-Drude and is difficult to calculate theoretically. Consequently we assumed that the conductivity at 19K is totally due to free electrons and that at 2K some of these electrons become localized. The semiconducting part can then be expressed as

Figure 3.15

Plot of the normalized (to 2 K) integrated intensity of peak A' (see Fig. 3.14) versus temperature (solid circles). The abrupt rise in intensity signifies the formation of SDW. The shift in frequency (open circles) also shows a rapid change for $T < 14$ K. The lines were drawn as a guide to the eye.



$$\sigma_I = \sigma(2K) - X\sigma(19K) \quad (3.11)$$

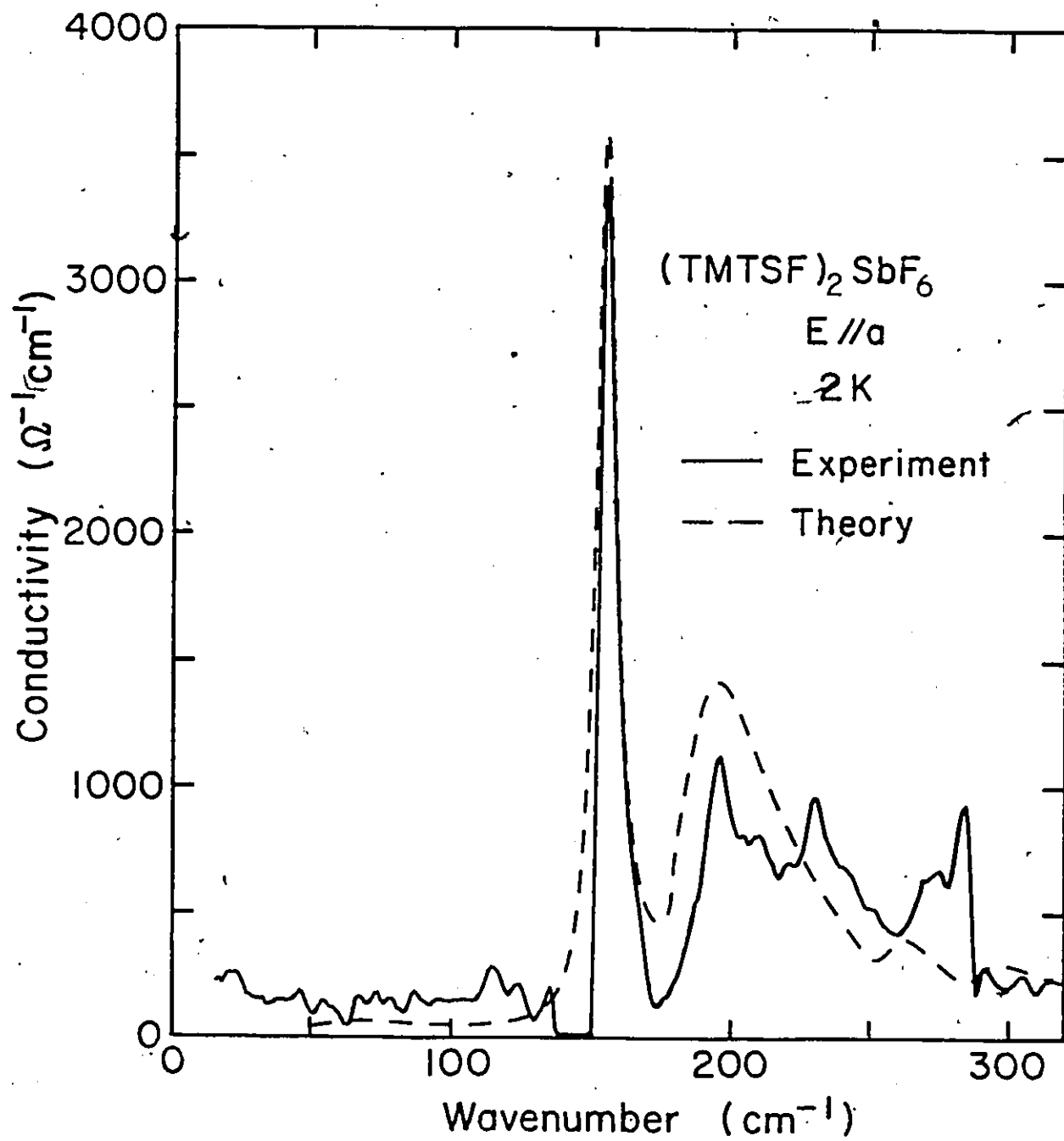
where X is a constant chosen to allow for a temperature dependence of the free electron part. In Fig. 3.16 (solid line) we show the resulting conductivity for $X = 0.75$. There is a gap-like region of low conductivity and a sharp and symmetric phonon line. The threshold in conductivity at $\approx 180 \text{ cm}^{-1}$ is identified as the onset of single particle excitations across a gap, $2\Delta_{\text{SDW}}$.

We will outline briefly the theory of M.J. Rice [57, 58]. When a CDW state is formed, there is intermolecular distortion. However, for organic charge transfer salts, there are, in addition, intramolecular distortions. These distortions have small CDW amplitudes, but are strongly coupled to the intramolecular vibrations. The phases of the CDWs can oscillate about their equilibrium positions which gives rise to anomalous infrared activity. These oscillations are called 'phase phonons'. The oscillator strength is electronic in origin rather than lattice. Since the intermolecular distortion is along the chain axis, the CDW oscillation couples those phonons that are perpendicular to the chain or in the plane of the molecules. That is to say, the modes excited are the symmetric (or a_g) phonon modes which are usually infrared non-active.

Detailed calculations show that the conductivity of intramolecular-vibration stabilized CDW is given by

Figure 3.16

Obtained by subtracting $0.75 \sigma(19 \text{ K})$ from $\sigma(2 \text{ K})$ (solid line). The threshold in conductivity at $\approx 180 \text{ cm}^{-1}$ is identified as a SDW gap, 2Δ . Dashed line, theoretical fit using equation 3.12 for $T = 0 \text{ K}$.



$$\sigma(\omega) = \frac{\omega^2}{4\pi i \omega} \frac{p, CDW}{\omega} [f(\tilde{\omega}) - f(0) - \tilde{\omega}^2 f(\tilde{\omega})^2 \lambda D_\phi(\omega)] \quad (3.12)$$

where $\frac{1}{8} \omega^2 p, CDW$ is the oscillator strength applicable to the CDW part, and $\tilde{\omega} = \omega/2\Delta$. The first two terms inside the square bracket give the single particle excitation across a gap, 2Δ . Below 2Δ , $\text{Re}[f(\tilde{\omega}) - f(0)] = 0$; whereas, at 2Δ , there is a threshold in $\sigma_1(\omega)$. The full expression was derived by Lee, Rice and Anderson [85] and is quoted below.

$$f(y) = \{\pi i + \ln[(1-S)/(1+S)]\} / (2S y^2) \quad (3.13)$$

where $S = \sqrt{1-y^{-2}}$. The e-p coupling λ is the sum of the coupling between the condensed electrons and all of the a_g phonons, $\omega_n(q_0)$ i.e. $\lambda = \sum_{n=1}^G \lambda_n$, G being the number of a_g phonons. The phase phonon propagator, $D_\phi(\omega)$, is given by

$$D_\phi(\omega)^{-1} = \left\{ - \sum_{n=1}^G (\lambda_n/\lambda) \omega_n^2(q_0) / [\omega_n(q_0)^2 - \omega^2 - i\omega\Gamma_n] \right\}^{-1} \\ + 1 - \frac{v}{\Delta} + \lambda \tilde{\omega}^2 f(\tilde{\omega}) \quad (3.14)$$

where Γ_n is the natural linewidth of the phonons, and $2v$ is the gap which becomes 2Δ with the e-p interaction turned on. Equation (3.14) gives Lorentzian-type lines for frequencies less than 2Δ . Above 2Δ , the lines are mixed in with the single particle continuum and have Fano or dispersive-like lineshapes [77].

Fig. 3.16 (dashed line) shows the conductivity found

using equation (3.12). The total e-p coupling, λ , was estimated to be 0.22 from mean field theory in the tight-binding approximation [86], $2\Delta = 8E_F[-1/\lambda]$ where the Fermi energy [13], $E_F = 0.276$ eV. This value of λ is lower than λ_{tr} which results from a summation over the whole Fermi surface rather than just the gapped part contributing to the SDW. The parameters used are listed in Table 3. All of the lines were given a width of $\Gamma = 12$ cm^{-1} . The total oscillator strength is taken to be 6% of $\frac{1}{8} \omega_p^2$. In addition, the fit was done with $2V = 150$ cm^{-1} from which the static dielectric constant $\epsilon_s = 1 + (\omega_p/2\Delta)^2 [\frac{2}{3} + \lambda\Delta/v]$ (equation (6), ref. 58) for the SDW part was calculated to be 2900. By subtracting $\epsilon_1(19\text{K})$ from $\epsilon_1(2\text{K})$ a similar value was obtained. In addition to the observed phonon lines there are ten more intramolecular phonon modes with frequencies higher than our measured data. These lines were arbitrarily assigned to a single frequency at 500 cm^{-1} with line width 50 cm^{-1} and e-p coupling 0.03. A more careful fit of the higher modes would alter the fitted values of λ_n . Low-lying intermolecular modes also couple to the electrons but are not expected to be optically active. They are given an arbitrary single frequency at 70 cm^{-1} with $\Gamma_{13} = 50$ cm^{-1} and $\lambda_{13} = 0.1$.

We will now discuss the reasonableness of the value of the gap $2\Delta = 180$ cm^{-1} (22 meV). The ratio $2\Delta/k_B T_{SDW} = 18 - 21$ is not too unreasonable where $T_{SDW} = 12 - 14\text{K}$ and k_B

Table 3

Mode	Frequency ω_n (cm^{-1})	Fitted λ_n
$a_g^v 11$	256	0.01
$a_g^v 12$	173	0.07
SbF ₆ line ?	288	0.01

Arbitrarily assigned lines

$$a_g^v 13, \omega_{13} = 70 \text{ cm}^{-1}, \Gamma_{13} = 50 \text{ cm}^{-1}, \lambda_{13} = 0.1$$

$$a_g^v 1-10, \omega = 500 \text{ cm}^{-1}, \Gamma = 50 \text{ cm}^{-1}, \lambda = 0.03$$

Other parameters used in the fit

$$2\nu = 150 \text{ cm}^{-1}$$

$$2\Delta = 180 \text{ cm}^{-1}$$

$$\omega_{p,CDW} = 2500 \text{ cm}^{-1}$$

is the Boltzmann's constant. Within mean field theory, this ratio follows a BCS-type description [80], i.e. $2\Delta/k_B T_{mf} = 3.5$. However, if fluctuation effects are included this value will change. For example, in an incommensurate Peierls transition [87], $T_{mf} \approx 4T_{SDW}$ giving $2\Delta/k_B T_{SDW} = 14$. In view of the crudeness of this calculation, the agreement is all that one can expect. A condition for the coexistence of a metallic and semiconducting state is that $2\Delta < 4 t_b$. For the SbF_6 salt, the transverse transfer integral [68] t_b is 18 meV. The band width in the b-direction is, then 72 meV. This implies that only a small portion of the Fermi surface is gapped. One then expects the metallic state to persist at low temperatures. This is borne out by our results. In addition, the absence of the phase phonon peaks in the perpendicular direction (Fig. 3.12) is in agreement with the prediction [57] of Rice's theory. Also, we did not observe a measurable magnetic field dependence up to 7 kgauss.

It is natural to extend the phase phonon argument to the ClO_4 salt where two lines at 7 and 25 cm^{-1} were observed for $E||a$. The temperature dependence of these lines is shown in Fig. 3.17. In the $E|a$ direction there is a broad peak at $\approx 20 cm^{-1}$ that also changes with temperature, Fig. 3.18. As pointed out earlier, it is not clear whether a lower peak is present in this polarization.

Figure 3.17

Temperature dependence of the 7 and 25 cm^{-1} peaks of $(\text{TMTSF})_2\text{ClO}_4$. Note the shift to lower frequency in the minimum at 30 cm^{-1} as the temperature was increased. The shift occurred abruptly at 24 K.

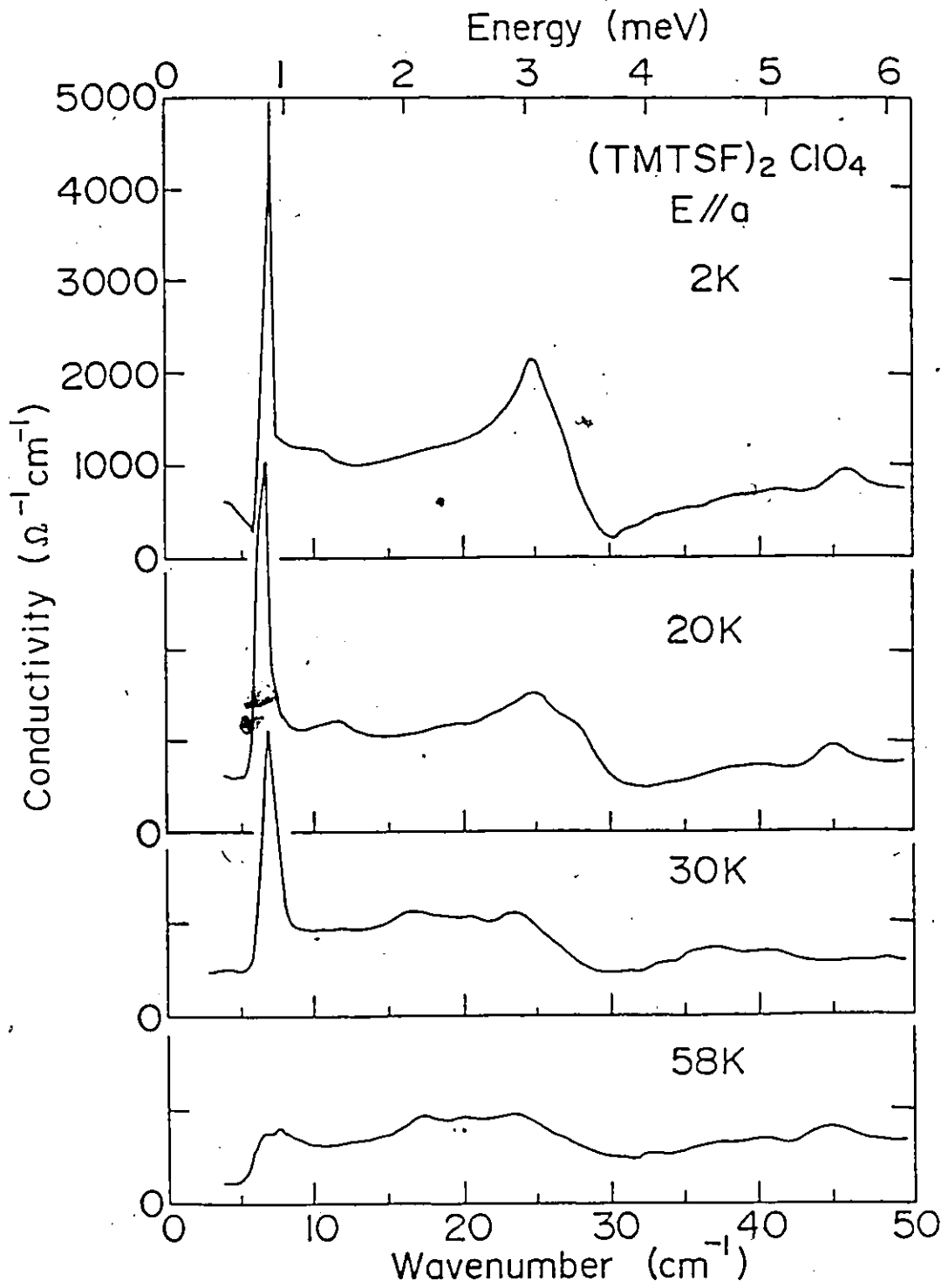
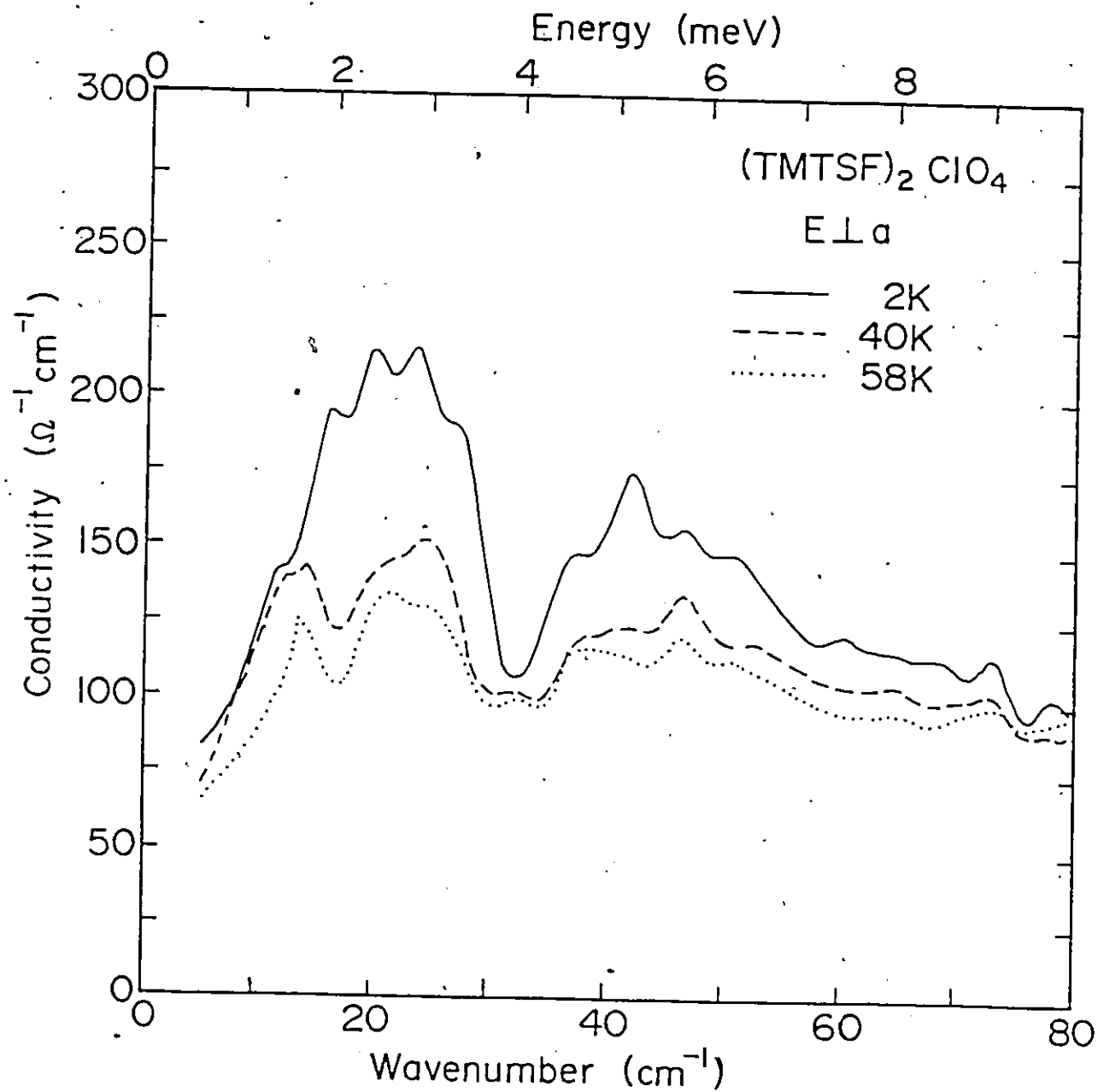


Figure 3.18

Corresponding temperature dependence of $\sigma_1(\omega)$ at low frequencies for $(\text{TMTSF})_2\text{ClO}_4$ in the $E \perp a$ direction. A shift in frequency is also observed in this direction.

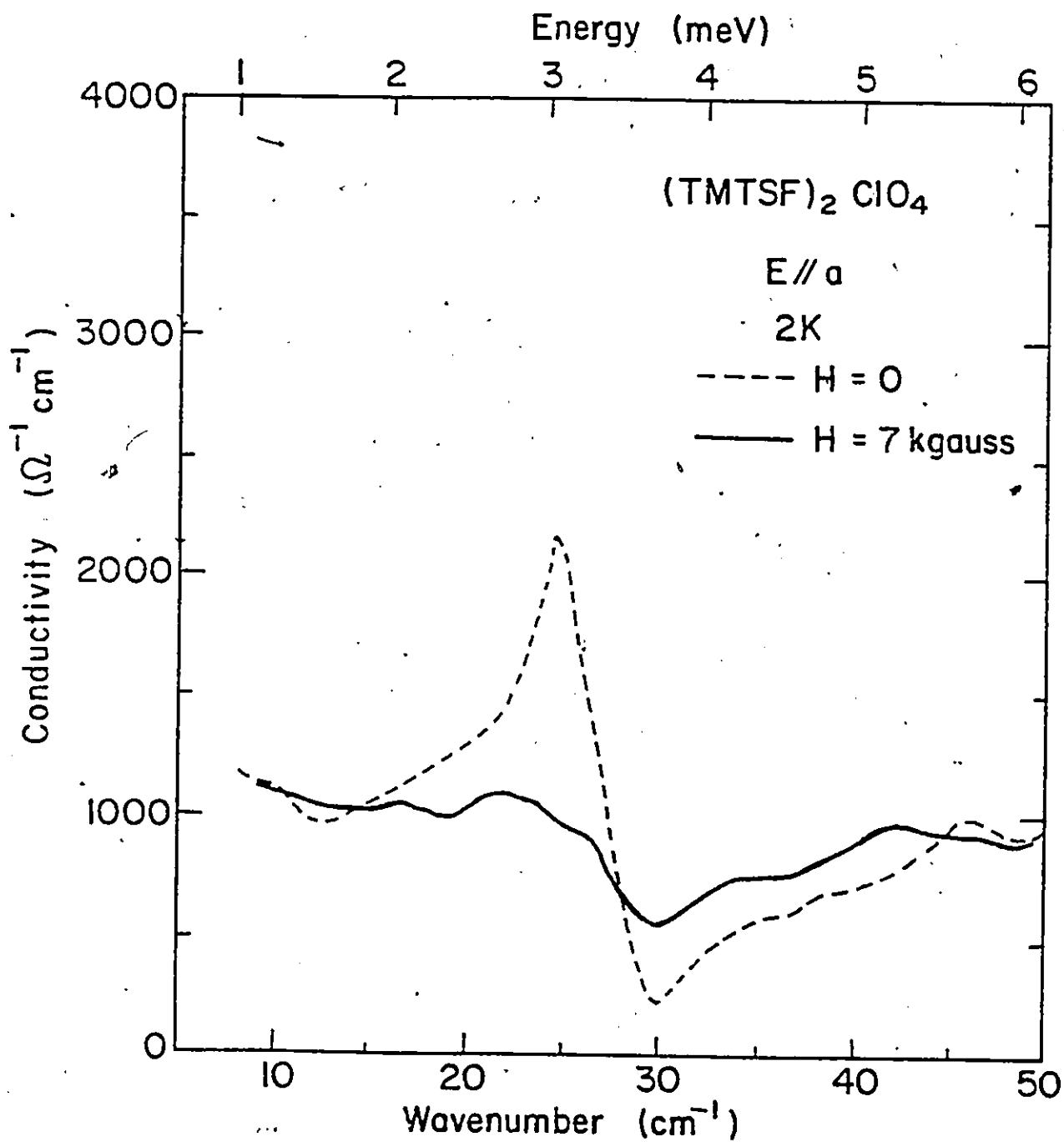


The phase phonon explanation, however, is difficult to justify for the following reasons. First, the peaks were observed up to temperatures of $\approx 60\text{K}$. If there is any phase transition at such high temperatures, then it should be seen in other measurements e.g. dc conductivity which would then have a MI transition in the $\approx 60\text{K}$ region. No such transition was observed [4]. Second, phase phonons originate from symmetric phonon modes. Group theory calculations show that there is no symmetric mode in this frequency region [59]. There are however, librational modes. It is not clear how these librational modes would couple to electrons since the results shown in Fig. 3.17 are for the R-state of the ClO_4 salt i.e. there should be no SDW or CDW state present. Third, there was an abrupt shift down by 2 cm^{-1} for the higher frequency peak as the sample was heated above 24K . This temperature is associated with the anion order/disorder. Thus it would appear that the ClO_4 anions do play a part, at least in the 25 cm^{-1} peak. Fourth, the 25 cm^{-1} peak is magnetic field dependent. This effect is shown in Fig. 3.19 for $H = 7\text{ KGauss}$, and corresponds to the magneto-absorption experiments discussed in Section 2.5. Lastly, a similar temperature dependence in the $E_{\parallel a}$ direction, albeit different in peak position, and a shift at 24K strongly imply the observed features are not phase phonons.

In addition, the 29 cm^{-1} peak in the reflectance is

Figure 3.19

Magnetic field dependence of the 25 cm^{-1} peak. A small magnetic field washes out the peak and fills in the minimum at 30 cm^{-1} .



sensitive to radiation damage [59]. A 100 ppm damage reduces the intensity by 60% while a 1000 ppm damage completely destroys the peak. It is difficult to understand these observations if it is a direct phonon. It should also be noted that radiation damage reduces the dc conductivity significantly [38].

The persistence of the peaks to high temperatures, and the magnetic field dependence present difficulties in trying to explain the results shown in Fig. 3.16. It is not clear as to the physical origin of the two peaks. The explanation for our observations may lie in a better understanding of the role the anions play in this compound.

As indicated earlier, the disorder in the anions can be frozen in if the sample is quenched. We show in Fig. 3.20 the reflectance and the corresponding $\sigma_1(\omega)$ of the ClO_4 compound at 2K when cooled at a rate of 40 - 50K/min from $\approx 70\text{K}$. By cooling at a faster rate $\approx 70\text{ K/min}$ from 30K, the reflectance in the R-state and Q-state, both at 2K, show a difference in the position of the edge (at 29 cm^{-1} and 27 cm^{-1}) that we associate with anion disorder (Fig. 3.21). The Q-state edge at 2K is similar in position to that at temperatures above 24K for the R-state. The conductivity in Fig. 3.20 shows an asymmetric peak at 22 cm^{-1} with threshold at 20 cm^{-1} . By using the first two terms in equation (3.12) and also equation (3.13), this peak is identified as a SDW

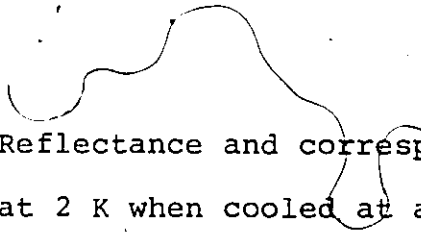


Figure 3.20

Reflectance and corresponding conductivity of $(\text{TMTSF})_2\text{ClO}_4$ at 2 K when cooled at a rate of $\approx 40\text{-}50$ K/min from ≈ 70 K. The asymmetric peak is identified as being due to single particle excitations across a SDW gap.

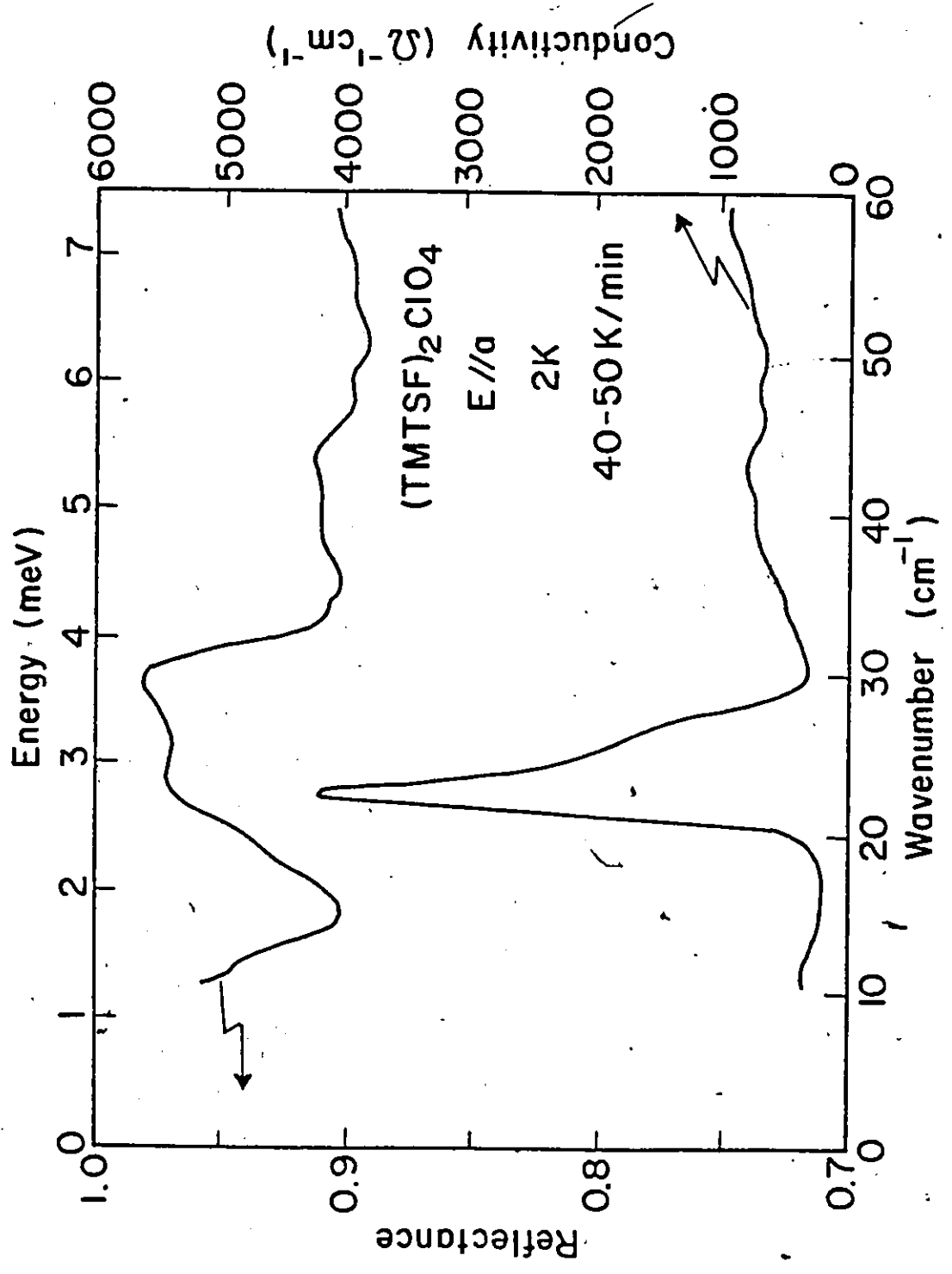
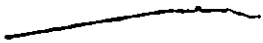
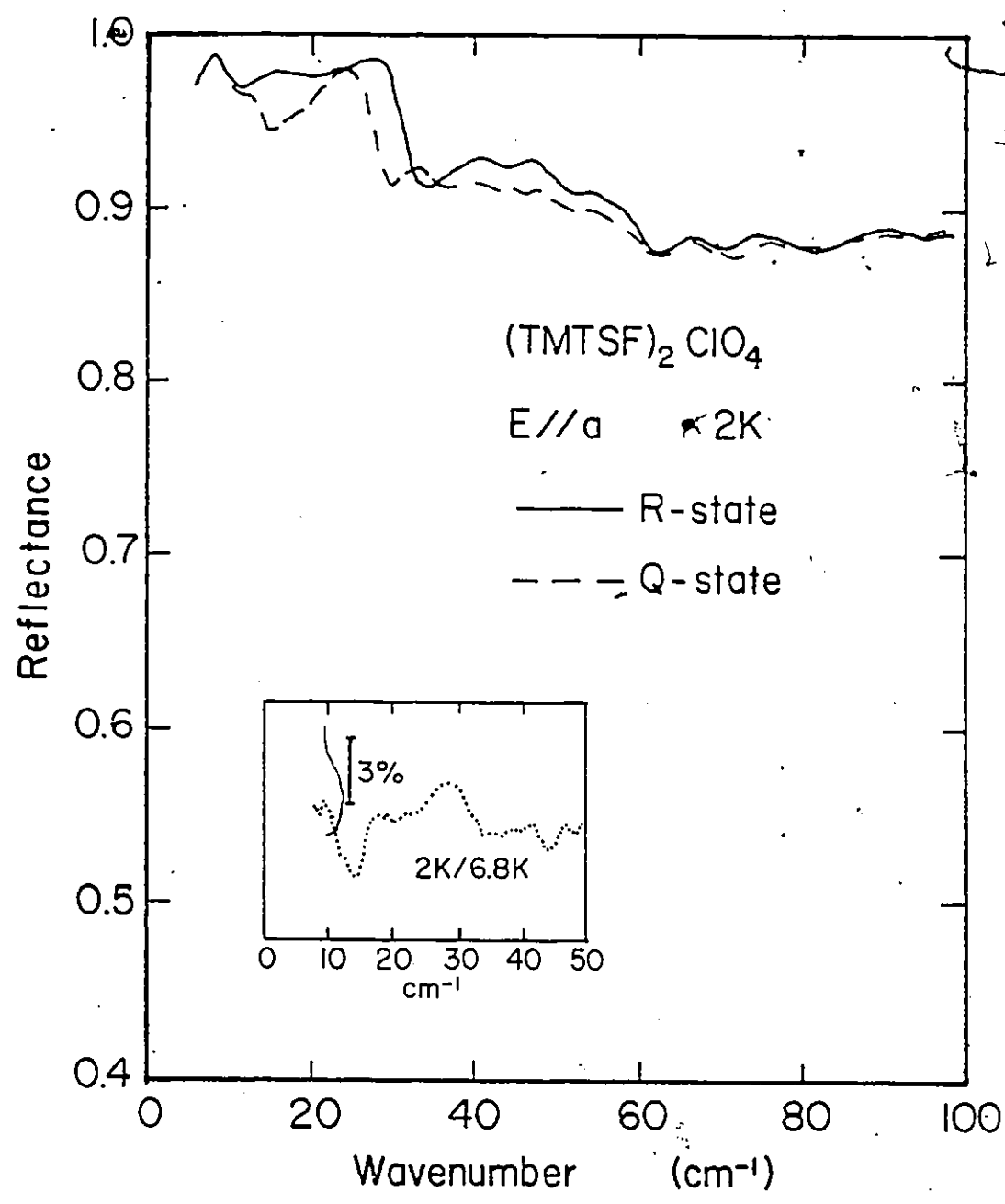


Figure 3.21

Reflectance of $(\text{TMTSF})_2\text{ClO}_4$ in the R-state and Q-state, both at 2 K. The Q-state was obtained when cooled at a rate of ≈ 70 K/min from 30 K. This shows clearly that the shift observed in Fig. 3.4 can be associated with anion order/disorder. The inset illustrates the disappearance of the 14 cm^{-1} dip in the reflectance at 6.8 K.



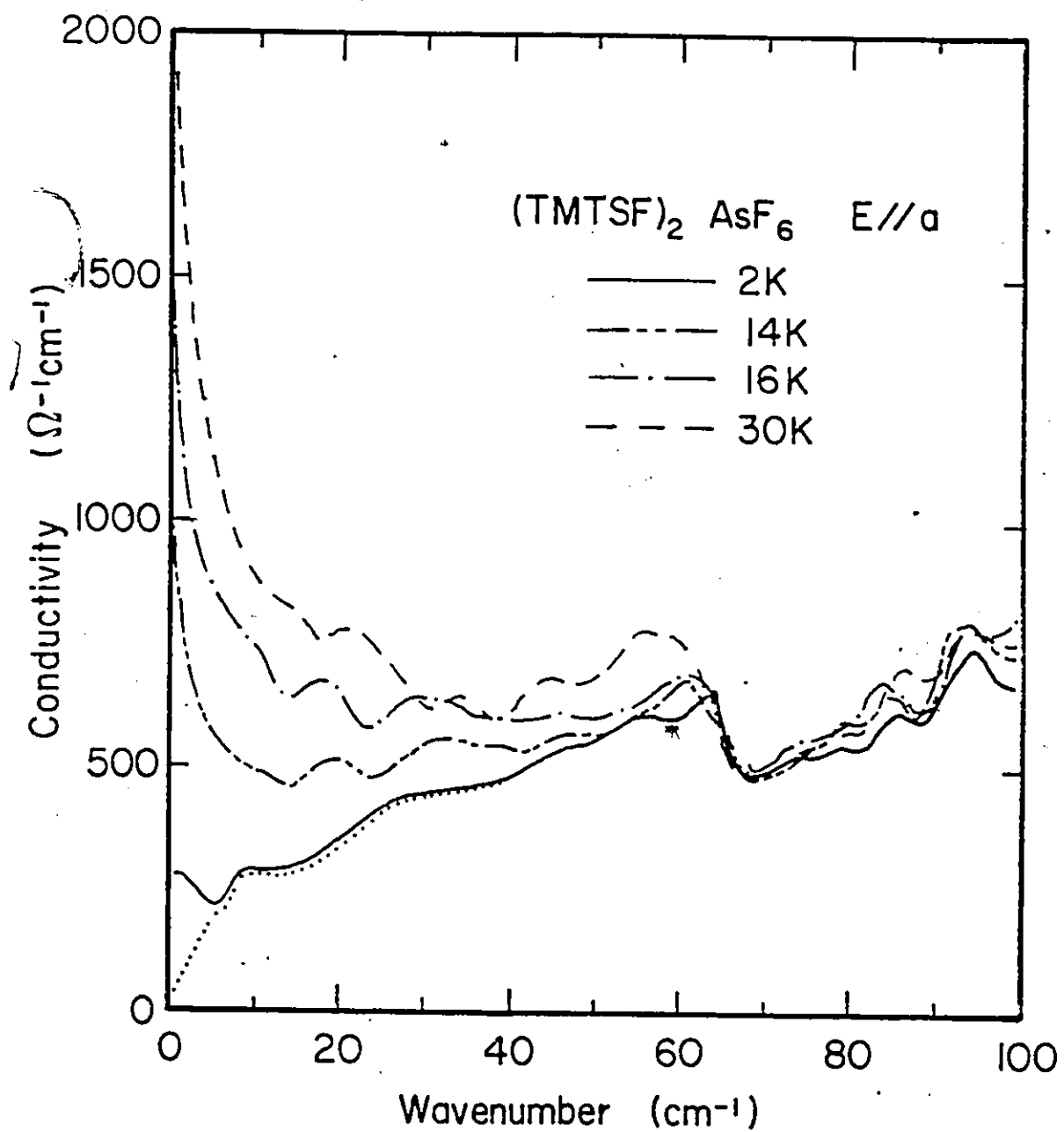


gap with $2\Delta_{\text{SDW}} = 20 \text{ cm}^{-1}$. There are other factors that suggest that the peak is due to single particle excitation across a SDW gap. It disappears by 7K, i.e. above the SDW transition temperature. This is shown in the inset of Fig. 3.21 where the thermal reflectance was taken. It shows an increase in reflectance for the 14 cm^{-1} dip as the temperature was raised to 6.8K. Also, we did not observe any magnetic field dependence of the peak up to 7 k Gauss. The presence of a magnetic field, at most, will flip the spin over but will not affect the SDW gap.

We now turn to the last of the three compounds, the AsF_6 salt, in the low frequency end. Fig. 3.22 illustrates the decrease in $\sigma_1(\omega)$ as the temperature was decreased to 2K i.e. as the sample changed to a SDW state. This decrease is not confined to $E \parallel a$ but is also observed in the $E \perp a$ direction, Fig. 3.13. At 2K, two choices in the extrapolation to $\omega = 0$ were done in the reflectance, Fig. 3.6. The dotted line (Fig. 3.22) which represents the extrapolation to $R(\omega=0) \approx 94\%$ gives the correct dc conductivity. Note that the dc conductivity is not zero but $\approx 30 (\Omega \cdot \text{cm})^{-1}$. This implies that there is a partial presence of a metallic state. At two other temperatures, 14, and 16K, the extrapolated dc values agree very well with the measured dc conductivity [88]. This represents the first optical observation of an extrapolation to the correct dc values as a function of temperature for an organic charge transfer salt.

Figure 3.22

Detailed conductivity of $(\text{TMTSF})_2\text{AsF}_6$ for $E||a$ at the low frequency end. At the three lower temperatures, the extrapolated dc conductivity agrees very well with direct dc measurements. The dotted line shows the conductivity with the extrapolation shown in Fig. 3.6. Below $\approx 8 \text{ cm}^{-1}$ the conductivity was obtained by extrapolating the reflectance to unity.



The measured dc value at 30K is much larger than our extrapolated value. We note that as the temperature decreases there is a decrease in oscillator strength. If there is any pinned SDW mode (as in CDW, refs. 30 and 31) below our lowest measured frequency $\approx 7 \text{ cm}^{-1}$, then as the material goes into the SDW state, the oscillator strength should redistribute itself at higher frequencies. In other words, there should be an increase in oscillator strength at $\approx 10 \text{ cm}^{-1}$ if there is a pinned SDW mode. The fact that we did not observe any increase suggests that there is no pinned SDW mode.

In Figs. 3.9 and 3.19 we have shown the overall conductivity spectrum for $E \parallel a$ and $E \perp a$ respectively. There does not appear to be any region in $\sigma_1(\omega)$ which can definitely be associated with a SDW gap. For both polarizations, there is a curious decrease in $\sigma_1(\omega)$ below $\approx 62 \text{ cm}^{-1}$ ($\approx 67 \text{ cm}^{-1}$ in $E \perp a$). Whether this represents a SDW gap is not clear. There is no theoretical justification to take this decrease as a SDW gap. If it is a SDW gap, then there is a slight anisotropy in the gap.

c. Effects of Thermal Cycling

Almost all of the results presented above were obtained from the first cryogenic run. The results from the first run were reproducible i.e. the samples can be cycled over the temperature range studied without any visible differences in the results. Various effects were observed af-

ter recycling. A virgin crystal has a shiny black surface. After three or four thermal cyclings, the surface has a matte appearance. Also, tiny cracks could be seen on the surface under a lower power microscope. The cracks were probably due to stress induced during the cooling process.

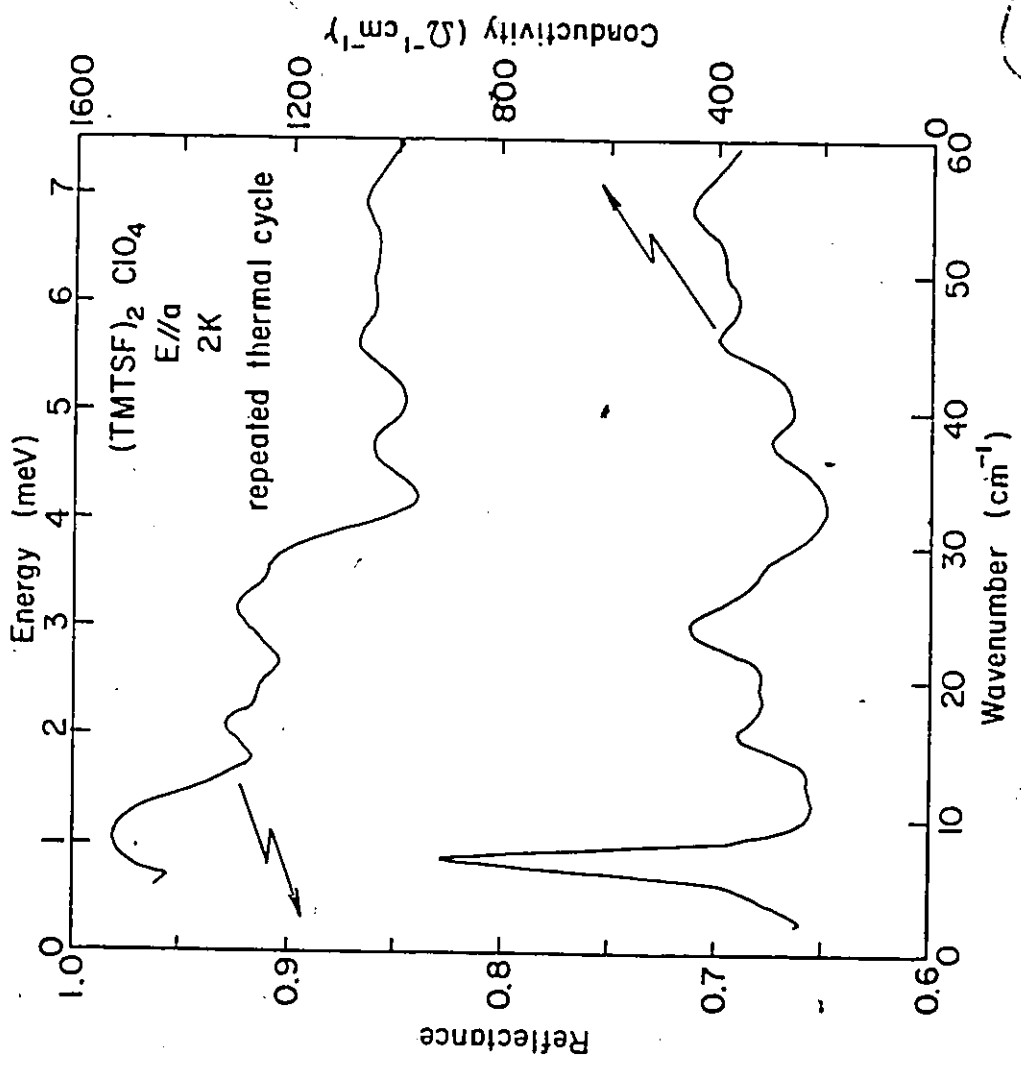
In Fig. 3.23 we show the reflectivity and conductivity of the ClO_4 compound after ≈ 5 thermal cycles. Note that the two peaks in $\sigma_1(\omega)$ are still visible though reduced in strength. There is also an increase in diffraction related structures. We found that by scraping the surface of the mosaic and then washing it with dichloromethane (CH_2Cl_2), we were able to reproduce the results shown in Fig. 3.4. This suggests that the changes observed under repeated thermal cycling are due to impurities that diffused into the surface rather than due to the cracks.

The magnetic field effect shown in Fig. 3.19 was observed during the first cooling and in the R-state. We were not able to see the effect after one thermal cycle. In the last ClO_4 mosaic studied, the magnetic field dependence was only observed in the first spectrum. It would appear that the field effect is not easily reproducible and may explain why Challener failed to observe this effect [59].

For the SbF_6 compound, two mosaics M1 and M2 from the same batch were studied. Only the initial cryogenic run on M1 has the strength of the lines (A, B and C) shown. The second mosaic M2 which was kept in a dessicator for about

Figure 3.23

An example of the effect of thermal cycling on a sample of $(\text{TMTSF})_2\text{ClO}_4$. The 7 and 25 cm^{-1} lines are still visible, though reduced in strength.



three months prior to measurements gave much weaker A, B and C lines. Line D however, was unchanged. The level of reflectance for both mosaics is comparable. For E_{1a}, the lines were again of different strength (except line D); being stronger in M2 than M1.

The above observations for the SbF_6 material imply that lines A, B and C are not simply phonons. It is difficult to conceive of phonons being so strongly influenced by impurities. Our interpretation shows that they are of collective origin. The probable reason why the lines are weaker in M1 is that impurities diffused into the crystals or that $(\text{TMTSF})_2\text{SbF}_6$ may have decomposed.

Thermal cycling did not affect the results shown in Fig. 3.6 significantly. After four cycles, the same results were obtained by taking thermal reflectance i.e. the changes in reflectance as a function of temperature were not affected by impurities that may have diffused into the crystal. In the actual reflectance, diffraction peaks caused by cracks could be seen. A probable reason for the compound not being strongly influenced by thermal cycling is that the compound is less pure in the first place [80].

CHAPTER 4

SUMMARY AND CONCLUSION

In this chapter, a summary of the results will be presented. In the metallic state, the results will be discussed both in terms of fluctuation superconductivity and a single particle transport picture. Suggestions for future experiments will be given at the end of this chapter.

The first part of this project involved measuring the transmission through a grid of $(\text{TMTSF})_2\text{ClO}_4$ crystals. This method was used to enhance the absorption in the presence of a magnetic field and is suitable for measuring the energy gap of ordinary superconductors. However, there is a lack of absolute calibration i.e. the changes in the conductivity are not known. This technique applied to the organic compound showed an increase in absorption below ≈ 3.8 meV when a field of 0.2 Tesla was applied. The frequency region affected by the magnetic field is in agreement with measurements done using the reflectivity method.

By Kramers-Kronig transformation of the reflectance, one can get $\sigma_1(\omega)$. The metallic state of the materials can be characterized by two lifetimes: τ_c that describes the lifetime of the zero frequency mode, and τ_p that gives the frequency dependent relaxation time due to scattering by phonons. The latter process has a conductivity profile that

shows an initial increase as a function of frequency before levelling off at the limiting value of $\frac{1}{\tau_p}$. As each phonon branch (or internal phonon mode) comes in, thresholds in $\sigma_1(\omega)$ are observed. This is most pronounced in the AsF_6 salt. The calculated values of τ_c show that the zero frequency mode has an extremely long lifetime ($> 10^{-11}$ s). Since τ_p is of order $10^{-14} - 10^{-15}$ s, the Holstein process occurs in the relaxation region of the zero frequency mode. The strength of the e-p coupling for the three compounds is between 0.5 - 0.95; the highest value is for the ClO_4 salt. These values are very reasonable and support the Holstein mechanism.

The low conductivity in the $10 - 100 \text{ cm}^{-1}$ region shows that the dc conductivity cannot be described by a single particle transport model (Drude's mechanism). This model has a ω^{-2} dependence in $\sigma_1(\omega)$ for $\omega\tau > 1$ and in the $10 - 100 \text{ cm}^{-1}$ region would show a decrease instead of an increase (as our results indicate) as a function of frequency. Thus, a single particle transport picture cannot adequately account for the huge dc conductivity.

As pointed out in Section 1.3, $\sigma_1(\omega)$ for FSC would be characterized by low conductivity inside the pseudo-gap after which it would rise sharply to a normal metal response. For the ClO_4 salt at 2K, $\sigma_1(\omega)$ does have this character and, together with the magnetic field dependence, would suggest the existence of FSC. However, detailed temperature

dependence studies of $\sigma_1(\omega)$ indicate that the low conductivity at 30 cm^{-1} does not tie in with a pseudo-gap. As the temperature is increased, the pseudo-gap would be filled in. This would give a corresponding increase in conductivity in the low frequency end. Our results did not show a filling in of the gap up to 58K, far above the fluctuation temperature. Moreover, in the Holstein process with a superconducting gap, the thresholds in $\sigma_1(\omega)$ would be shifted up by the value of the energy gap 2Δ , when compared to the normal state [89]. No such shifts were observed in our results.

Our results strongly indicate the existence of a collective (or zero frequency) mode that is responsible for the high dc conductivity. We were not able to identify the mechanism responsible for this mode. This mode is necessary to account for the high measured dc conductivity. We estimate the half-width for the two centrosymmetric compounds to be $\approx 0.3 \text{ cm}^{-1}$ while that for the ClO_4 salt is almost two orders of magnitude smaller. The effective mass, M^* , of the mode is 250 - 650 m^* .

In the SDW state, the results for the three compounds appear diverse. The ClO_4 salt in the Q-state gives a clear threshold at 20 cm^{-1} in $\sigma_1(\omega)$ and an asymmetric peak. This threshold is identified as the SDW gap. For the SbF_6 salt, sharp phase phonons can be observed. This represents the

first observation of phase phonons in the SDW state. The SDW gap in this compound is $\approx 180 \text{ cm}^{-1}$. The AsF_6 salt, on the other hand, did not show any identifiable SDW gap. The zero frequency mode appears to freeze out as the compound goes into the SDW state.

These three compounds do not show a well formed SDW gap. For example, in the SbF_6 salt the conductivity below the gap is not zero. This indicates the coexistence of a SDW state and metallic state.

4.1 Suggestions for Future Experiments

The ClO_4 salt is the most interesting of the $(\text{TMTSF})_2\text{X}$ compounds. It undergoes a transition to a superconducting state in the R-state under ambient pressure, the first organic material to show such behaviour. The extremely narrow zero frequency mode that is responsible for the high dc conductivity deserves further study.

There are two possible ways to broaden the half-width of the zero frequency mode: one, radiation damage on the sample reduces the dc conductivity considerably, and two, doping with known amounts of impurities e.g. $(\text{TMTSF})_2(\text{ClO}_4)_x(\text{ReO}_4)_{1-x}$. Both of these methods should increase the scattering rate. If the mode is due to single particle transport, then the mode would broaden with the same amount of oscillator strength. It would then become accessible to far-infrared spectroscopy. On the other hand, a collective

mode may become pinned at a finite frequency or disappear by transferring its oscillator strength to higher frequencies [85]. Thus, by doping (or radiation damage) one can make a more detailed study of the zero frequency mode. In addition, as impurity scattering becomes more dominant, the Holstein process would be washed out. The resulting conductivity would show an increase in the low frequency end.

Within the organic materials, a new group of compounds *bis*-(ethylenedithiolo)tetrathiafulvalene (BEDT-TTF):X where X is a similar group of radical anions also become superconducting although under pressure [90]. One of the compounds, $(\text{BEDT-TTF})_4(\text{ReO}_4)_2$, has a MI transition at 81K. It would be interesting to do a parallel study on these compounds to study the mechanisms for transport and to see whether a zero frequency mode exists in these compounds.

APPENDIX

Energy	$1 \text{ meV} = 8.066 \text{ cm}^{-1}$	
Temperature	$1 \text{ K} = 0.695 \text{ cm}^{-1}$	
Scattering half-width Γ (cm^{-1})	$= \hbar/\tau$	
	$= 5309.2/\tau_{15}$	where τ_{15} is in units of 10^{-15} s
Conductivity	$1 (\Omega \cdot \text{cm})^{-1} = 4.78 \text{ cm}^{-1}$	
Resistivity	$1 \mu\Omega \cdot \text{cm} = \frac{1}{9} \times 10^{-17} \text{ s}^{-1}$	
Wavenumber	$1 \text{ cm}^{-1} = 29.98 \text{ GHz}$	
	$= 1.884 \times 10^{11} \text{ rad/s}$	
Boltzmann's constant	$k_B = 8.617 \times 10^{-2} \text{ meV/K}$	

BIBLIOGRAPHY

- 1 K. Bechgaard, C.S. Jacobsen, K. Mortensen, H.J. Pedersen and N. Thorup, *Solid State Commun.* 33, 1119 (1980)
- 2 D. Jérôme, A. Mazaud, M. Ribault and K. Bechgaard, *J. Physique Lett.* 41, 95 (1980)
- 3 R.L. Greene and E.M. Engler, *Phys. Rev. Lett.* 45, 1587 (1980)
- 4 K. Bechgaard, K. Carneiro, M. Olsen, F.B. Rasmussen and C.S. Jacobsen, *Phys. Rev. Lett.* 46, 852 (1981)
- 5 K. Mortensen, Y. Tomkiewicz and K. Bechgaard, *Phys. Rev.* B25, 3319 (1982)
- 6 J.B. Torrance, H.J. Pedersen and K. Bechgaard, *Phys. Rev. Lett.* 49, 881 (1982)
- 7 W.M. Walsh, Jr., F. Wudl, E. Aharon-Shalom, L.W. Rupp, Jr., J.M. Vanderberg, K. Andes and J.B. Torrance, *Phys. Rev. Lett.* 49, 885 (1982)
- 8 S. Tómic, J.P. Pouget, D. Jérôme and K. Bechgaard, *J. Physique*, 44, 375 (1983)
- 9 P.M. Chaikin, Mu-hong Choi, J.F. Kwak, J.S. Brooks, K.P. Martin, M.J. Naughton, E.M. Engler and R.L. Greene, *Phys. Rev. Lett.* 51, 2333 (1983)
- 10 M. Ribault, D. Jérôme, J. Tuchendler, C. Weyl and K. Bechgaard, *J. Physique Lett.* 44, L-953 (1983)
- 11 D.B. Tanner, C.S. Jacobsen, A.F. Garito and A.J. Heeger, *Phys. Rev.* B13, 3381 (1976) and refs. therein

- 12 K. Bechgaard, *Mol. Cryst. Liq. Cryst.* 79, 1 (1982)
- 13 P.M. Grant, *J. Physique*, C3-44, 847 (1983)
- 14 C.S. Jacobsen, K. Mortensen, M. Weger and K. Bechgaard, *Solid State Commun.* 38, 423 (1981)
- 15 C.S. Jacobsen, D.B. Tanner and K. Bechgaard, *Phys. Rev. Lett.* 46, 1142, (1981) also *Mol. Cryst. Liq. Cryst.* 79, 25 (1982)
- 16 K. Mortensen, *Solid State Commun.* 44, 643 (1982)
- 17 J.F. Kwak, J.E. Schirber, R.L. Greene and E.M. Engler, *Phys. Rev. Lett.* 46, 1296 (1981) also *Mol. Cryst. Liq. Cryst.* 79, 121 (1981)
- 18 P. Garoche, R. Brusetti, D. Jérôme and K. Bechgaard, *J. Physique Lett.* 43, L-147 (1982)
- 19 M. Choi, P.M. Chaikin, R.L. Greene and E.M. Engler, *Solid State Commun.* 41, 225 (1982)
- 20 P.M. Chaikin, Mu-Yong Choi and R.L. Greene, *J. Physique*, C3-44, 783 (1983)
- 21 M. Weger, *J. Physique*, C3-39, 1456 (1978)
- 22 P.M. Chaikin, P. Haen, E.M. Engler and R.L. Greene, *Phys. Rev.* B24, 7155 (1981)
- 23 H.J. Schulz, D. Jérôme, A. Mazaud, M. Ribault and K. Bechgaard, *J. Physique Lett.* 42, L-313, (1981) also H.J. Schulz, *Mol. Cryst. Liq. Cryst.* 79, 199 (1982)
- 24 R.E. Peierls, *Quantum Theory of Solids*, Oxford University Press, London p. 108
- 25 J. Bardeen, *Solid State Commun.* 13, 357 (1973)
- 26 H. Frölich, *Proc. R. Soc.* A223, 296 (1954)
- 27 L.B. Coleman, M.J. Cohen, D.J. Sandman, F.G. Yamagishi, A.F.

- Garito and A.J. Heeger, *Solid State Commun.* 12, 1125 (1973)
- 28 D. Allender, J.W. Bray and J. Bardeen, *Phys. Rev.* B9, 119 (1974)
- 29 P.A. Lee, T.M. Rice and P.W. Anderson, *Solid State Commun.* 14, 703, (1974)
- 30 D.B. Tanner, K.D. Cummings and C.S. Jacobsen, *Phys. Rev. Lett.* 47, 597 (1981)
- 31 P. Brüesch, S. Strässler and H.R. Zeller, *Phys. Rev.* B12, 219, (1975)
- 32 J.P. Pouget, R. Moret, R. Comes, K. Bechgaard, J.M. Fabre and L. Giral, *Mol. Cryst. Liq. Cryst.* 79, 129 (1982)
- 33 A. Andrieux, C. Duroure, D. Jérôme and K. Bechgaard, *J. Physique Lett.* 40, L-381 (1979)
- 34 H.J. Schulz, D. Jérôme, A. Mazaud, M. Ribault and K. Bechgaard, *J. Physique*, 42, 991 (1981)
- 35 C. More, G. Roger, J.P. Sorbier, D. Jérôme, M. Ribault and K. Bechgaard, *J. Physique Lett.* 42, L-313 (1981)
- 36 A. Fournel, C. More, G. Roger, J.P. Sorbier, J.M. Delrieu, D. Jérôme, M. Ribault, K. Bechgaard, J.M. Fabre and L. Giral, *Mol. Cryst. Liq. Cryst.* 79, 261 (1982)
- 37 A. Fournel, C. More, G. Roger, J.P. Sorbier and C. Blanc, *J. Physique*, C3-44, 897 (1983)
- 38 R.L. Greene, P. Haen, S.Z. Huang, E.M. Engler, M.Y. Choi and P.M. Chaikin, *Mol. Cryst. Liq. Cryst.* 79, 183 (1982)
- 39 G. Deutscher, Y. Imry and L. Gunther, *Phys. Rev.* B10, 4598 (1974)
- 40 J.H.P. Watson and G.M. Graham, *Can. J. Phys.* 41, 1738 (1963)
- 41 S. Wolf and B.S. Chandrasekhar, *Phys. Rev.* B4, 3014 (1971)
- 42 D. Djurek, M. Prester, D. Jérôme and K. Bechgaard, *J. Phys. C*, 15,

- L-669 (1982)
- 43 J.F. Kwak, J.M. Williams, M.A. Beno and D.D. Cox, *Bull. Am. Phys. Soc.* 29, No. 3, 376 (1984)
- 44 M. Choi, P.M. Chaikin, E.M. Engler and R.L. Greene, *Bull. Am. Phys. Soc.* 29, No. 3, 376 (1984)
- 45 D.U. Gubser, W.W. Fuller, T.O. Poehler, J. Stokes, D.D. Cowan, M. Lee and A.N. Bloch, *Mol. Cryst. Liq. Cryst.* 79, 225 (1982)
- 46 J.E. Eldridge and F.E. Bates, *J. Physique*, C3-44, 1469 (1983) and refs. therein
- 47 W.M. Walsh, Jr., F. Wudl, G.A. Thomas, D. Nalewajek, J.J. Hanser, P.A. Lee and T. Poehler, *Phys. Rev. Lett.* 45, 829 (1980)
- 48 P.M. Chaikin, G. Grüner, E.M. Engler and R.L. Greene, *Phys. Rev. Lett.* 45, 1874 (1980)
- 49 P.H. Martin and E. Puplett, *Infrared Phys.* 10, 105 (1969)
- 50 T. Timusk and F.K. Lin, *Proc. of the 35th Symposium on Molecular Spectroscopy*, Columbus, Ohio, p. 68
- 51 D.H. Drew and A.J. Sievers, *Applied Optics*, 8, 2067 (1969)
- 52 H.R. Navarro-Contreras, *Ph.D. Thesis*, McMaster University
- 53 W.A. Challener, P.L. Richards, S.C. Zilio and H.L. Garvin, *Infrared Phys.* 20, 215 (1980)
- 54 R. Ulrich, *Infrared Phys.* 7, 37 (1967)
- 55 E.A. Lewis and J.P. Casey, *J. Appl. Phys.* 23, 605 (1952)
- 56 K.D. Moeller and W.G. Rotschild, *Far-Infrared Spectroscopy* (Wiley) 1971
- 57 M.J. Rice, *Phys. Rev. Lett.* 37, 36 (1976)

- 58 M.J. Rice, L. Pietronero and P. Brùesh, *Solid State Commun.* 21, 757 (1977)
- 59 W.A. Challener, *Ph.D. Thesis*, Lawrence Berkeley Laboratory
- 60 P. Garoche, R. Brusetti and K. Bechgaard, *Phys. Rev. Lett.* 49, 1346, (1982)
- 61 H.K. Ng, T. Timusk, J.M. Delrieu, D. Jérôme, K. Bechgaard and J.M. Fabre, *J. Physique Lett.* 43, L-513 (1982)
- 62 M. Ribault, *J. Physique*, C3-44, 827 (1983)
- 63 D. Jérôme, *Mol. Cryst. Liq. Cryst.* 79, 155 (1982)
- 64 J.F. Kwak, *Phys. Rev.* B26, 4789 (1982)
- 65 F. Wooten, *Optical Properties of Solids*, Academic Press (1972)
- 66 T.S. Moss, *Optical Properties of Semi-Conductors*, Butterworths Publications Ltd., London (1959) p. 25
- 67 F. Stern, *Solid State Phys.* 15, 299 (1963)
- 68 C.S. Jacobsen, D.B. Tanner and K. Bechgaard, *J. Physique*, C3-44, 857 (1983)
- 69 K. Kikuchi, I. Ikemoto, K. Yakushi and H. Kuroda, *Solid State Commun.* 42, 433 (1982)
- 70 T. Holstein, *Phys. Rev.* 96, 539 (1954) and *Ann. Phys.* (New York), 29, 410 (1964)
- 71 H. Scher, *Phys. Rev. Lett.* 25, 759 (1970)
- 72 P.B. Allen, *Phys. Rev.* B3, 305 (1971)
- 73 H. Bilz and W. Kress, *Phonon Dispersion Relations in Insulators* give a good collection on phonon density of states.
- 74 K. Iwahana, H. Kuzmany, F. Wudl and E. Aharon-Shalom, *Mol. Cryst. Liq. Cryst.* 79, 39 (1982)

- 75 R. Bozio, C. Pecile, K. Bechgaard, F. Wudl and D. Nalewajek, *Solid State Commun.* 41, 905 (1982)
- 76 B. Mitrović, H.G. Zárate and J.P. Carbotte, *Phys. Rev.* B29, 184 (1984)
- 77 L.P. Gor'kov and E.I. Rasha, *Solid State Commun.* 27, 1211 (1978)
- 78 Initial M.Sc. project
- 79 Private communication with R.L. Greene
- 80 Private communication to T. Timusk from J.F. Kwak who pointed out that $(\text{TMTSF})_2\text{AsF}_6$ consistently give the lowest dc conductivity of the TMTSF salts.
- 81 I.P. Ipatova, A.A. Maradudin and D.L. Mills, *Solid State Commun.* 8, 561 (1970)
- 82 E. Fenton and G. Psaltakis, *Solid State Commun.* 47, 767 (1983)
- 83 Private communication to T. Timusk from A. Griffin
- 84 L.J. Azevedo, J.E. Schirber and E.M. Engler, *Phys. Rev.* B27, 5842 (1983)
- 85 P.A. Lee, T.M. Rice and P.W. Anderson, *Solid State Commun.* 14, 703 (1974)
- 86 M.J. Rice and S. Strässler, *Solid State Commun.* 13, 125 (1973)
- 87 P.A. Lee, T.M. Rice and P.W. Anderson, *Phys. Rev. Lett.* 31, 462 (1973)
- 88 J.B. Torrance, *J. Physique*, C3-44, 799 (1983)
- 89 R.R. Joyce and P.L. Richards, *Phys. Rev. Lett.* 24, 1007 (1970)
- 90 S.S.P. Parkin, E.M. Engler, R.R. Schumaker, R. Lagier, V.Y. Lee, J.C. Scott and R.L. Greene, *Phys. Rev. Lett.* 50, 270 (1983)